QATAR UNIVERSITY

COLLEGE OF ENGINEERING

EFFICIENT ELECTROMAGNETIC ANALYSIS AND DESIGN TECHNIQUES IN JET ENGINES

BY

APARNA KRISHNA

A Dissertation Submitted to

the Faculty of the College of

Engineering

in Partial Fulfillment

of the Requirements

for the Degree of

Doctor of Philosophy in Electrical Engineering

Jan 2018

Committee

The members of the committee approve the Dissertation of Aparna Krishna defended on 17 Jan, 2018:

Tamer Khattab

Dissertation Supervisor

Aya. F. Abdelaziz

Dissertation Co-Supervisor

Walaa Hamouda

Committee Member

Abdulla Kadri

Committee Member

Nizar Zorba

Committee Member

Approved:

Khalifa Al-Khalifa, Dean, College of Engineering

Abstract

Krishna, Aparna, :

Jan: 2018, Doctor of Philosophy in Electrical Engineering

Title: Efficient Electromagnetic Analysis and Design Techniques in Jet Engines

Supervisor of Dissertation: Tamer Khattab

A statistical electromagnetics based approach is proposed for efficient analysis of electromagnetic propagation inside harsh environments, like jet engines, to establish a communication channel inside the environment. The study of electromagnetic propagation inside the jet engine compressors that are close to turbine blades faces several difficulties due to the design complexity. The jet engine environment is an extremely complex geometry and exhibits random behavior due to the presence of moving metallic parts. The complex geometry environment combined with the inhomogeneous volumetric target render traditional analytical and simulation modeling techniques highly inefficient. To address this issue, two different approaches are proposed. The first is an innovative dynamic simulation approach based on statistical electromagnetic methods and inspired by analysis of mechanically stirred reverberation chambers.A dimension scaling method is introduced along with the dynamic simulation approach to solve the complex jet engine environment. Furthermore, the effect of excitation on the field characteristics of the dynamic system has been analyzed to prove that the dynamic system is statistically linear.

In the second approach, a novel statistical excitation method is applied to develop an equivalent model for the fields generated by a fixed excitation inside a jet engine with dynamic rotating blade. Hence, the jet engine is considered as a static system without blade rotation, but with a random excitation. The dynamic and static systems have been compared using full wave simulation method and numerical methods. The results proved that there is a statistical

equivalence between the dynamic and the static systems. The effect of the Doppler frequency shift on the electric field strength inside a jet engine is analyzed by using a stepwise stationary blade rotation method. The results show that the amplitude deviation due to frequency shift is negligible at all receiving probe locations. Later, the effect of blade rotation on the electric field phase variation is also analyzed. The results are very promising for the future modeling of the jet engine Doppler shift in terms of field phase time variation.

A new low profile microstrip antenna array is proposed and analyzed for wireless sensor applications in extremely harsh jet engine environments. This design is to establish a communication link between the wireless sensors inside the jet engine with the receiving antennas and hence the entire system is designed for ISM band of frequency. Due to the environmental constraints, the antenna is designed to be extremely thin and flexible. The proposed antenna is designed to have a canonical beam pattern. Three different models of patch antenna arrays, circular, half circular, and hybrid rectangular circular models are designed, simulated, fabricated and experimentally measured. The proposed antennas radiate symmetrically around the normal axis Z, with a null in the boresight direction. The radiation pattern of the proposed antenna is promising for real-time applications inside a jet engine since the strongest radiation field of the antenna is pointed towards the engine blades.

Dedication

To My Vichu,

Acknowledgements

I would like to express my sincere gratitude towards the *God Almighty* whose abundant grace and mercy enabled the successful completion of this thesis.

I must first express my sincere thanks to Dr. Tamer Khattab, who accepted me as his Ph.D. student and mentored me with invaluable advice. He had a clear vision for this thesis, and encourage me to follow the correct direction. He was able to provide me with insight when I needed it, while at the same time allowing me the liberty to do the work independently. I would also like to express my heartfelt gratitude to my co-supervisor Dr. Aya. F. Abdelaziz for her guidance and valuable comments. This work would not have been possible without her patience and involvement, on a daily basis from the start of the project till date. Under her guidance, I successfully overcome many difficulties. Thank you Dr. Aya for all your support. You are an amazing person and a great mentor. I would also like to thank Prof. M. Guizani, for his valuable suggestions and advice during this journey. I would like to express my profound gratitude to all the faculties, TA's and non-teaching staff of electrical engineering department who have inspired and motivated me to make this thesis a success. I would also like to express my sincere gratitude towards Dr. Khalifa Al-Khalifa (Dean, College of Engineering), Dr. Nasser Ahmed Al-Emadi (H.O.D), Dr. Nader Meskin (program coordinator) and all the staff in the Graduate Office for their support and suggestions. I would also like to extend my sincere gratitude towards the examining committee for their valuable suggestions and comments. I would especially like to acknowledge for all the technical support that I have received from CREMA, CUSAT, India and Texas A&M, Qatar.

I would like to thank my wonderful family: my parents, my brother, sister-in-law and all my cousins for being such a huge support throughout my life. My

parents gave their unconditional love to me and exerted their best to support my study. Thank you for never giving up on me and always remaining by my side. My sincere regard goes to my family-in-law for their love and support. I express my sincere thanks to all my friends, fellow PhD students in the college and relatives, for supporting me and motivating me.

I would like to thank a very special person, my husband, for his great support and understanding during this journey. When I thought that it is impossible to continue, you were there to motivate and guide me. Without you, this thesis would not have been written. Last but not the least, I want to say a big thanks to our little prince, '*Vaishnav*' for being world's best son. Words can never express how thankful I am to both of you for standing beside me with your unconditional love, care and patience, without which I could not have achieved the biggest dream in my life.

Part of this work was supported by a graduate student scholarship, GTA, from Qatar University.

This research work was made possible by grants number NPRP 08-700-2-296, NPRP 6-1326-2-532 and NPRP 7-923-2-344 from the Qatar National Research Fund, QNRF (a member of the Qatar Foundation, QF). The statements made herein are the sole responsibility of the authors.

Contents

List of Tables

List of Figures

List of Symbols and Acronyms

DS Dimension Scaling

DSA Dynamic System Approach

DSS Dynamic System Simulation

EM Electromagnetic

FDTD Finite Difference Time Domain

FEM Finite-Element Method

GO Geometrical Optics

HF High Frequency

HFSS High Frequency Structural Simulation

IPO Iterative Physical Optics

LF low frequency

MIMO Multiple Input Multiple Output

MM Mode Matching

MoM Method of Moment

PDF Probability Density Functions

PO Physical Optics

PTD Physical Theory of Diffraction

RC Reverberation Chamber

RCS Radar Cross Section

RPM Revolutions Per Minute

RX Receiver

SA Statistical Antenna

SAT Statistical Antenna Theory

SBR Shooting and Bouncing Ray

SE Statistical Excitation

SSA Static System Approach

STEM Statistical Electromagnetics

TX Transmitter

WSN Wireless Sensor Network

Chapter 1: Introduction

Analysis of Electromagnetic (EM) propagation inside harsh environments is one of the most challenging and important research subjects due to its applications in civil and military fields. We define EM harsh environments as unreliable and unbounded cavity propagation environments due to their complex geometry and the presence of moving metallic parts within the propagation path. The EM modeling of such type of complex cavities is extremely difficult. Therefore, the deployment of provably reliable wireless system is challenging. However, to monitor the environment attributes such as temperature, pressure, strain, etc; and to ensure the personal and environmental safety, deployment of Wireless Sensor Network (WSN) inside harsh environment is becoming more appealing due to high cost of material and maintenance of wiring. A WSN can been positioned inside the harsh environment and then it can transmit the information to a receiver placed outside the environment wirelessly. Hence, it is highly important to study the characteristics of the wave propagation inside the complex and harsh environment to develop a provably reliable wireless communication system inside such environment.

One of the two main threads of this research is to analyze the characteristics of EM field propagation inside harsh environments; particularly jet engine environments as shown in Fig. 1.1. This analysis will help to design a reliable communication system inside the environment enabling the extraction of the engine parameters with the help of wireless sensors. In order to properly eval-

uate the communication networks from the inside environment to outside, the transmitters will be positioned at the proposed locations inside the jet engine turbines and the receiving devices antenna will be positioned in front of the jet engine inlet. The relevance of this analysis is twofold with the mounting pursuit for fly-by-wireless [1]. Wherein the costly wired systems in different components of the aircraft, including those inside jet engines, can be substituted by wireless sensors and actuators. It's desirable to use wireless sensors installed on the stationary parts inside the jet engine, instead of the extremely expensive wired system. Existing wired systems are extremely complex, troublesome, heavy and easily undergo damage and deterioration due to harsh environment. Moreover, wireless sensors can be installed on the rotating parts of the jet engine, such as blade rotors. Thus, it is essential to have WSN installation because of the benefits such as; weight reduction, ease of maintenance and an increased monitoring capability [1, 2, 3, 4].

The jet engine design and analysis techniques are not only limited to aircraft applications but they extend to different areas of research such as industrial gas turbines, electrical power generation by natural gas, etc. It is exceptionally challenging to extract the field values from arbitrarily shaped model geometries with large sizes, complex terminations, and cross section variations. Over the years, numerous studies have been performed on the analysis of jet engine inlets and their components [5, 6, 7, 8, 9, 10, 11]. Early studies have expectedly been of theoretical nature, focusing mainly on very simple geometrical structures, such as simple circular cylinders without complex terminations [5, 6]. However, the complexity of the configurations has been steadily increasing, leading to practical computational results for fairly realistic structures [8, 12].

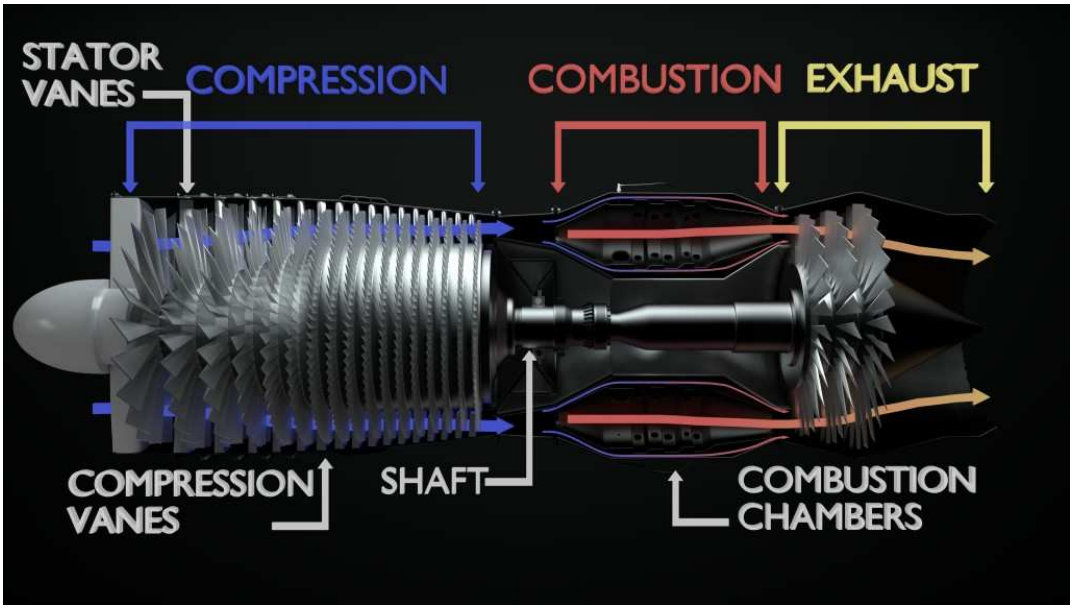

Figure 1.1 Cut away diagram of a jet engine.

1.1 Motivation

Modeling of wireless communication channel inside harsh environment is gaining momentum, due to the increasing interest in measuring parameters that earlier were impossible or difficult to measure with wired telemetry systems. In a typical sensing and wireless communication system inside the jet engine environment the sensors are installed on the turbine blades or compressors and will transmit the required information wirelessly to a receiver placed outside the engine. The interest towards wireless communication channel characteristics inside the jet engines stems from the trend towards using wireless sensors to evaluate different parameters related to the operation of the engine such as strain, temperature, pressure, gas emission and fuel consumption. This trend constitutes the so called $fly-by-wireless$ technology [1, 3, 4]. To develop a reliable wireless transmission inside the jet engine environment, the EM wave propagation has to be characterized and new antennas have to be designed

and modeled. The main work presented in this thesis attempts to cover both challenges.

The first part of the thesis outlines a brief overview of analysis of the EM field propagation inside the jet engine for addressing the challenges in modeling the wireless communication channel inside the environment. To establish a wireless communication channel inside the harsh environment, it is essential to have some prior knowledge of the characteristics of the EM propagation inside the environment. As we know, the metallic jet engine environment, the dynamic rotation of the fan blades and the stators between the transmitters and receiver will affect the performance of the EM propagation. Thus, the analysis of EM propagation inside the jet engine is essential to find the exact location of receivers with designed EM properties. Moreover, to successfully build a wireless network that works in harsh jet engine environment, an antenna system that is thin, possess desired radiation properties and conformal to the curved jet engine surfaces need to be designed and developed. The design of the antenna will be the main contribution in the second part of the thesis.

In order to take into consideration the challenges of the analysis of EM propagation inside harsh EM environments, two different approaches are put forth in the literature; the deterministic approach and the statistical approach. As the environment and the system of concern become more complex, the deterministic approach becomes less viable. The deterministic approach is applicable only to a known cavity geometry with canonical shapes. Hence, Statistical Electromagnetics (STEM) approach is introduced as an alternative method to analyze propagation in complex geometries

STEM is proposed as a novel approach for analyzing complex systems such as jet engine environment, without dealing with the complex details inside the engine cavity by using a probabilistic approach [13]. This method helps in expecting the field precisely inside a medium, which has a mix of small

and large dimensions simultaneously. STEM was first applied in analyzing the EM propagation inside the jet engine by Abdelaziz *et al*, [13]. In order to analyze the statistical characteristics of the EM field inside the jet engine, the concept of Reverberation Chamber (RC) approach had been applied. The statistical properties of the EM field as a function of the stirrer position were determined and compared to those of the mechanically mode stirred RC. The study proved that the jet engine cavity resembles the interior of an RC; it generates statistically uniform fields. This new analytical method motivates the idea of analyzing jet engine environment using the RC approach.

When analyzing a jet engine model with rotating blades by using STEM approach, we must consider the effect of different factors, such as number of blades, number of rotations, orientation of blades, Doppler frequency, etc;. Moreover, analyzing the whole jet engine blade rotation is time consuming and needs a more complex simulation procedure. Hence, a Statistical Excitation (SE) concept was introduced as a novel efficient approach for analyzing jet engines using the STEM approach [14]. The concept of SE has been adopted from Statistical Antenna (SA) hypothesis which has been applied in many applications to characterize the natural randomness that arises during the design or manufacturing process of large antenna systems [15, 16, 17, 18].

1.2 Objectives and Contributions

The overarching objective of this thesis work is to develop efficient techniques for the analysis of EM propagation in harsh environments (jet engines) and propose suitable novel antenna designs that enable reliable wireless connections in such environments. The detailed objectives of this thesis are multifold.

(1) Study the propagation characteristics of the EM waves inside complex dynamic harsh environments like jet engines.

(2) Endorse STEM as an efficient tool for the analysis of EM propagation inside complex cavities by considering the jet engine environment, as a mechanically stirred RC with the blades acting as a stirrer.

(3) Adopt the SE concept to develop an equivalent static model (fixed blades and random excitation) for the field generated inside a jet engine originally due to rotating blades and fixed excitation. Since the blades in the SE approach do not rotate, the simulation complexity is reduced and the system behave as a linear system. Hence, SE method is adopted as a best alternative for the dynamic system.

(4) Study the effect of Doppler frequency shift on the electric field characteristics inside the jet engine. The propagation characteristics of the EM wave is analyzed at different operating frequency from the Doppler spectrum to evaluate the effect of frequency deviation on the field magnitude and phase.

(5) Design a novel low profile two element array of microstrip patch antennas. The antennas are simulated and measured for wireless sensor applications in extremely harsh environments like jet engines. Due to the environmental constraints, the antenna is designed to be extremely thin and flexible. The entire system is designed for ISM band with maximum operating frequency at 2.45 GHz for the communication.

1.3 Challenges

Jet engine analysis and modeling are considered as extremely important problems because it is involved in the civilian and military needs. The ideas here are not limited to cases of jet engines and gas turbines because these problems can be generalized for the study of EM propagation inside any large, complex-geometry cavities containing rotating metallic objects. Different models and numerical techniques were used to get an approximate approach for calculating

the field inside the engine. Exact field calculations inside a real engine seems to be extremely difficult due to the complex nature of the problem. Researchers are facing many challenges to analyze such a complex medium and to determine the field distribution inside the engine. Basically, the complexity arises from the large jet dimensions, its complex design geometry, and its dynamic rotating parts. Characterizing the EM propagation through such an environment is extremely challenging. Moreover, the dynamic jet engine environment has a time varying characteristics and introduces Doppler frequency shift and phase noise in the received electric field. However, neither current state-of-the-art analytic methods nor simulation methods can capture the dynamics of a system resulting from rotating parts. Only experimental results can capture the time-dynamic behavior, but it is quite expensive and prohibitively restricted due to the sensitivity of jet engine technology. This complex geometry environment and inhomogeneous volumetric target leads to applying the concept of STEM as an alternate approach to this problem. STEM methods takes into account several parameters and hence end up with results which are more globally valid. However, to achieve good statistical model fit of the EM propagation inside the jet engine, using STEM requires a careful optimization of the statistical parameters as well as segmentation of the complex jet engine geometry.

Furthermore, one of the most significant challenges is the antenna design process. The main objective during antenna design is to reduce the size of the antenna with a desired radiation pattern. As the size of the antenna compared to the wavelength reduces, the directivity of the antenna is reduced and so the radiation pattern of the antenna becomes more isotropic. However, the requirements of the wireless sensing link is to have a null in the broadside direction and have the pattern pointed towards the jet engine fan blade. In order to achieve this, a patch antenna array geometry is proposed. Moreover, due

to the environmental constraints the proposed antenna needs to be extremely thin and this introduces high losses in the substrate. The antenna radiation efficiency is reduced considerably due to the thin substrate. This was another major challenge during the antenna design process.

1.4 Thesis Outline

The outline of the remaining parts of this thesis is as follows:

Chapter 2 introduces the general overview of different techniques used for the analysis of EM propagation through jet engine. This includes different kind of numerical analysis methods, experimental methods followed by STEM methods for analyzing complex cavities. Experimental measurements play a significant role to understand the nature of EM propagation inside complex cavities. This is followed by a comprehensive review of some of the most interesting aspects in the literature regarding SA concepts and conformal patch antenna concepts. Chapter 3 describes the two different aspects of the analysis of the propagation characteristics of the EM wave inside the jet engine environment. The segmentation details of the complex jet engine environment is also provided in this chapter.

Chapter 4 explains the dynamic system approach details and describes the propagation characteristics of the EM wave inside the jet engine environment with the help of a simplified jet engine model with different set of rotating blades. The model is simulated by using Ansoft High Frequency Structural Simulation (HFSS), a full wave simulation environment, and characterizes the jet engine environment as being similar to a mechanically stirred RC. The EM fields are extracted and analyzed statistically using STEM approach. Meanwhile, the effect of jet engine dimensions on the standard deviation (σ) of the electric field inside the jet engine is also analyzed.

In Chapter 5, different investigations are performed to identify the effect of various jet engine parameters, such as Transmitter (TX) antenna position, number of blades and the dimensions of the cylindrical structure, on the characteristics of the EM field inside the jet engine environment. The analysis shows that the jet engine environment resembles a lossy RC when the TX antennas are located at a position other than λ distance from the center of the axis.

Chapter 6 presents a Static System Approach (SSA) and proposes SE as a novel application of STEM. An equivalent model for the rotating fan blades inside a simplified jet engine is developed with random excitation and fixed fan blade position. Moreover, the static and dynamic systems are compared to prove the assumptions made initially by using both full wave simulation and numerical evaluation. In Chapter 7, a detailed analysis of the effect of Doppler frequency shift on the propagation characteristics is presented. The phase and the amplitude deviation due to the Doppler frequency shift are analyzed.

In Chapter 8, three different patch antenna models that can be used inside the jet engine environment for wireless communication applications are proposed and analyzed. The antennas are designed to have a radiation pattern that has null in broadside direction. Hence, the dimensions of the antennas are optimized to obtain the required radiation characteristics. The simulated results are validated through experimental measurements.

Finally, in Chapter 9 a detailed conclusion of the thesis is given and the notion for the supplementary research are entrenched in the future work.

Chapter 2: Literature Survey

The analysis of EM propagation inside the jet engine turbine is very important in applications, such as radar scattering phenomenology, radar cross section reduction, non co-operative target identification, and communication channel modeling inside turbines, for the purpose of wireless sensors installations. The analysis is not limited to the cases of jet engines and gas turbines, since the problem can be generalized as the study of EM propagation inside large complex geometry cavities containing rotating metallic objects. A comprehensive survey on different techniques found in the literature for the analysis of the EM wave propagation inside jet engines (or gas turbines) is provided in this chapter. Different numerical and measurement methods were used to get an approximate approach for calculating the field inside the engine [8, 9]. Here, we tried to facilitate the in-depth understanding of the challenges and proposed solutions of the addressed problem. The main analysis methods found in the literature can be summarized as: (i) analytical methods (or exact solution methods), (ii) numerical methods, (iii) measurement (or experimental) methods, and (iv) the STEM method, which is the most recent. In the following, a quick overview of the time line and progress across the different methods followed by a detailed discussion on each method in a separate section is provided.

Analytical (or exact calculation) methods use a mode matching technique with a scattering matrix analysis. The first trial of analyzing the jet engines relied on analytical methods [5, 6, 11]. These trials were limited to very simple

or small canonical structures. The complexity of these methods were increased drastically with the diameter of the structure [11]. Analytical methods are too complex to define arbitrary cross sections or non uniform geometries.

A variety of numerical algorithms have been used to improve the performance of analytical results. Numerical methods are divided into low frequency (LF), High Frequency (HF) and hybrid methods. LF methods are applicable only to electrically small structures. The arbitrary shaped complex cavities can be modeled with great precision by using LF methods [10, 19]. Whereas, the application of HF methods such as geometric optics method, physical optics method, ray methods, etc., are limited to electrically large system with uniform surfaces [20]. Consequently, hybrid method consisting of both LF and HF methods are used for the analysis of complex environment like jet engines. When a cavity is small, numerical techniques such as the Method of Moment (MoM), the Finite-Element Method (FEM), and their combinations can be applied [10, 19]. The arbitrary shaped complex cavities can be modeled with great precision by using FEM. Similarly, when the cavity is very large compared to the wavelength, high frequency techniques based on ray tracing and physical optics methods can be used [11, 20, 21]. However, high frequency methods are suitable only for very simple terminations and they are not able to handle the complexity of actual terminations. A very good review of literature related to early trials and techniques used to study electromagnetic scattering from inlets, cavities and open ducts before 2003 can be found in [11].

Experimental measurements play a significant role to understand the electromagnetic propagation nature inside complex cavities. Researchers need to verify their analytical studies with real life data. But limited resources are available in literature due to the set up complexity [7, 22, 23, 24]. Then, STEM has been used to analyze electrically large cavities with complex details [25, 26, 27, 28].

In this chapter, after surveying classical approaches for studying electromagnetic propagation inside jet engines, we discuss applying STEM approach in the new area for analyzing the field propagation inside jet engines. The intuition for this approach stems from the argument that in order to analyze the overall characteristics of electric field inside complex cavities containing rotating metallic objects, statistical analysis can be adopted.

2.1 Analytical Methods

Early approaches to the problem have been heavily surveyed in [11] as previously mentioned. Anastassiu *et al.* have used an analytical method based on the Mode Matching (MM) method to treat straight inlets with simple terminations, exploiting the inherent cylindrical periodicity [8]. Although accurate, the MM technique faces serious limitations related to the shape and size of the inlets. The MM technique can be applied only to canonical structures, where the fields can be expressed analytically. Also, the resulting system demonstrates slow convergence and requires a large number of modes because of the number of internal reflections. This method is still used as a reference solution to validate other numerical and analytical results.

Recently, a combination of mode-matching and scattering matrix were used to obtain an analytical solution for reducing radar cross section (RCS) of a simplified jet engine structure [29]. The jet engine structure was treated as an open ended corrugated circular waveguide cavity structure to reduce the RCS of the jet engine. Many small-sized corrugations compared to the size of the jet engine were inserted into the waveguide cavity. Instead of using a hybrid method of high frequency and low frequency methods, the structure was analyzed using the mode matching method at the open end and the scattering matrix at the corrugated waveguide section. Hence, a closed form RCS solution

was obtained and the results were validated with MoM by using a commercial simulation software. The suggested method converges rapidly and provides computational efficiency.

The analytical approach is quite limited in its ability to capture the different features of complicated geometries and typically uses an approach based on modules of simplified geometry, which quickly gets complicated for real-world structures.

2.2 Numerical Analysis

Numerical techniques play an important role in analyzing complex cavities. The basic requirement for the numerical analysis is that the complex geometry should be separable into low frequency and high frequency regions. Applying numerical techniques can be divided into low frequency methods, high frequency methods, and hybrid methods according to the size and shape of the cross section of the ducts.

Low frequency methods give precise results only to electrically small structures (with respect to wavelength). The basic numerical techniques applied to the analysis are FEM, Finite Difference Time Domain (FDTD) and MoM [10, 11, 30, 31, 32]. The FEM approach is well suited for the analysis of complex structures with complex material composition. The traditional FEM analysis is based on a partial differential equation method and uses sparse matrix method to solve complex inhomogeneous structure. However, FEM still has problems while handling the entire system due to large computational requirements. On the other hand, the FDTD method helps to model the real-time behavior of EM fields; consequently, this method is suitable for impulsive and transient analysis. However, FDTD method is not suitable for modeling curved sur-

faces because of the computational complexity as it requires large number of iterations to solve electrically large structures.

HF methods, such as ray methods, Geometrical Optics (GO), Physical Optics (PO), Physical Theory of Diffraction (PTD), and Iterative Physical Optics (IPO), are applicable to electrically large systems but are infeasible to complex terminations which contain electrically small details. These methods are based on local interaction of EM fields [11, 33, 34, 35, 36, 37, 38]. Hence, the computational complexity of these methods are less than the low frequency numerical methods. The time required for the simulation is also very less. However, these methods are geometry dependent. These methods are unable to account for the fields arising from discontinuities like edges and tips inside the cavities. The PO method has been widely used for the Radar Cross Section (RCS) analysis because of its relatively high accuracy. The PO method is computationally more efficient than other HF methods and is very easy to implement. However, it is applicable only to very large and smooth surfaces. This method faces difficulties to handle the fan and the hub inside a jet engine inlet. Hence, several modified versions of PO method like IPO have been developed to increase the speed and the accuracy of the PO method. A forward-backward (FB) iterative algorithm combined with IPO techniques (FBIPO) were also used as a modification to PO method for analyzing the EM propagation inside a jet engine [34]. FB algorithm helps to solve EM propagation, that exhibit both one-way and two-way directions. The FB method updated the IPO currents on the cavity walls in forward and backward directions along the waveguide axis. The algorithm starts with sequential ascending numbering of discrete current elements starting from zero. To improve the efficiency and to reduce the computational cost of FBIPO, a fast far-field approximation was applied. A detailed implementation procedure and numerical results for FBIPO were available in [34, 39]. Since FBIPO algorithm is a classical iterative method there is a possibility that

this method may diverge. Since, the FBIPO algorithm is not guaranteed to converge, it is stopped when a sufficiently low residual error has been attained, or the solution begins to diverge. The residual error threshold should be chosen carefully to attain sufficient accuracy and this is the major draw back of this method.

Neither low frequency methods nor high frequency methods can produce an efficient and accurate analysis of EM propagation inside large complex bodies containing small structures. So, hybridization of these methods is important for the analysis of complex cavities. Applications of these methods are well reviewed in [11, 40]. Taking into consideration, the complexity of the jet engine's face complexity and the length of its inlet, hybrid methods are required for efficient analysis of EM propagation inside jet engines. Hybrid methods have been utilized to analyze cavities containing complex terminations by combining both LF and HF methods to overcome the short coming of either methods [11, 22, 30, 41]. Hybridization employs HF techniques in the empty part of the inlet and LF methods in the loaded section [41]. So here, we do not intend to develop a detailed and complete procedure about first two techniques. A detailed and well written review on these techniques were available on [11]. Limiting our attention to hybrid technique, since this becomes one of the most appropriate technique for the analysis of complex cavities, we can define its advantages over other two numerical analysis technique.

To analyze a jet engine cavity using hybrid method, the computational region is decomposed into a HF region, which constitutes the inlet section and a LF region with an inner object. Figure. 2.1 represents the two regions of analysis. Plane C0 is an aperture plane and plane C1 is a virtual interface which separates the HF region from the LF region [42].

The HF region is analyzed to track the fields at C1 plane either by Shooting and Bouncing Ray (SBR) or IPO techniques. The SBR technique decomposes

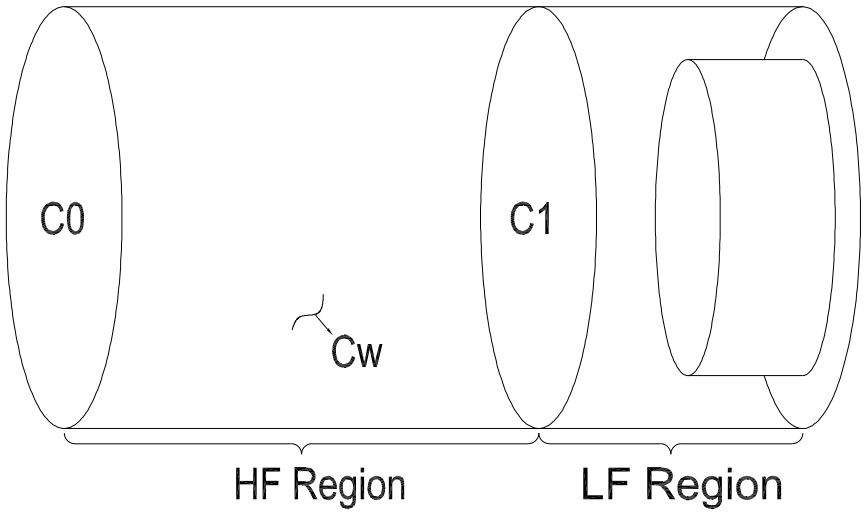

Figure 2.1 Jet engine model. [31]

the field values from the aperture to a set of parallel rays. Using the laws of optics, the rays are tracked into the cavity. The HF region is modeled using square flat facets and analyzed using IPO. The density of this region depends on the constraints on computational time and available memory. To find the incident field at plane C1 using IPO method, the initial currents at the center point of every facet on the inner side wall is calculated iteratively until convergence is reached using the ray tracing method. These initial currents become the source of the transmitted fields, which can be calculated at the center of every facet. The incident field at plane C1, calculated by SBR or IPO, becomes the excitation source for the termination region, which is modeled by LF method. The FDTD method were used to analyze the LF region. The region is modeled by FDTD cells with a density of 20 cells per wavelength. Field values at the centers of the FDTD cells can be determined using the field values of nearest IPO facet. The numerical analysis of the jet engine model with both SBR-FDTD, and IPO-FDTD is available in [42]. The IPO method provides more accurate results than SBR method at C1 plane, when the

structure has complicated LF region with blade terminations. However, in [42] the IPO method uses two different types of approaches (AIPO-CR and AIPO-RT) to determine the iteration number from the result of ray path tracing or the change rate of facet currents. This reduces the calculation error due to the insufficient iteration number, but this methods took more time to estimate the scattering pattern of an open-ended circular cavity with the complex inner object. Moreover, it is evident from the paper that as the system complexity increases, it is difficult to depend on a single method.

Another hybrid method called IPO-MoM was used to analyze the wave propagation inside jet engine. The jet engine model is decomposed into two regions as shown in Fig. 2.1 and the HF region is analyzed using IPO method and LF region by MoM [43]. However, the IPO method uses a fixed number of iterations during the analysis and hence the accuracy of the estimated RCS of the open ended cavities may degrade if the number of iterations is very small. In order to avoid the limitation of this method, an AIPO method was introduced [33]. AIPO-MoM hybrid method is used for the calculation of jet engine modulation during stationary and dynamic cases of blades [33]. AIPO method uses the change rate of current method (AIPO-CR) to find the number of iterations and hence requires more computational time. AIPO method is used to analyze the HF region, modeled by square flat facets. The MoM method is used to analyze the electrically complex LF region, modeled by triangular flat facets. After wards the AIPO and the MoM regions are connected through a simple connection mechanism. In the dynamic case, the jet engine modulation is incorporated using a modified impedance equation to reduces the computational complexity [33].

2.3 Measurement Method

Experimental data of realistic jet engine structures is desired to study the physical EM interpretation of jet engines and the properties of internally propagating waves. Moreover, it is important to validate the reliability of numerical results through comparison against measured values. Although there are many efforts to model the complex jet engine cavities and turbines, there is a lack of experimentally measured data of real jet engines to validate the numerical and simulation models. Early measurement based methods used scaled down jet engine models to obtain experimental data [7, 24, 44].

A small-scale simple jet engine structure terminated with an array of straight blades with inner diameter 15 cm and outer diameter 30 cm is used to collect measured data in earlier literature as shown in Fig. 2.2 [7]. The length of the hollow section is 20 cm and the blade termination is 10 cm. The inlet is terminated by a perfectly conducting plate. The measured data is compared to the analyzed data, calculated using modal analysis (Mode Matching (MM)) and shows good agreement [7, 8].

In [7], a smooth S bend cavity, known as *Cobra* and proposed by Aerospatiale Matra Missiles (AMM), is used for computational purposes. The *Cobra* has a cross sectional dimensions of 0.09 m $\times$ 0.11 m, and a length of 0.35 m. A cap is added above the aperture during the computational process as shown in Fig. 2.3.

The study revealed that the measured data and the computed one did not match well due to the cavity complexity and the uncertainties on the measurement method [22]. The subscale inlet model data cannot reliably validate the numerical results nor reliably predict the full scale results, both of which are essential for understanding the EM characteristics of a realistic jet engine structure.

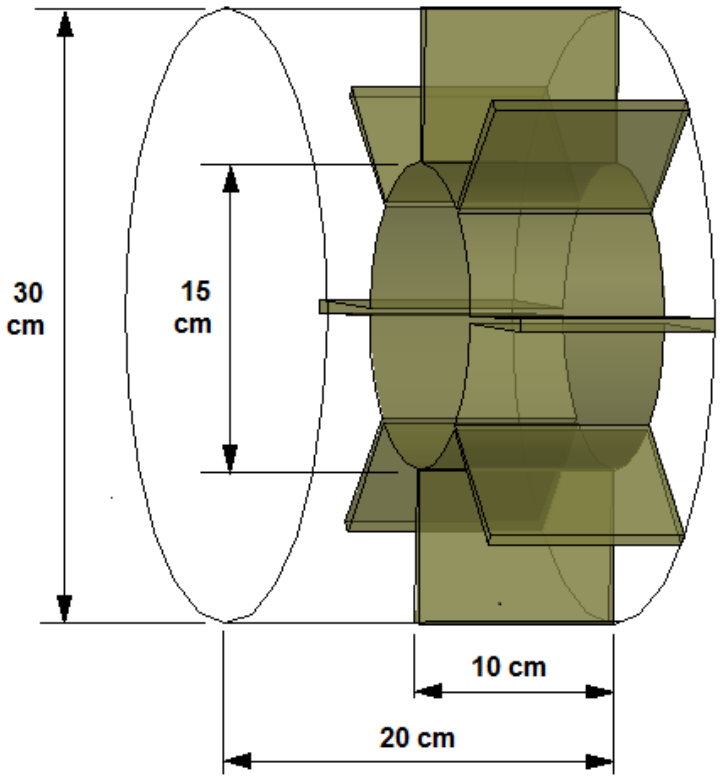

Figure 2.2 Small scale simple jet engine model.[3]

To the best of our knowledge, the availability of the experimental data for a full size engine model is scarce. Recently, an experimental setup of a full scale jet engine structure was tested and experimental data was drawn [24, 44]. The model consists of a parabolic hub and a single stage stator blades attached to the hub. The fan blades are simple, flat rectangular shaped with dimensions of 24.6 cm $\times$ 10.4 cm and thickness 0.16 cm. Each blade is set at a 45 $^\circ$ angle with respect to the axial axis of the duct. The engine model is mounted on a rotating platform attached to a computer controlled motor to rotate the platform. The measured data from this structure is shown to be more reliable than the small scale engine measured data. However, the structure remains simple with only one stage of blades.

Recognizing the field behavior and distribution inside a jet engine is essential for modeling the wireless communication channel inside this cavity. The interest towards wireless communication channel characteristics inside the jet engines stems from the trend towards using wireless sensors to evaluate different parameters related to the operation of the engine such as strain, temperature, pressure, gas emission and fuel consumption. This trend constitutes the so called $fly - by - wireless$ technology [1]. It's desirable to use wireless sensors installed on the rotating disc holding the blades, instead of the extremely expensive wired system. In recent literature, a close to realistic jet engine structure modal was designed and fabricated to enable measurements of data for varying blades position angles and frequencies [45]. The model has three stages of rotor blades attached to a rotating shaft at a 35° slantwise angle and connected to a motor. The dimensions of the blades and engine geometry are

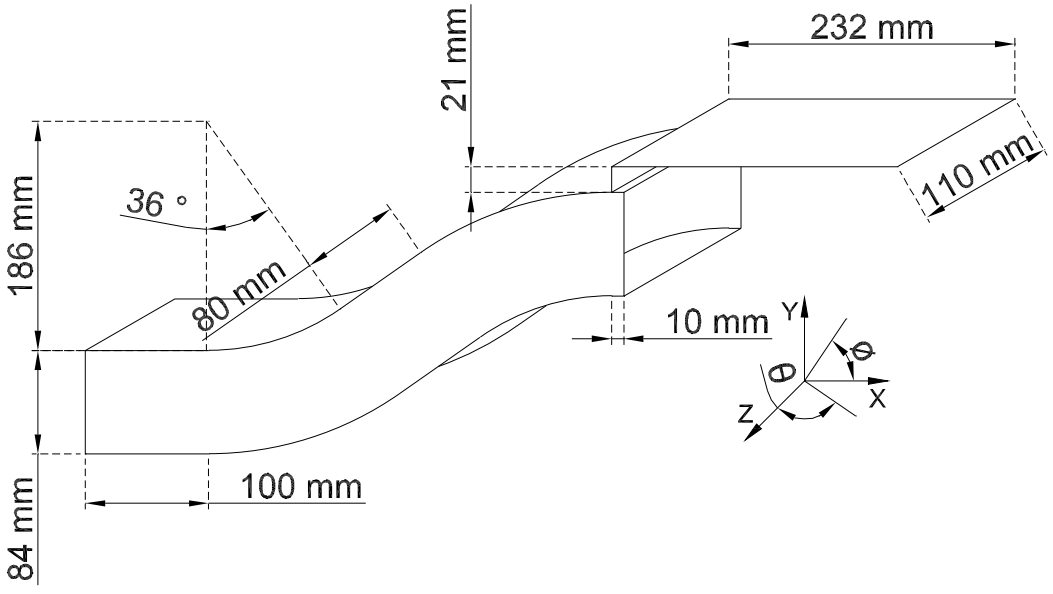

Figure 2.3 S bend cavity.[17]

given in [45]. The measured data from the model is compared to the numerical results, deduced from SBR method.

Measurements and simulations of EM wave propagation parameters inside the jet engine fan are performed to demonstrate the possibility of a radio communication inside the jet engine [46]. A half-scale jet engine model is used for the experimental measurements. The model is tested in complete isolation from any wireless applications in the surroundings. The wave propagation inside the jet engine is measured using a monopole antenna inserted into boreholes located on the rotor discs of the model. The measurements portrays a fading channel environment inside the jet engine, which can be owed to the multiple turbine blades. Simulations are performed on the same half scale model using CST microwave studio®, and the theoretical and empirical results are compared for verification. Since the simulations could not incorporate rotation of the blades, the simulated and empirical data exhibits large deviations. Nevertheless, the literature succeeded in claiming the possibility of radio communication inside the jet engine. Moreover, it was proven that the jet engine environment is a fading environment and the time between two consecutive fading dips is enough for transmitting a data package if the entire package can be transmitted in a time period that is shorter than 120 μs[46]. The fading characteristics of the communication channel inside a jet engine are described by the K-factor, and the path loss between the transmitting (TX) and receiving (RX) antenna. The effect of frequency on the fading characteristics of the radio environment of a jet engine was analyzed and it was proven that there is a possibility to reduce the fading by changing the operating frequency of the WSN [47].

Different modal, numerical and measurement methods used for the analysis of EM scattering from jet engine inlets and their components were discussed in the previous sections. It is important to mention that as the complexity of the

jet engine increases the existing deterministic techniques become less reliable and there arise the importance of STEM.

2.4 Statistical Electromagnetic Analysis

The STEM is a novel approach that can model EM behavior inside jet engine systems without dealing with the complex details inside the engine cavity. The STEM method addresses the problem of treating interior responses of complex field enclosures or systems by modeling the problem using a probabilistic approach. RC is the classical application of STEM. RC is an enclosure consisting of metal walls with metallic stirrers forming a high quality factor cavity with continuous variable boundary conditions as shown in Fig. 2.4 [48]. The fields inside the RC can be considered as random processes, which are characterized by its n-th order statistics. The Probability Density Functions (PDF) for the real and imaginary components of the electric and magnetic fields inside an RC are normally distributed. Hence, the field magnitudes are Rayleigh distributed and the powers are exponentially distributed [48]. The concept of STEM and RC modeling are applied for many configurations where large cavity with complex environments are encountered [48, 49, 50, 51].

Modified RC techniques are used to study the effect of EM fields on aircrafts [52, 53]. Moreover, the same techniques are used to find the effect of HIRF on aircraft and avionic systems. The test procedure for issuing the certificate for HIRF response goes through multiple steps. First, the aircraft is illuminated from outside while being exposed to different aspect angles. Then, the internal cavity electromagnetic environment (EME) is measured for every external illumination and a mode mixing technique is used to characterize the cavity EME which is compared against an RC model [52]. The theoretical and measured data are compared using a cumulative density functions (CDF) deduced

for different aircraft. The theoretical CDF shows a good agreement with the measured one when stirring ratio is greater than 30 dB [52].

In [53] two different techniques, used for electromagnetic vulnerability (EMV) testings, are explained and conducted on a large navy aircraft P-3 and a simulated EMV test on an E-2C aircraft. The effect of the mode stirring during EMV testing is explained in details. Field probes are used for the measurement and are distributed at different locations near to different aircraft equipments, which are exposed during the test. Measurements are taken from these probes for one revolution of the stirrer. The mode stirring is then removed for repeating the test on the P-3 aircraft. Similarly, on the E-2C,

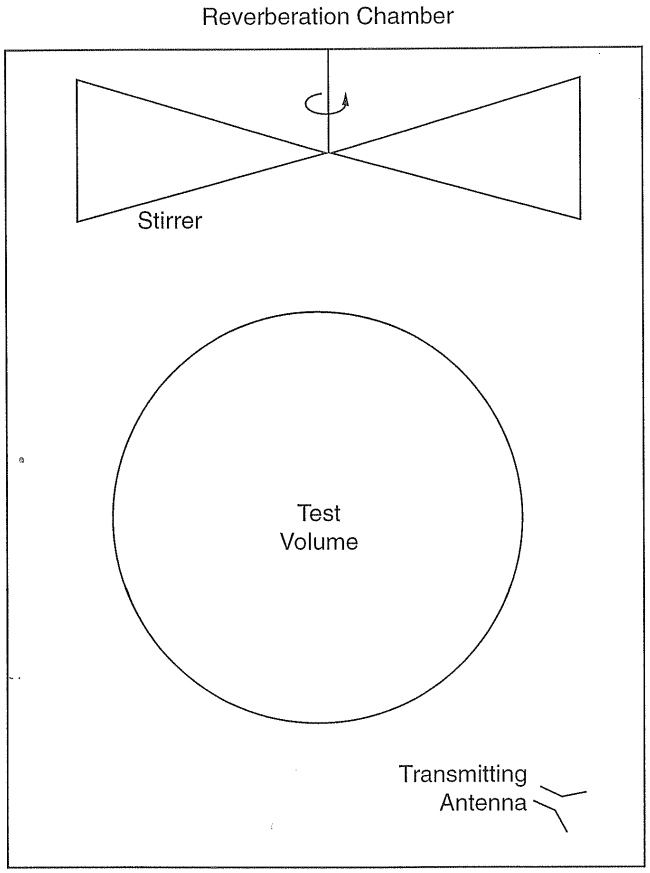

Figure 2.4 Mechanically stirred reverberation chamber.

a transmit antenna is used to simulate an actual antenna position used during the standard EMV test. Field probe measurements are taken for different frequency ranges with and without mode stirring. The results show that the mode stirring based EMV testing improved the accuracy of the resulting field distribution without using different aspect angles [53].

In [26, 27] an approach based on STEM and RC is used to find out the effect of the penetration of high intensity radiated fields on fuselage. A mechanically stirred RC approach is used to characterize the EM environment inside an aircraft cavity. A simple fuselage model is illuminated with an incident plane wave and the measured field values are processed statistically to find out the distribution of the electric field inside the fuselage and the shielding effectiveness [26]. A mode stirrer is placed inside a simplified fuselage model to measure the penetrating fields for various stirrer rotating positions. The field values are measured using probes installed at different locations. Measured data are statistically analyzed and the probability distribution of the penetrating fields are evaluated. Later, the measured CDF values are compared with the theoretical values and the measured data statistical characteristics are confirmed by performing goodness-of-fit test. These studies concluded that the interior of fuselage, resembles the interior of an RC, if they are mode stirred [27].

2.5 Statistical Antenna Concept

The concept of SA is previously owned and has been accepted several decades back in order to appraise the performance loss of antennas and arrays, when random perturbations occur with respect to an ideal design [54]. The concept of SA has been applied to many applications to characterize the natural randomness that arises during the design or manufacturing process of large antenna systems. The randomness affects the performance of the antenna sys-

tems. Briefly, Statistical Antenna Theory (SAT) is the theory of antenna with random sources. SAT is a state-of-art idea that helps to describe the antenna properties embedded in their device casing and under the perturbing influence of close objects or bodies statistically . The benefit of this approach is similar to other statistical descriptions of the radio link, such as the radio channel, intending to provide a more realistic description of the antenna part of this channel.

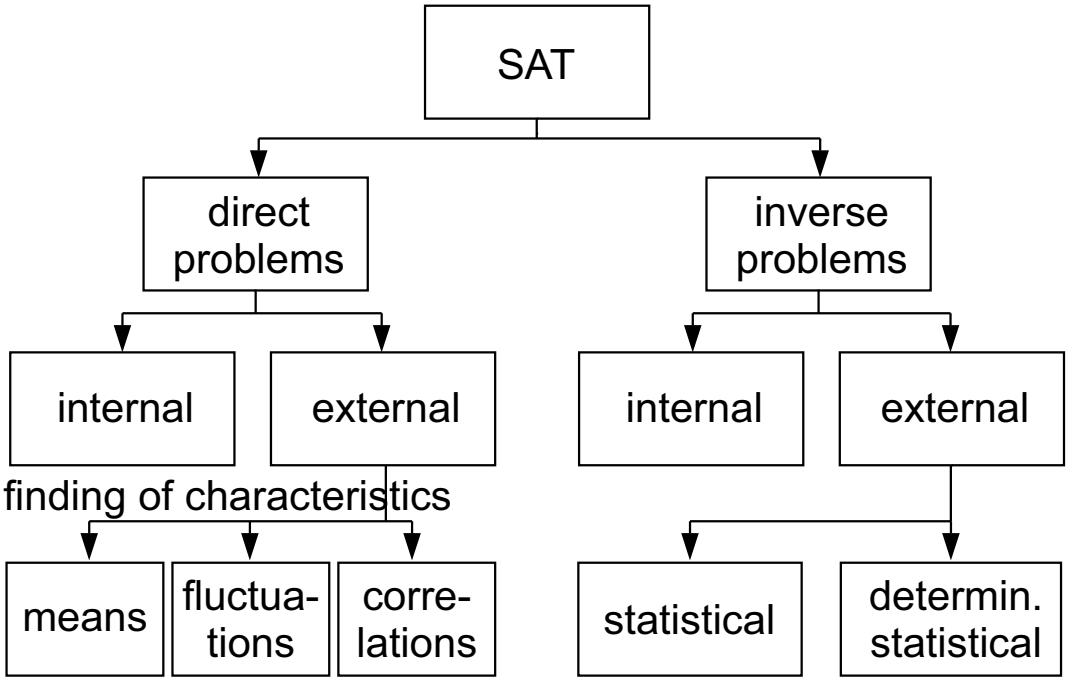

Figure 2.5 Concept of SAT [43].

The amplitude, phase, and the orientation of an antenna can be random due to the inaccuracies in antenna manufacturing process or due to their parameter instability. The fluctuations or random errors affect the antenna performance. It is really important to identify the reasons of the randomness and their nature,

to be able to compute their influence on the antenna parameters. SAT was used mainly to identify the influence of random antenna deformation and damages on its performance [17, 54]. Figure 2.5 shows the basic concept of SAT. SAT can be divided into direct and inverse problems. The direct problem focuses on determination of the antenna radiation field statistics stemming from different origins of randomness. The SAT inverse problem is interned to define the antenna "statistical" structure given its radiation field statistics [54].

However, in this thesis SA concept is used to provide the randomness inside the jet engine. The rotation of the blades inside the dynamic jet engine system is translated to a random excitation with specified characteristics and hence it is named SE. Chapter 6 contains a detailed analysis of the jet model based on this novel approach.

2.6 Microstrip Antennas

In wireless Communication, the antenna plays an important role. For wireless communication inside harsh metallic environment, the antenna should be compact, conformal and efficient. One of the most suitable antenna technologies for such requirement is the microstrip antenna technology [55]. Microstrip patch antennas consist of an area of metal over the substrate and is supported by the ground plane as shown in Fig. 2.6.

Microstrip antennas allow the conductor part to take any shape with respect to the X-Y axis direction. The main characteristics of the patch antenna with principal conductor shapes such as; rectangular, square, circular, elliptical, and triangular, are mostly similar. The fundamental mode has a broadside radiation pattern irrespective of the shape of the patch. Hence, the tuning of higher order modes turns to be a more challenging process compared to the

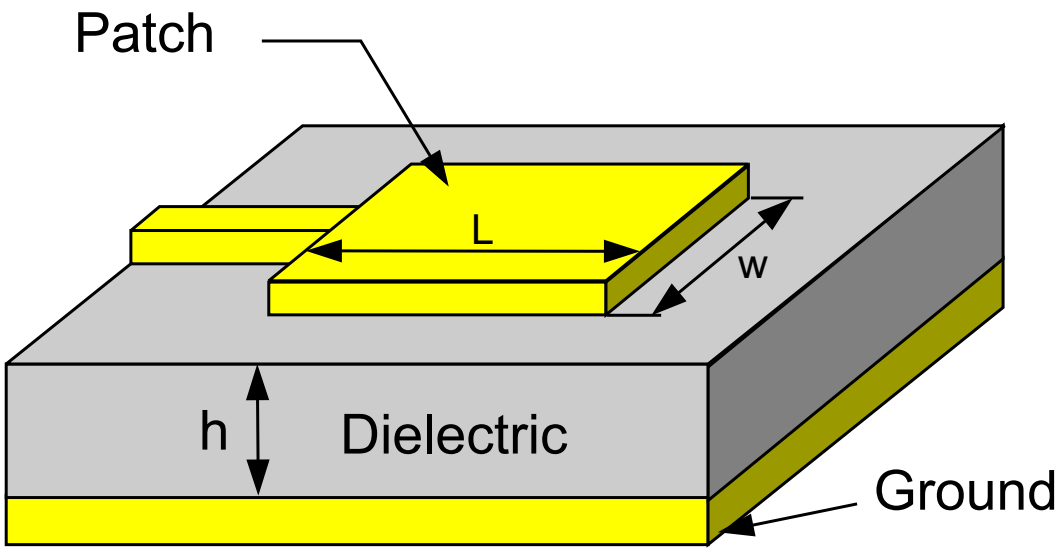

Figure 2.6 Microstrip Patch Antenna.

fundamental mode tuning. The higher the mode, the more complex tuning is going to be [55].

The significant challenges that arise during the development of the antennas for harsh environment are the physical constraints of the environment, and the size and weight restrictions of the TX and Receiver (RX) antennas. The planar antennas developed by using conventional methods are difficult to attach to the curved surfaces of a jet engine. Moreover, the behavior of the antenna will change if the antenna is located in an environment with conducting materials. Hence, it is important to design the antenna that is conformal to its environment. Conformal antennas were introduced in the 1980s associated with the outer surfaces of aeroplanes, for reducing the aerodynamic drag and hence bettering the aircraft speed, fuel consumption, and gas emissions [56]. In recent times, conformal antennas are used in different harsh environment applications like maritime communication, aircraft applications, jet /gas tur-

bine applications, etc. Microstrip patch antennas are one of the most popular planar antennae for the conformal application because of its features such as low profile, light weight, low cost and ease of fabrication. Moreover, it can be made conformal to its environment easily. Hence, patch antennas are suitable for aircraft and missile applications. These antennas can withstand shock and vibration and also they are mechanically robust [55].

2.6.1 Design of Antenna for the Wireless Communication inside Harsh Environment

Recently, researchers have developed a conformal patch antenna system for applications inside harsh metallic environments [57, 58, 59]. The antenna is designed and fabricated for ISM frequency band to be used inside train wagon. A two layer patch antenna is designed with the feeding strip in between the layers. The bottom and the top layer substrate are made of FR-4 and rogers RO3003 material; respectively as shown in Fig. 2.7.

They chose a thick substrate with low permittivity in order to achieve good radiation efficiency. The antenna has the form of a rectangle with a semi-circle at the feeding side. At the opposite end of the feed, the antenna is short-circuited to ground through a layer of copper tape having the same size as the width of the antenna. This helps to reduce the physical size of the antenna. Authors were able to prove that the antenna is a good radiator inside the metallic environment with two radiation peaks and a null in the broadside direction [58].

Later, an array of patch antennae that can be mounted on the external surface of the jet engine is designed. The patch antenna usually radiates perpendicular to the ground plane of the antenna (broadside). However, for this particular application radiation pattern needs to be pointed towards the fan of

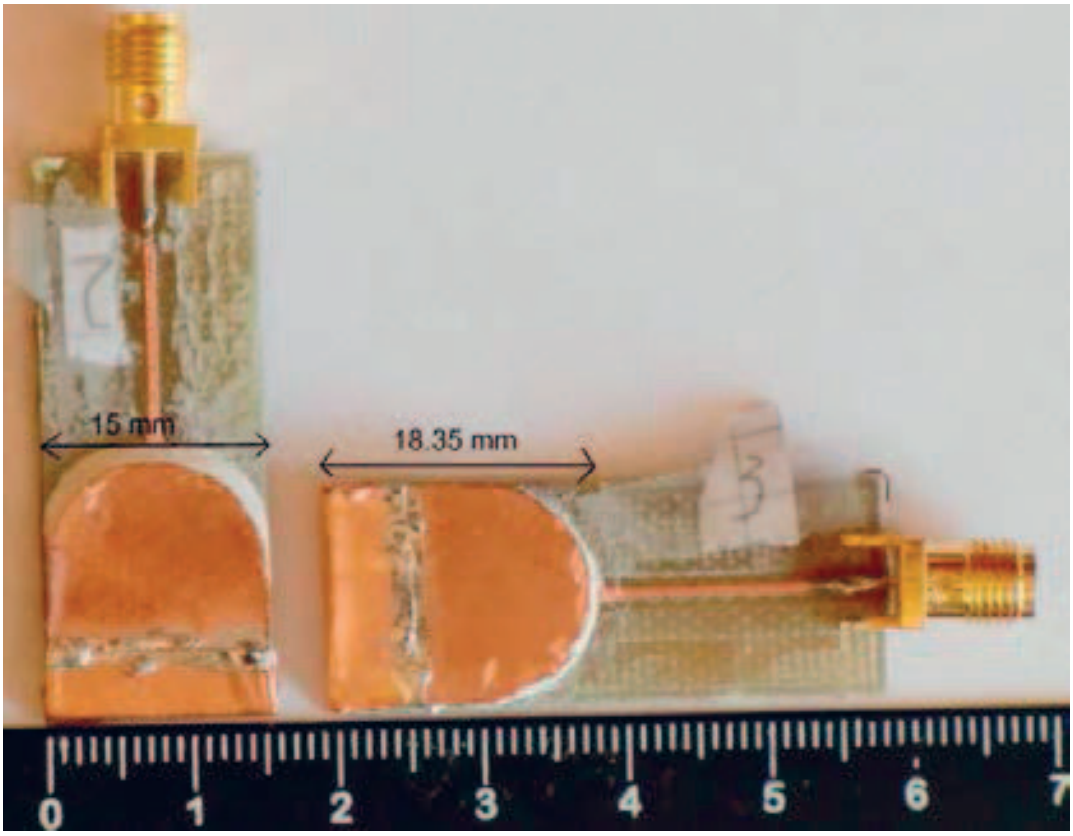

Figure 2.7 Microstrip patch antenna for wireless applications inside train wagon. [47]

the engine. Hence, an array of rectangular patches was designed to be used inside jet engines as shown in Fig. 2.8 [57]. The fabricated antenna was designed to operate in the ISM frequency bands. In order to make the antenna both flexible and thin, Rogers ULTRALAM 3850 material was used for the substrate with a thickness of 0.1 mm. The radiation efficiency of the antenna was -13 dB due to high losses in the substrate.

In this thesis, a new antenna system that can operate in extremely harsh and metallic environment is developed. A circular microstrip patch antenna that radiate a dual beam pattern is designed, simulated and fabricated. Designed antenna is conformal to both planar and cylindrical surfaces and has a null at the broadside direction of the radiation pattern.

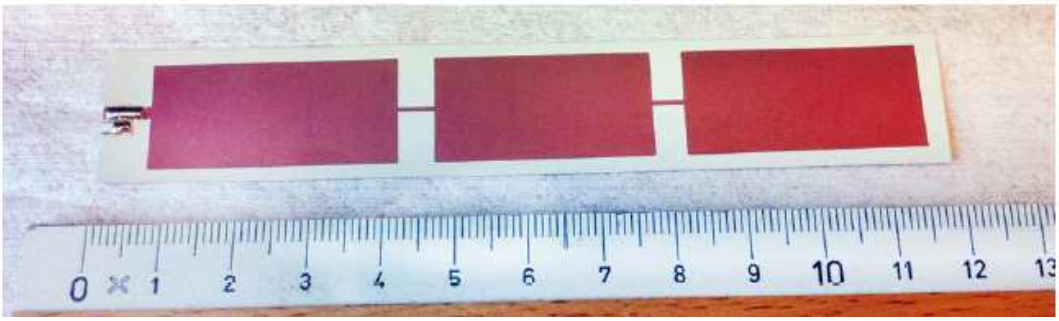

Figure 2.8 Microstrip patch antenna for wireless application inside jet engine. [48]

2.7 Summary

In the present chapter, a comprehensive overview of different techniques used for analyzing the propagation of EM fields inside the jet engine environment which are excited either internally or by an external source is provided. Different analytical, numerical, and measurement-based methods have been analyzed. Analytical methods are generally considered extremely challenging due to the slow convergence rate of the mathematical functions associated with such methods, which decreases with frequency. Numerical methods like MoM, finite-difference methods, and related transmission-line matrix methods are grounded in well-established Maxwell's equation based techniques and can be applied to solve various systems. Later, a more viable option is analyzed that can still capture the time-dynamic effects while providing feasible and accurate results through the use of STEM. We have found that this method is sufficiently accurate yet simple enough to describe the fields inside a complex and dynamic cavity environment using statistical methods instead of the classical deterministic perspective. Finally, a brief review of conformal antennas inside the complex jet engine environment is provided.

Chapter 3: Statistical Electromagnetics Inside Jet Engine

3.1 Introduction

Modeling of EM propagation through complex cavities is very difficult due to their complex geometry and the harsh surrounding environment, as well as the rotating metallic parts they contain. In addition, it is extremely difficult to extract the field values from an arbitrarily shaped model geometries having large sizes, complex terminations, and cross-section variations. The jet engine environment consists of curved surfaces and different stages of rotors and stators mounted on a central shaft as shown in Fig. 3.1. Researchers are facing many challenges during the analysis of such a complex structures to determine the field distribution inside the engine.

The analysis of the EM propagation through jet engine has evolved from the numerical approach to the STEM models. STEM approach was introduced as a novel method to analyze the jet engine cavity. However, it is worth to ask why STEM approach is applicable for a system like jet engine turbine. This is mainly because the exact evaluation of the electrically large system to analyze the field characteristics depending on different engine parameters are extremely complex. The complete analysis of such a complex system using deterministic approach is exceptionally problematic because of the dependency of the analysis to the details of the cavity's dimensions, material property, and

the frequency spectrum of the excitation. These problems have excited the generation of the statistical description, such as "the most convenient solutions must be *statistical in nature*" [60].

The intuition for this approach stems from the argument that to analyze the overall characteristics of the electric field inside the complex cavities containing rotating metallic objects, statistical analysis can be adopted. STEM approach successfully analyzes the complex systems such as the jet engine environment, without dealing with the complex details inside the engine cavity by using a probabilistic approach. This method helps in analyzing the field precisely inside the medium, which has a combination of small and large dimensions parts simultaneously [61, 62]. In order to deal with the STEM approach, the jet engine environment has been decomposed into different **segments**, which is favorable to solve electrically large scale problems, as illustrated in Fig. 3.2. From Fig. 3.2 (a), it is clear that the dimension of each segment is varying in nature.

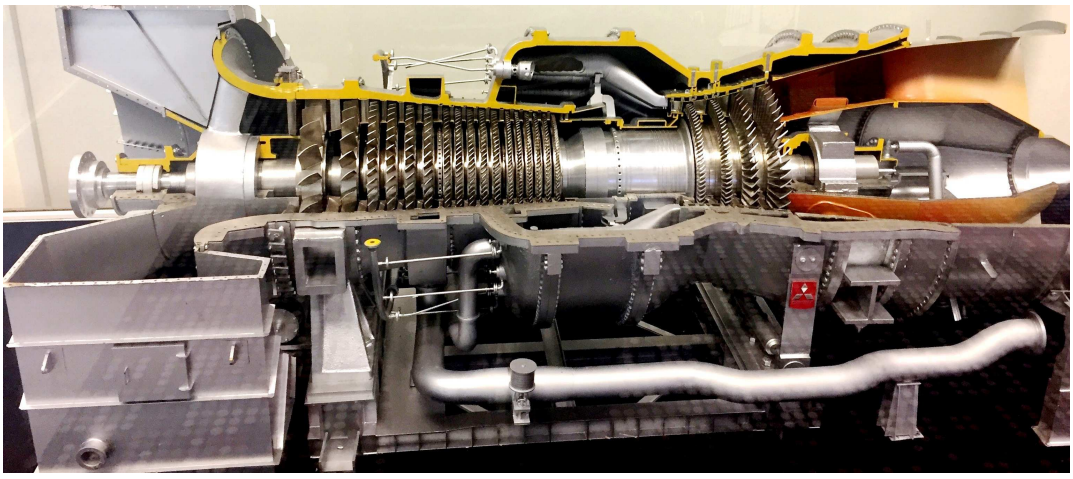

Figure 3.1 Photograph of jet engine model (@ Qatar University).

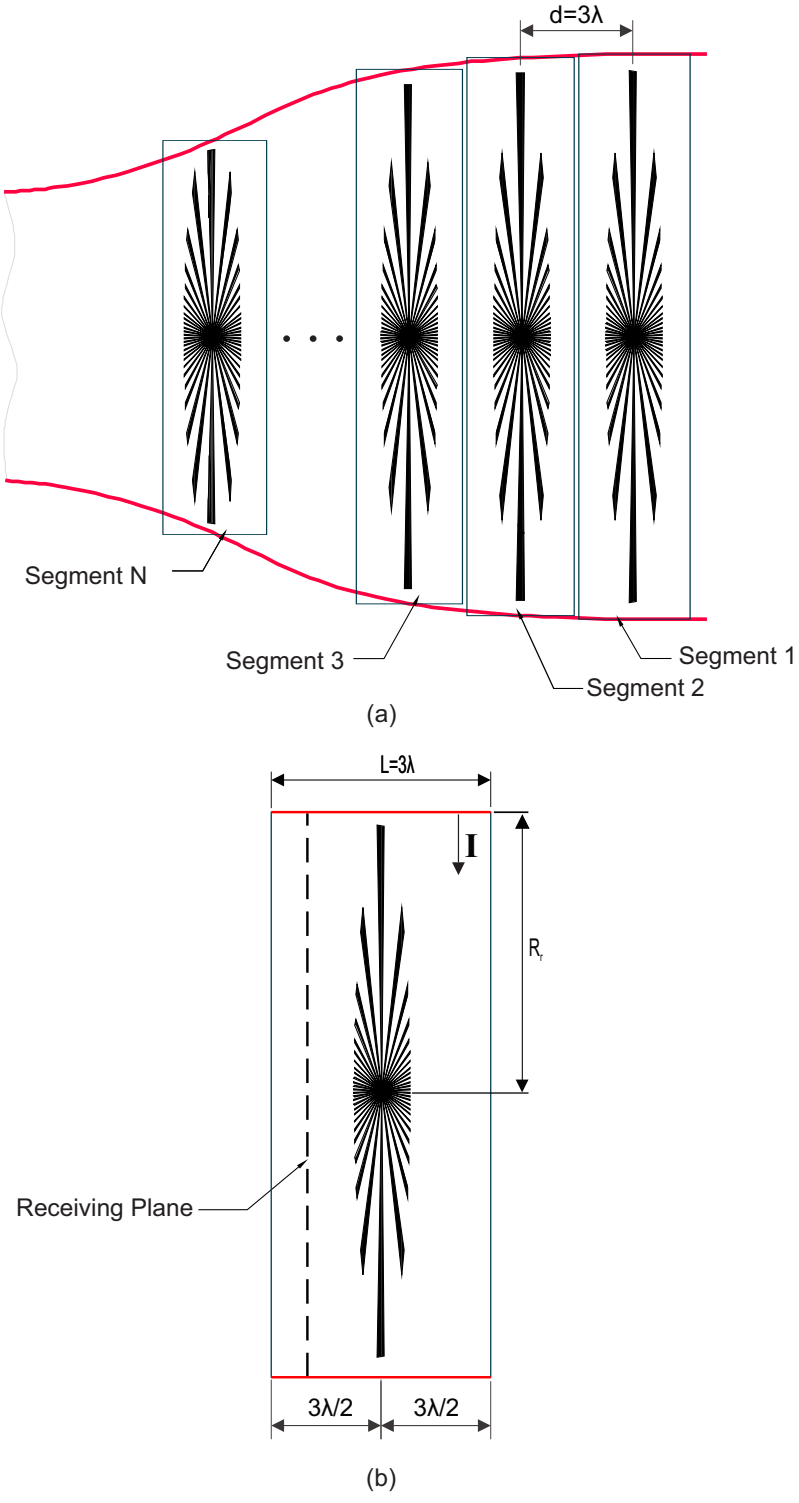

Figure 3.2 Jet engine model: (a) Segmentation of the model. (b) Details of single segment.

3.2 Segmentation Approach

The segmentation approach decompose the jet engine environment into different segments and each segment is occupied by a single stage of fan blade in the middle of the segment and we assume uniform spacing between the blades as shown in Fig. 3.2 (b). Later, the segments are cascaded in such a way that the output field of each segment will act as an input excitation to the next segment. However, in this analysis each jet engine segment is assumed to have an identical characteristics and hence, the characteristics of the EM propagation are analyzed through only one segment (**segment1**). The most important requirement of this segmentation method is that the solutions of all the segments should be recombined (cascaded) to get a solution of the entire system.

The **segment1**, which represents a simplified jet engine model, consists of a single stage of rotating blades and is characterized by the length (**L**) and a radius (R_r) as shown in Fig. 3.2 (b). A single frequency continuous wave (I) is used to excite the jet engine system internally and the field characteristics are extracted from a particular receiving plane which is $\approx$ at λ distance from the center of the axis. The **segment1** can be considered as a mechanically stirred RC with the blades acting as a stirrers. Hence, all the hypothesis related to RC environment can be applied for the EM analysis inside **segment1**.

In this thesis, two different methodologies have been used to evaluate the EM propagation through the jet engine environment using STEM approach. In the following, a quick overview of the two methodologies used for the jet engine EM analysis followed by a detailed discussion on each methodology in separate subsections is provided.

3.3 Methodology

The **segment1** of the jet engine environment is modeled into two different perceptive to study the EM propagation through jet engine environment. The proposed system methodology can be represented as shown in Fig. 3.3, where Fig. 3.3 (a) represents dynamic system model and Fig. 3.3 (b) represents static system model. The dyanamic system is characterized as a fixed excitation (I(a)) and blade rotation (random environment). $E_D(a)$ is the magnitude of the electric field resulting from the fixed antenna excitation, a. The mean and the standard deviation of the electric field in the dynamic system are represented by μ_D and σ_D; respectively. However, static system is modeled in such way that it has fixed blade position and random excitation (I($a + a + \Delta a$)). In the static system, $E_S(a + \Delta a)$ represents the magnitude of the electric field due to the randomized excitation. The mean and the variance of the electric field in

(a) Dynamic System

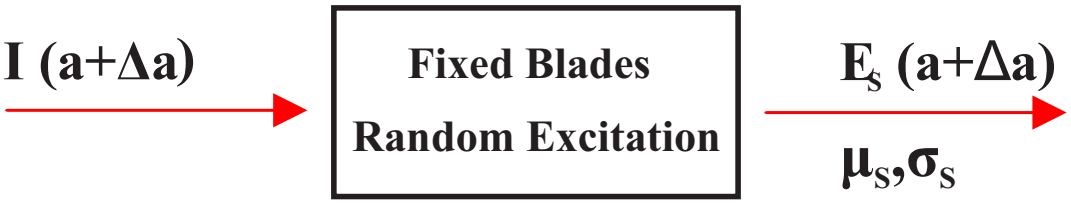

(b) Static System

Figure 3.3 Block Diagram of System Architecture: (a) Dynamic System. (b) Static System.

the static system is represented as, μ_S and σ_S; respectively. Later, to analyze the two system models, two different approaches are proposed as given below.

- Dynamic System Approach (DSA): The DSA adopt a combination of Dynamic System Simulation (DSS) and the Dimension Scaling (DS) method to solve the entire jet engine model. The DSS method analyze the characteristics of electric field due to the dynamic rotation of blades in the jet engine environment.

- Static System Approach (SSA): The SSA uses a combination of analytical method (AM) and a novel SE method to solve the EM propagation through the entire geometry.

The extremely large dimension of the jet engine environment makes the analysis procedure more complicated and hence, to avoid the system complexity the proposed methodology introduced on a simplified jet engine segment. Hence, for the initial analysis only **segment1** will be evaluated and it will be analyzed using both DSA and SSA approach.

3.3.1 Dynamic System Approach

The Dynamic System Approach (DSA) method is a dynamic simulation based semi analytical procedure for evaluating the field propagation characteristics. The **segment1** of the jet engine turbine model will be analyzed using the DSS method to extract the field characteristics. The characteristics of the EM propagation through the complex jet engine segment will be analyzed statistically. Later, rest of the segments can be modeled analytically using the DS method.

In DSS, the **segment1** will be considered as a simplified jet engine model and the analysis will carry out by assuming the jet engine environment is similar to a mechanically stirred RC environment. The randomness inside the

jet engine environment can be provided by changing the transmitting antenna position, or by rotating the metallic blades. The rotation of the blades can be configured in a step-wise or consecutive manner. It is important to mention that at every rotational step the field distribution inside the jet engine environment will change. The magnitude of the electric field characteristics is extracted along the jet engine environment and analyzed statistically. The analysis proved the initial hypothesis that the jet engine environment is similar to a mechanically stirred RC.

3.3.2 Static System Approach

SSA method is an alternative approach to the DSA method, which uses a combination of a novel SE method and an analytical method (AM) to solve the EM propagation through the entire geometry. SSA method aimed to model the EM propagation inside the jet engine environment without complex dynamic simulation method. In SSA approach, SE method is used to model the statistical characteristics of the output field parameters. The SE concept provides the randomness inside the jet engine without the need for multiple rotation position simulations. The rotation of the blades inside the dynamic jet engine system was translated to a random excitation with specific precalculated characteristics. Consequently, the blades in the new model are fixed, and the multiple-rotational position simulation runs are translated into multiple runs with a fixed blade position and an antenna fed by a random source with predefined characteristics. The SE analysis helps to predict the output field characteristics of the jet engine without considering the dynamic rotation of the blades by controlling the input feeding parameters.

3.4 Summary

In this chapter, we introduced STEM as an exceptional tool that can capture the time-dynamic effects of the jet engine environment while providing feasible and accurate results compared to the traditional deterministic approach. Moreover, this method is sufficiently accurate yet simple enough to describe the fields inside the complex and dynamic cavity environments using the statistical methods. Two different methodologies have been introduced for efficient and accurate analysis of EM propagation inside a complex jet engine system. The dynamic system approach analyzes the behavior of EM propagation through dynamic jet engine system, where the randomness is provided by the rotation of the blades. The dynamic approach still requires a large number of simulation procedures, which increases the complexity of the analysis. We also introduced the concept of the SE as a method to translate the source of randomness inside a dynamic jet engine resulting from the blade rotation into a randomness resulting from varying the excitation randomly. The proposed approaches provide a new and efficient methodologies for analyzing the engine environment compared to existing deterministic approach.

Chapter 4: Dynamic System Approach

4.1 Introduction

The dynamic system approach is one of the STEM methodology used to analyze the jet engine environment. This approach follows a combination of dynamic system simulation and the dimension scaling method to solve the entire jet engine model. In this chapter, a simplified jet engine model is developed to analyze the field characteristics using DSS and DS method. The design, and the analysis of the jet engine model with different number of rotating blades are also presented here.

4.2 Dynamic System Simulation (DSS)

In DSS, a simplified model similar to the jet engine segment (**segment1**) with one set of rotating blades are outlined. Later, the rotation of the blades are ensured by the dynamic simulation of the blades in many different angular positions with equal angular increases each time to establish an arbitrary environment inside the jet engine cavity. The field propagation inside the jet engine is analyzed through full wave simulation analysis and the outcomes are analyzed statistically. This work begins by stating a hypothesis that the jet engine environment resembles a mechanically stirred RC with rotating blades acting as the stirrer.

4.2.1 Modeling of simplified jet engine cavity segment

The first step to analyze the propagation of EM field inside a complex jet engine environment begins with the modeling of a simplified jet engine segment. Each segment of jet engine cavity consists of a cylindrical cavity and one set of rotating blades which act as stirrers in the environment as shown in Fig. 3.2. The simplified model is developed using Ansys® HFSS simulation tool. In order to analyze the propagation characteristics within the jet engine environment, the power being transmitted by the TX antenna, and the field characteristics are analyzed at different fixed RX locations.

Cavity model

The simplified jet engine model is represented by a large metallic cavity of dimension R_r x **L**. The cavity is an open cylinder with a radius (R_r) of 19 cm, length **L** of 18 cm as shown in the Fig. 4.1. A shaft made of pec material is used for attaching the blades and it has a radius of 3 cm. The shaft and the attached blades are located at $(3/2)\lambda$ from the center of the axis.

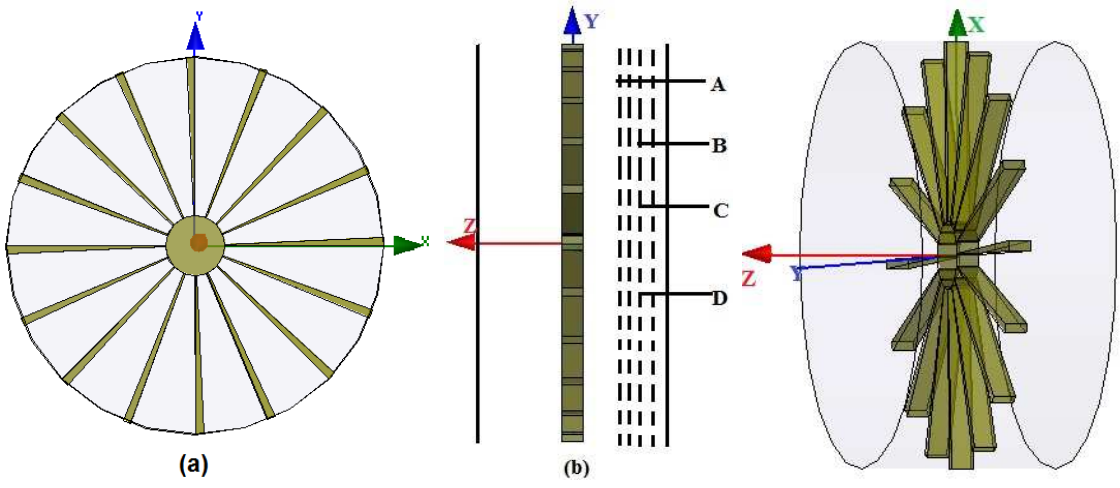

Figure 4.1 Simplified jet engine model: (a) Front view. (b) Side view. (c) 3-D engine view.

TX antenna

The source of EM fields (excitation) for the analysis of EM propagation is provided by the simulation environment. An incident Hertzian dipole excitation (a) represents a simple transmitting antenna which is provided by the HFSS full wave simulation environment simulates the field of an elementary short dipole antenna. The excitation is positioned at $X-Z$ plane at λ position (TX1, 19 cm , 6 cm), away from the center of the axis. The Hertzian dipole excitation inside the simulation environment is characterized by the current (a) multiplied by the dipole length (dl) as shown in Fig. 4.2. The unit of excitation is Am and is equal to 0.012 Am in the initial simulation procedure.

Blades (Stirrer)

The blades in this simplified jet engine model is similar to mechanical stirrers and the rotation of the blades inside the engine environment will help to pro-

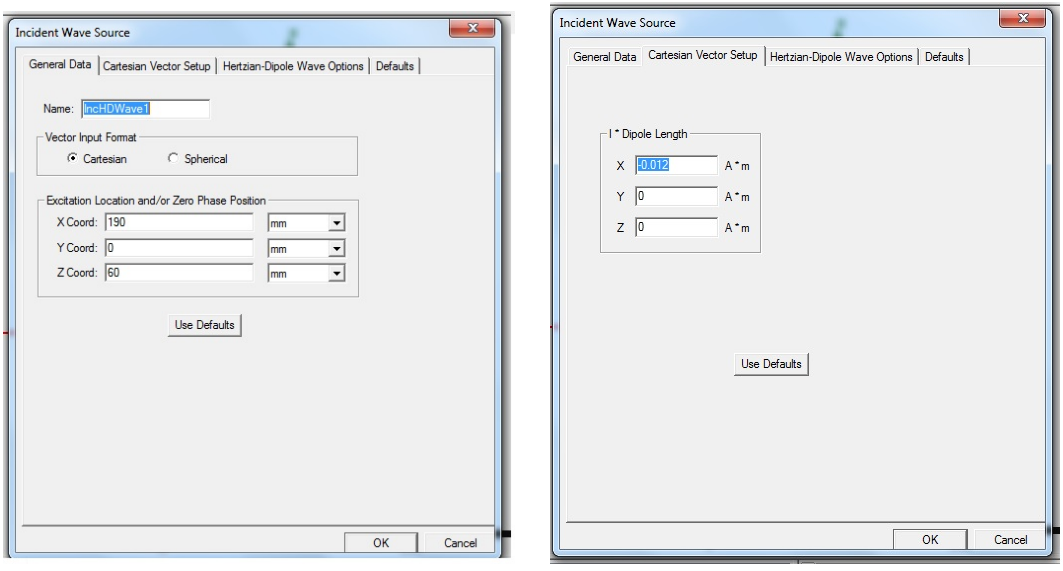

(a) (b)

Figure 4.2 (a) Location setting of excitation. (b) Excitation characteristics.

vide independent field samples as possible. The blades can rotate either in a continuous or stepwise manner and are designated as mode-tuned or mode-stirred; respectively. In this thesis, we targeted only the stepwise rotation (mode stirred) of the blades to generate randomness inside the environment.

In order to distribute the energy inside the jet engine environment, the blades have to be electrically large as possible with respect to the size of the engine cavity. The blades are attached on the central shaft and the angular thickness of the blade is 2.5° as shown Fig. 4.3. Initially, the model carries 16 blades, which are uniformly distributed around the shaft and extended to the wall of the cylinder as shown in Fig. 4.1 [13]. Later, the number of blades are increased to study the effect of complexity on field characteristics.

Receiver Location

The electric field values are extracted for each and every blade position at different planes inside the environment and these planes are set at distances 54 mm(A), 60 mm (B), 66 mm (C) and 72 mm (D) from the center along the $-Z$ axis as shown in Fig. 4.1(b). These planes are circular planes and is chosen to be approximately in the middle of the outer cylinder and the central shaft as shown in Fig. 4.4. However, it is important to mention that for a large complex cavity the electric filed characteristics due to different blade positions will be independent of the position in the cavity, as long as the re-

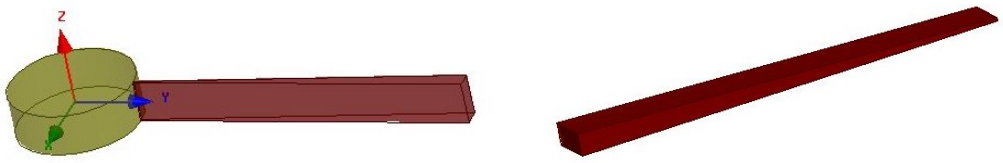

(a) (b)

Figure 4.3 (a) Architecture of blade and central shaft. (b) Geometry of blade.

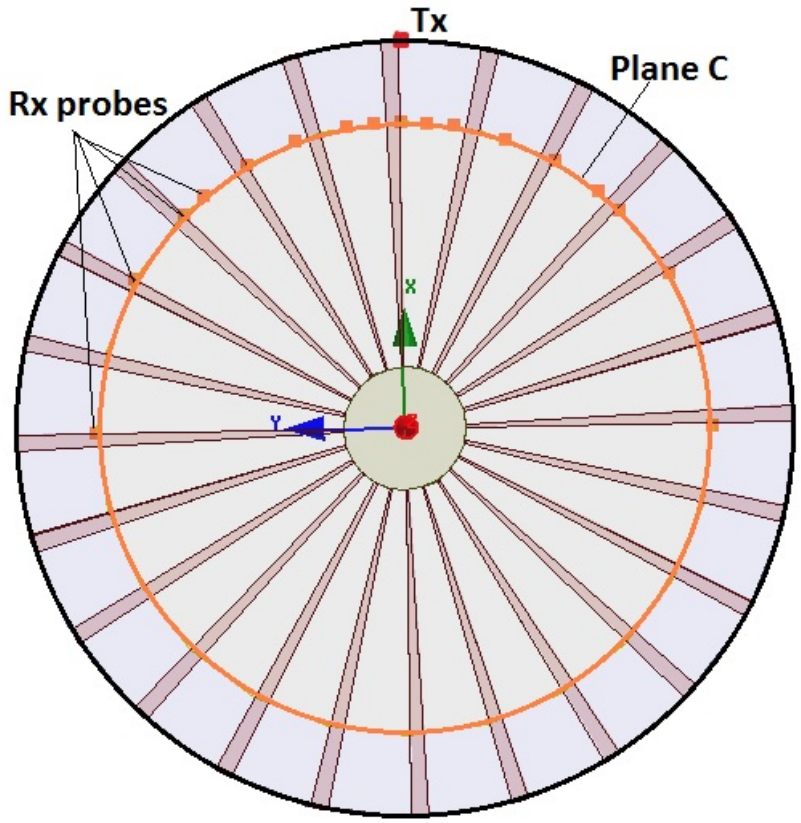

Figure 4.4 Representation of jet engine model with receiver plane C and probe location.

ceivers are half of the free space wavelength away from any metallic and moving structure . Hence, to satisfy this hypothesis all the electric field values are extracted upon the receiver probes that are scattered over a circle which has a 150 mm radius as shown in Fig.4.5. It is important to mention that, 17 receiving points are situated on the circle around each plane and are located at $\theta = \pm 90\,^{\circ}, \pm 60\,^{\circ}, \pm 45\,^{\circ}, \pm 40\,^{\circ}, \pm 30\,^{\circ}, \pm 20\,^{\circ}, \pm 10\,^{\circ}, \pm 5\,^{\circ}$, and $0\,^{\circ}$ on the circle as shown in Fig. 4.5. The electric field values are extracted from these receiving points are saved as *.reg* files and later the results are post processed using MATLAB functions.

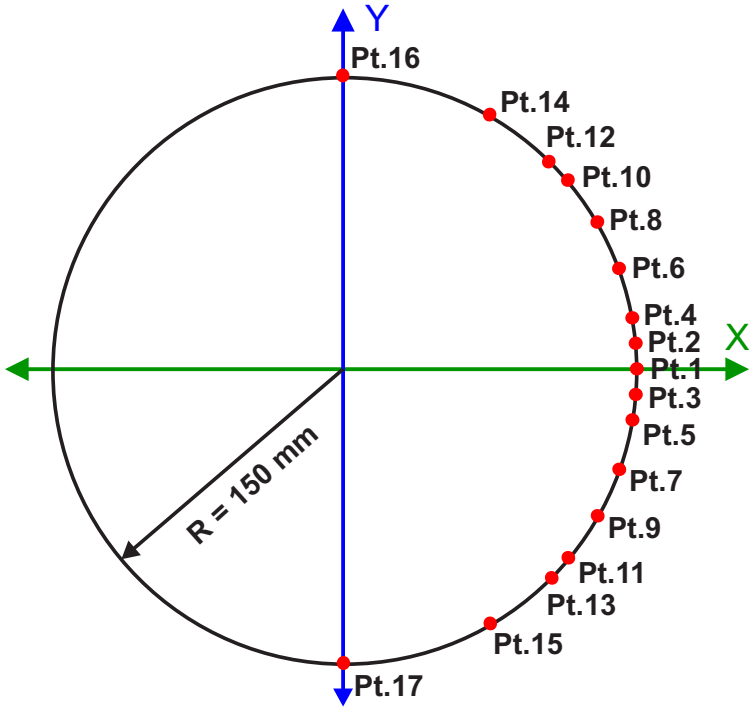

Figure 4.5 Location of receiver points on a circular plane.

System specifications

The used system is Intel(R)Xenon(R)CPU with 2.40 GHz, 2.39 GHz, 2 processors and 48GB RAM.

4.2.2 Modeling of the Simplified Jet Engine Environment

The jet engine model as explained in above section is modeled using the HFSS FEM software as shown in the Fig. 4.1. The model contains 16 coplanar rotating blades, which are uniformly distributed around the shaft and extended to the wall of the cylinder. The proposed model cut down the complexity of the jet engine problem. However, this simplified model gives a profound judgment into the EM propagation characteristics inside complex jet engine cavity. The transmitted signal is provided by a Hertzian-dipole excitation, which is placed one wavelength (λ) from the center of the engine along $+Z$ axis according to a

geometrical view. The blades were rotated 90 times with 0.25 ° each time. The frequency used in the simulations is 5 GHz [13].

The electric field values were extracted for each and every stirrer position at different receiver planes and average field values at different points over all the blade rotation positions were calculated. It was proven that the squared magnitude of any of the electric field components propagating inside a large complex cavity such as RC with mechanical mode stirrer, has an exponential distribution [48]. Hence, the average squared magnitude of the electric field values are tested against our statistical modeling hypothesis. Comparisons between empirical and theoretical PDF are performed by curve fitting tools (CFT). It is found that the squared magnitude of the fields ($|E_z|^2$) has an exponential distribution compared to the theoretical exponential distribution proved in the RC model as shown in Fig. 4.6. It is clear from the figure that there is a great agreement between the two curves for the field component E_z, and hence, the main hypothesis is successfully applied.

4.2.3 Generalized Jet Engine Model with more rotating blades

In order to generalize the jet engine analysis, and to analyze the effect of number of blades on the EM field characteristics, the jet engine structure with more number of coplanar rotating blades is designed and simulated as shown in Fig. 4.7. The structural characteristics of the jet engine model in Fig. 4.7 is similar to that of **segment1**. The model represents an open cylinder with a single stage of 24 coplanar rotating blades mounted on the central shaft.

The dimensions of the jet engine model is explained previously in section 4.2.1 and all the dimensions are scaled down by a factor of 10 from a typical jet engine dimensions in order to expedite the simulation while ensur-

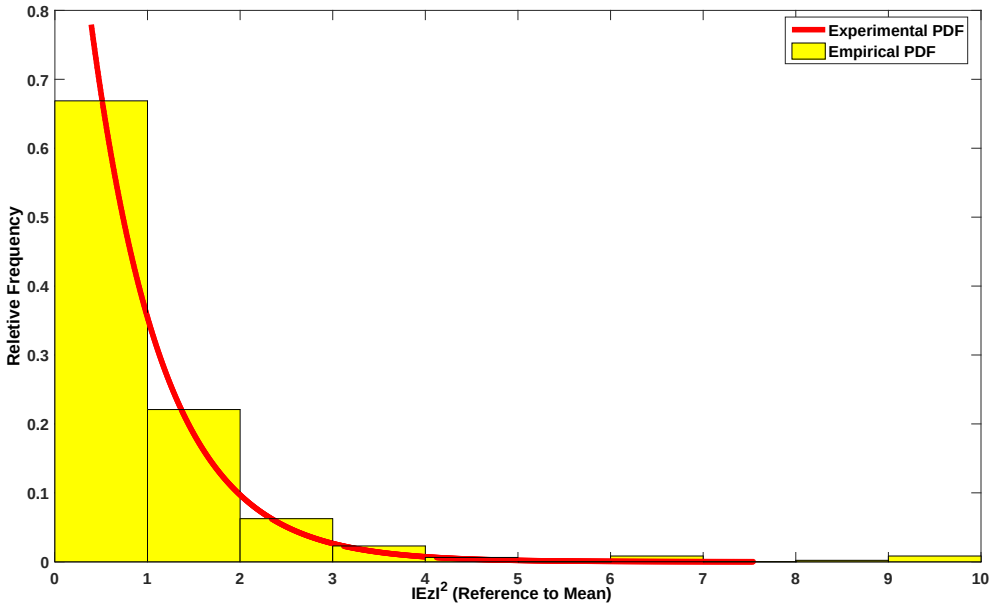

Figure 4.6 Data relative frequency histograms for the field along the jet engine for 16 blades.

ing its accuracy. The scaled frequency used in the simulations is 5 GHz (for an actual frequency of 500 MHz). The source of EM fields (excitation) in the design is provided by the simulation environment. An incident Hertzian dipole excitation (**a**) represents a simple transmitting antenna provided by HFSS full wave simulation environment simulates the field of an elementary short dipole antenna as explained in previous sections. Figure 4.7 (a) represents the front view for the simplified model, Fig. 4.7 (b) represents the side view and Fig. 4.7(c) represents the 3-D view for the engine. In order to ensure the randomness inside the jet engine environment, the blades are simulated for 120 distinct position with an angular rotation step (**R**) of 0.125 degrees. Hence, the blades are acting as the mechanical mode stirrers for the RC approach. For each stirrer position, the statistical properties of the EM field as a function of the stirrer position is analyzed.

Statistical Analysis

The electric field values are extracted for each and every stirrer position at different planes and these planes are set at distances 54 mm(A), 60 mm (B), 66 mm (C) and 72 mm (D) from the center along the $-Z$ axis as shown in Fig. 4.7(b). These planes are circular planes, and for the purpose of the analysis all the electric field values are extracted upon receiver probes that are scattered over a circle which has a 150 mm radius as shown in Fig. 4.5.

The magnitude of the electric field values ($|E_z|$) are extracted at those 17 different points on each plane (**A, B, C, D, and E**), at 120 different blade positions. Then, average the field values to study the statistical characterization of the propagating field. The squared magnitude of the average fields are calculated and analyzed statistically. Figure 4.8 represents the relative frequency histograms and its comparison with the theoretical pdf exponential models according to (4.2) which represents the mathematical formulas for the

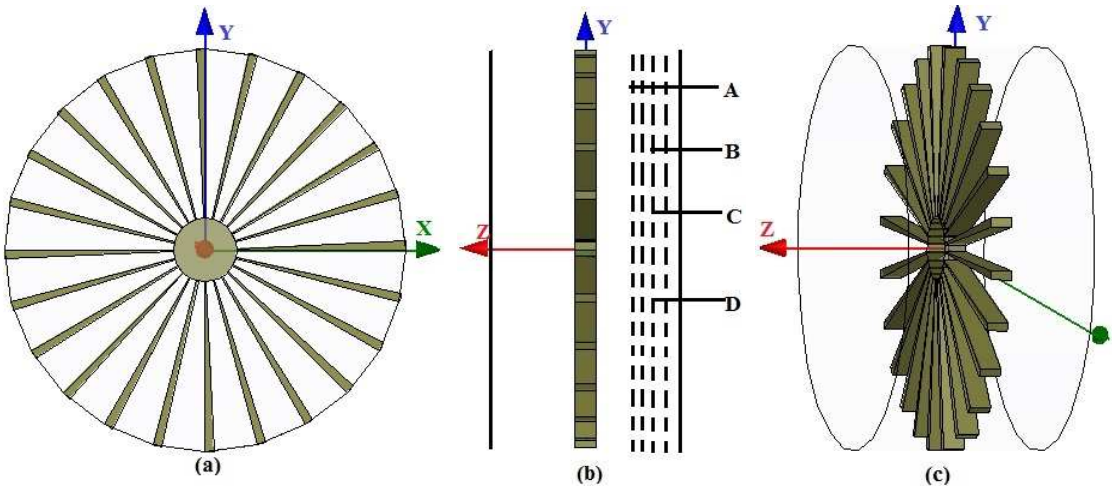

Figure 4.7: Simplified jet engine model with 24 blades :(a) Front view. (b) Side view. (c) 3-D engine view.

exponential PDF. The parameter (b) was estimated by calculating its maximum likelihood estimator and is equals to the mean average [63]. Here, we test the field characteristics against the statistical modeling hypothesis.

$$f_x(x) = \frac{1}{b} e^{-x/b} \tag{4.1}$$

$$f_x(x) = 1 - e^{-x/b} \tag{4.2}$$

It is found that $|E_z|^2$ has an exponential distribution compared to the theoretical exponential distribution proved in the RC model. The result for 24 blades is shown in Fig. 4.8. Hence, it is proved that the field component ($|E_z|^2$)

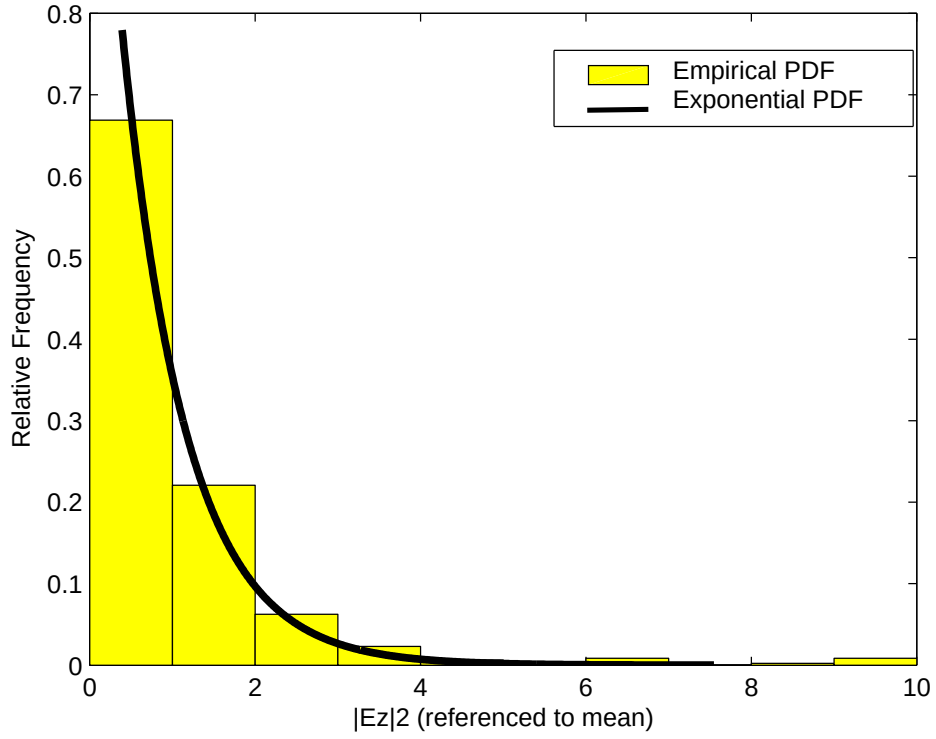

Figure 4.8 Data relative frequency histograms for the field along the jet engine for 24 blades.

along the engine axis is exponentially distributed when the antenna was at λ distance from the center of the axis. This means that the real and the imaginary components (E_{zr} and E_{zi}) of E_z have Gaussian distribution but with zero mean and are independent.

In order to generalize the best location for the receiving antenna, the average field value of $|E_z|^2$ at different receiving points over all the circular planes are calculated. It is worth to mention that, Plane **C** is considered as the best location for the receiving antenna as this plane is comparatively far from the blades and it gratifies the statistical theory. Hence, for the future jet engine analysis only the characteristics of Plane **C** will be analyzed. All the field values will be extracted only along the receiver points situated on Plane **C**.

The DSS analysis proved that the complex jet engine segment is similar to that of a mechanically stirred RC and generates statistically uniform electric field. Furthermore, to study the effect of dimension on field characteristics DS method is proposed. The DS method helps to characterize the EM propagation through the cascaded jet engine environment. At first, a mathematical model of the field characteristics as a function of the cavity dimension is outlined. Later, the assumption is verified using the DSS method.

4.3 Dimension Scaling Method

DS method is an analytical approach that can be used to model the EM propagation through complex jet engine segments. The fundamental requirement to solve the propagation characteristics using DS method is that the jet engine geometry should be separable. As explained before, the jet engine environment is decomposed into different segments to ease the complexity of STEM analysis and from Fig. 3.2, it is clear that each segment has a varying dimension.

Hence, to model the jet engine environment by using DS method the effect of dimension on field characteristics should be analyzed.

Since, the jet engine environment resembles a mechanically stirred RC, we can adopt all the statistical representations that have been evolved for the RC to resolve the EM field inside the jet engine.

4.3.1 Mathematical Modeling of Electric Field Component

The previous analysis proved that, the complex metallic jet engine cavity creates a statistically uniform electric field similar to RC, once excited by an internal EM source. Hence, the Hill's plane wave integral representation for RC field can be used to analyze the characteristics of the field components of an ideal jet engine environment [64]. Fig. 3.2(b) is considered as a well stirred ideal environment similar to a mechanically stirred RC and the environment generates a statistically uniform field. Then, We will analyze the statistical properties for one electric field rectangular component at one receiving point inside the jet engine cavity.

Based on a plane wave integral representation, the electric field at a particular position $\vec{r}$ inside a complex cavity can be represented as in (4.3), where Ω is the solid angle, $\vec{k}$ is the wave propagation vector and $F(\vec{\Omega})$ is the angular plane wave spectrum [64, 65].

$$\vec{E}(\vec{r}) = \int\int \left(F(\vec{\Omega}) exp(j\vec{k}.\vec{r}) d\Omega \right) \tag{4.3}$$

However, from the plane wave analysis it is clear that the mean value of the electric field, which is the sum of a large number of multipath rays with random

phase inside a well stirred cavity will be zero. i.e;

$$\left\langle \vec{E}(\vec{r}) \right\rangle = \int\int \left(\left\langle F(\vec{\Omega}) \right\rangle exp(j\vec{k}.\vec{r}) d\Omega \right) = 0 \tag{4.4}$$

Also, it is proved that the mean-square value of the electric field is independent of position as shown in (4.5), where E_0 is the plane waves amplitude.

$$\left\langle |\vec{E}(\vec{r})|^2 \right\rangle \equiv |E_0|^2 \tag{4.5}$$

$$\left\langle |E_x|^2 \right\rangle = \left\langle |E_y|^2 \right\rangle = \left\langle |E_z|^2 \right\rangle = \frac{|E_0|^2}{3} \tag{4.6}$$

$|E_0|^2$, can represent in terms of cavity parameters as shown in (4.7), where P_t is the transmitted power through the cavity, ϵ is the free-space permittivity, $\mathbf{Q}$ is the quality factor of the cavity, ω is the angular frequency and $\mathbf{V}$ is the cavity volume.

$$|E_0|^2 = \mathbf{Q} P_t / \omega \epsilon \mathbf{V} \tag{4.7}$$

From (4.6) and (4.7), the variance of the well stirred field component inside a complex cavity volume can be calculated as in (4.8).

$$\sigma^2 = \mathbf{Q} P_t / \omega \epsilon \mathbf{V} \tag{4.8}$$

ie;

$$\sigma^2 \propto \ 1/\mathbf{V} \tag{4.9}$$

From (4.9) it is clear that, the variance of the average electric field component is inversely related to the volume of the cavity. For the jet engine model; $\mathbf{V} = \pi \mathbf{R_r}^2 \mathbf{L}$ and we have considered $\mathbf{L}$ as a constant for all the segments as shown in Fig. 3.2. Hence, (4.9) can be represented as;

$$\sigma^2 \propto 1/\mathbf{R_r}^2 \tag{4.10}$$

Equation (4.10) proves that the variance of the axial electric field component inside the jet engine cavity is linearly related to the radius of the cavity model. Hence, the statistical parameters of the field components of any jet engine model can be deduced from these analysis.

4.3.2 Verification of DS mathematical model using DSS

In order to prove the relation between the radius of jet engine and sigma of electric field inside the jet engine environment and to find the effect of dimension of complex jet engine on the field characteristics, the simplified jet engine model (**segment1**) is simulated by using DSS method for varying dimensions. The **segment1** is simulated for different values of R_r. For each value of R_r, the simplified jet engine model as in Fig. 4.7 is simulated for 120 different blade positions with 0.125° angular increase each time to ensure the randomness of the medium. The TX antenna is positioned at λ distance from the center of the axis.

The magnitude of the electric field values are extracted around Plane **C** for 120 different blade rotational positions at those fixed 17 receiving positions as shown in Fig. 4.5. At each receiving point, the electric field values are analyzed statistically to evaluate the field characteristics. The analysis proved that the

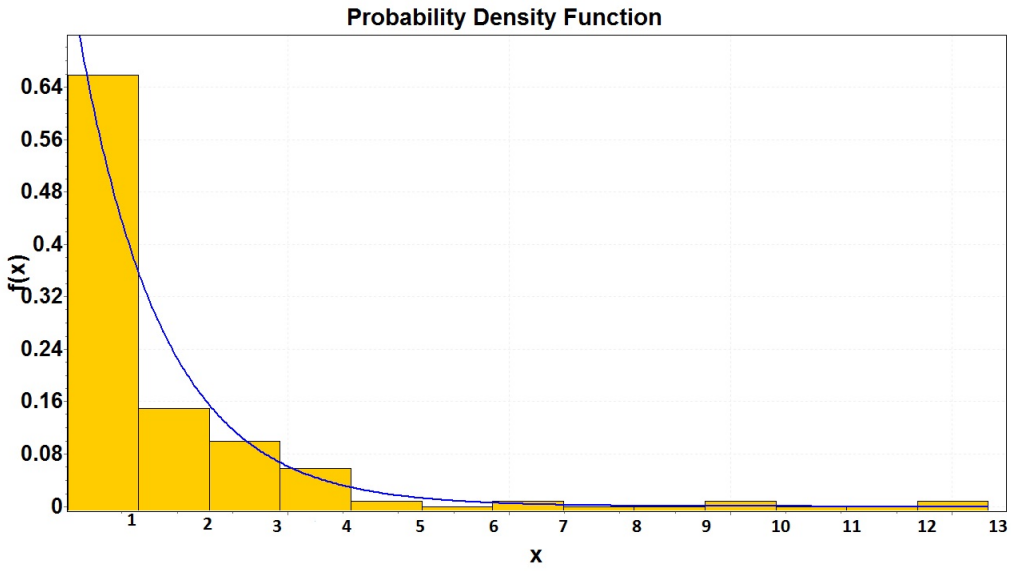

Figure 4.9 Data relative frequency histograms for the field along the jet engine for R_r=180 mm.

magnitude of the electric field component inside the jet engine environment for all the jet engine dimension follows the dynamic system hypothesis and generates a statistically uniform electric field. The analysis proved that the $|E_Z|^2$ follows an exponential distribution, for all the jet engine dimensions as shown in Fig. 4.9. The variation of the characteristics of the field component (σ) with varying dimension is analyzed statistically and is shown in Table 4.1. Table 4.1 shows the σ values of electric field magnitude for various jet engine dimensions at some fixed receiver positions.

Figure 4.10 proves the relation between the radius of jet engine environment and the standard deviation at a fixed receiver location, $\varphi = 45\,^\circ$. It is clear from Fig. 4.10 that as the radius of a jet engine increases the standard deviation decreases and is applicable to all other probe locations. These results validates our analysis in section 4.3 and prove that the σ of the field magnitude is inversely related to the radius of the jet engine **segment**. This means that it is possible to analyze the entire jet engine environment by using the combination

Table 4.1 Radius Vs Standard Deviation.

	$\varphi = 90°$	$\varphi = -90°$	$\varphi = -45°$	$\varphi = 45°$
R (mm)	σ	σ	σ	σ
190	19.9164	21.0578	14.7572	13.1172
186	24.7483	20.7343	18.746	15.9002
180	34.0473	30.9365	24.0655	25.0831
176	32.1018	37.0106	43.3144	46.9675
170	54.0813	54.9466	50.2509	47.1392

of dynamic simulation of **segment 1** and the dimension scaling approach for the rest of the **segments**.

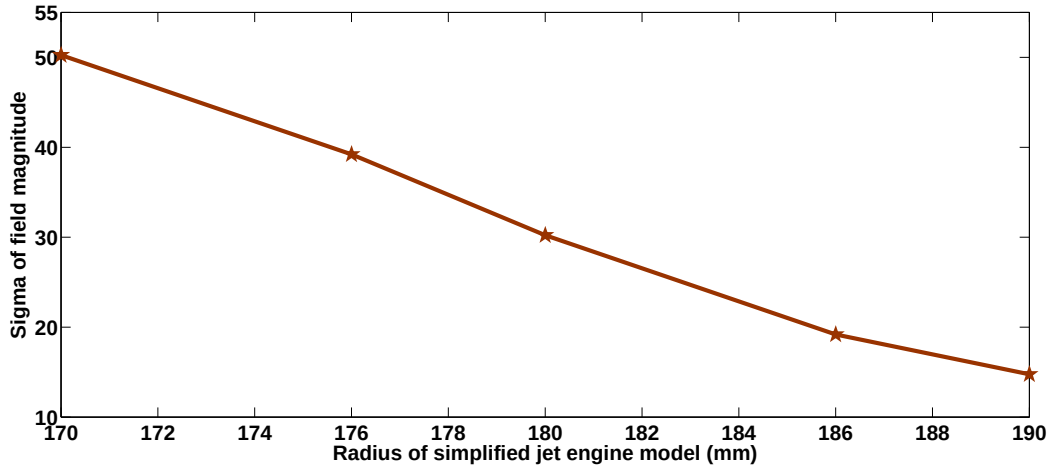

Figure 4.10 Relation between standard deviation and radius of jet engine at a fixed receiver location.

It is important to mention that, in the dynamic simulation method on **segment1** the randomness of the medium is established by simulating the blades in 120 different positions with equal angular increases. However, to increase the efficiency of the dynamic system analysis, an increased simulation positions with very small angular step size is required. This will ensure a continuous blade rotation, which means increasing the time and complexity of the computation. This will increase the time and complexity of computation. In order to reduce the system complexity, the static system approach is introduced. The outcome from this analysis helps to implement an alternative approach for the analysis of extremely complex and electrically large systems without considering the system complexity.

4.4 Summary

A simplified jet engine model is designed and simulated using the full wave simulation environment. The statistical characteristics of the electric field inside two different jet engine model with varying number of blades are analyzed. The results for 16 and 24 blade jet engine analysis support the hypothesis of using STEM for analyzing the EM field nature inside the engine. The primary analysis shows that, when the transmitting antenna is at λ distance from the center of the axis , $|E_z|^2$ has an exponential distribution function similar to the case of a mechanically stirred RC, which produces a normally distributed electric field. Later, the field characteristics inside the jet engine environment is modeled using the dimension scaling approach. The analysis proved that the statistical characteristics of the electric field magnitude is linearly related to the radius of the jet engine environment. The proposed methodology can be useful for the analysis of the complex jet engine structures without considering their complex design geometry due to the advantages of the statistical method.

Chapter 5: Effect of Jet Engine Parameters On Field Characteristics

5.1 Introduction

In this chapter, the effect of different jet engine parameters on the statistical characteristics of the electric field parameters are analyzed to generalize the complex jet engine analysis. The effect of excitation positions, and number of blades on the field distribution are analyzed by employing the notion of STEM. Later, the field uniformity of electric field component inside the complex jet engine environment is investigated by changing the number of blades and TX antenna positions. Furthermore, to model a reliable radio channel between the TX antenna and the receiving (RX) probes for the wireless communication inside jet engine, a correlation based modeling method is also presented in this chapter.

5.2 Statistical Distribution of Electric Field Inside Jet Engines for Different Excitation positions

In this section, an innovative approach is proposed for the analysis of EM field distribution inside the jet engine for different excitation positions by employing the notion of STEM. The DSS approach is used to analyze the field characteristics inside the engine environment. For the initial jet engine analysis, the

location of the excitation was at λ distance from the center of the axis along the $X-Z$ plane (190 mm, 60 mm). However, to generalize the jet engine analysis the effect of excitation position on the statistical nature of the electric field distribution inside the jet engine environment is analyzed. The excitation positions are changed with respect to initial excitation position. The new location of the excitations are represented as TX1: 190 mm, 45 mm, TX2: 190 mm, 75 mm, TX3: 180 mm, 45 mm, and TX4: 180 mm, 75 mm along the $X-Z$ plane.

5.2.1 Statistical Analysis of EM field for TX1

The simplified jet engine model with a single stage of 24 coplanar rotating blades as explained in Chapter 4 is used for the analysis. The blades are uniformly distributed around the shaft and for each TX antenna position the blades are simulated for 120 distinct positions with 0.125 degrees angular increase each time to ensure the randomness of the medium. The transmitted signal is provided by a Hertzian-dipole excitation (a), which is located at TX1 position, which is at $(3/4)\lambda$ from the center of the engine along $+Z$ axis according to the geometrical view. The field values are extracted from Plane **C** upon 17 points located over the circle which has a 15 cm radius as shown in Fig. 5.1. At each point, the magnitude of the E_z component is extracted at the different 120 blade positions. Then, average the field values to compare with the statistical models. Furthermore, the E_{zr} and E_{zi} of the axial field components along the engine axis are extracted and their probability distributions are studied.

It is clear from the analysis that there is a great agreement between the distributions of the E_{zr} and E_{zi} components and the Gaussian distribution as shown in Fig. 5.2. Figure. 5.2 shows the normal probability plots [66] for

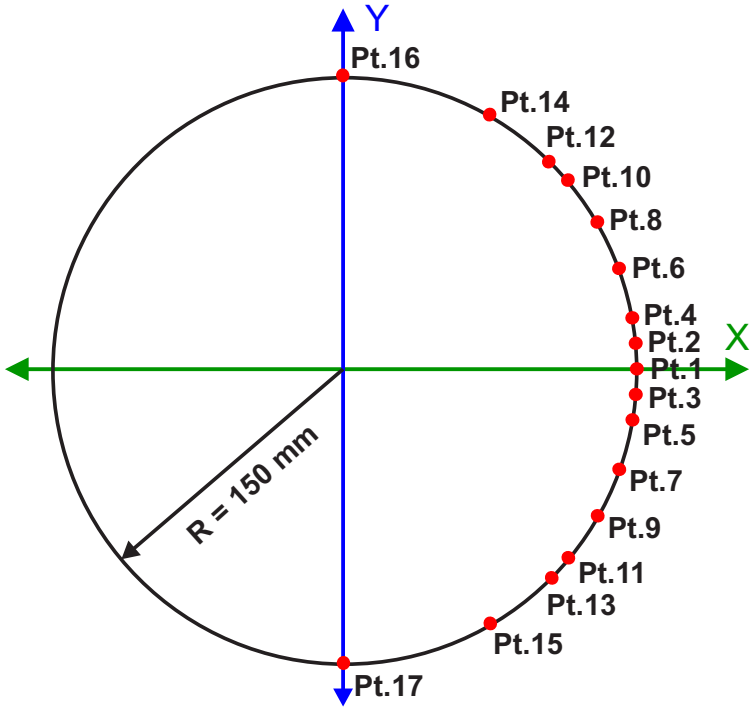

Figure 5.1 Location of receiver points on a circular plane.

the extracted field components at excitation positions TX1. Normal probability plot assess graphically whether the data could come from a normal distribution. The statistical analysis proved that, the E_{zr} and E_{zi} are Gaussian distributed with particular mean and variance and are dependent with each other. They possess high correlations as shown in Fig. 5.2.

Later, the statistical analysis of the propagating field inside the jet engine for three other excitation position is also presented to compare the results. The electric field values are extracted at the circular Plane **C** for 120 blade rotation for other three different antenna excitation (TX2, TX3, TX4) positions. The E_{zr} and E_{zi} of the axial field components along the engine axis are extracted for each excitation positions and then average the field values to study the statistical characteristics of the propagating field. Figures. 5.3, 5.4, and 5.5,

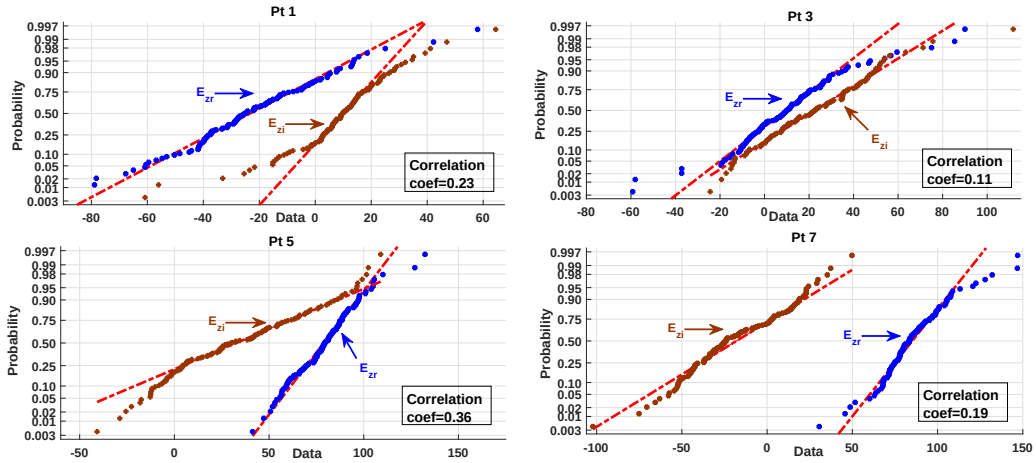

Figure 5.2 Normal probability plots for the field components along the cylindrical jet engine at excitation position 1.

show the normal probability plot of E_{zr} and E_{zi} component for three different excitation positions.

It is clear from the figures that, at all the TX antenna locations the distributions of the two field components have Gaussian distribution with particular

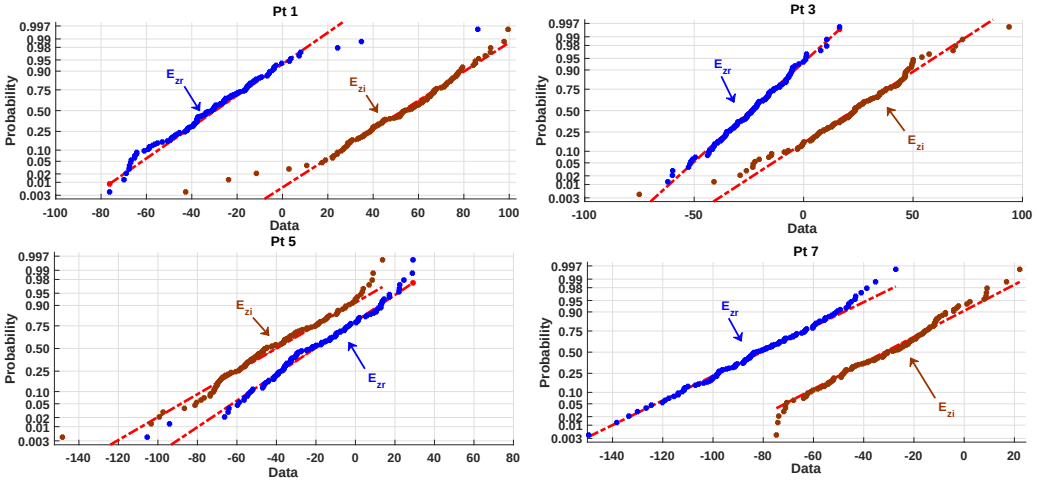

Figure 5.3 Normal probability plots for the field components along the cylindrical jet engine at excitation position 2.

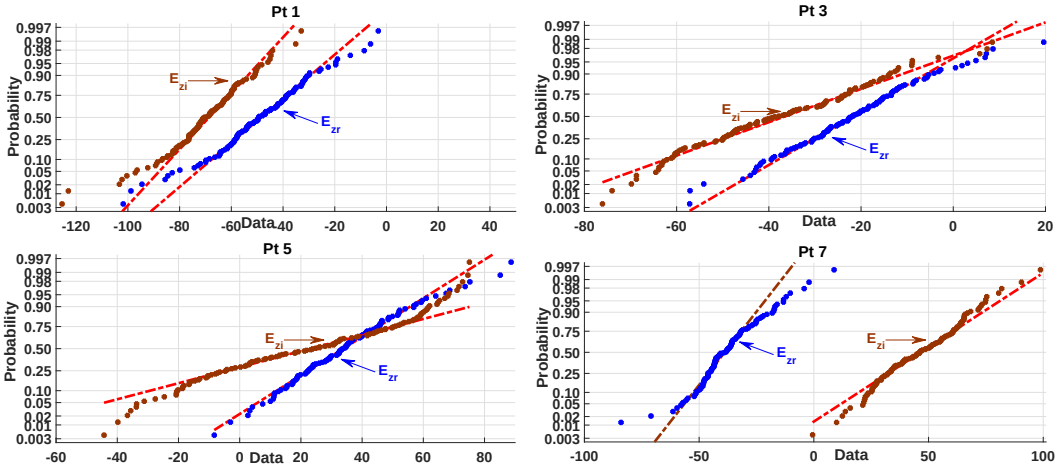

Figure 5.4 Normal probability plots for the field components along the cylindrical jet engine at excitation position 3.

mean and variance. However, except for the values of the data that have low probability, the distribution introduces curvature at the ends. This is because it needs more sample points to compare the theoretical results with simulation values resulting in increasing the time of simulations. The two field components

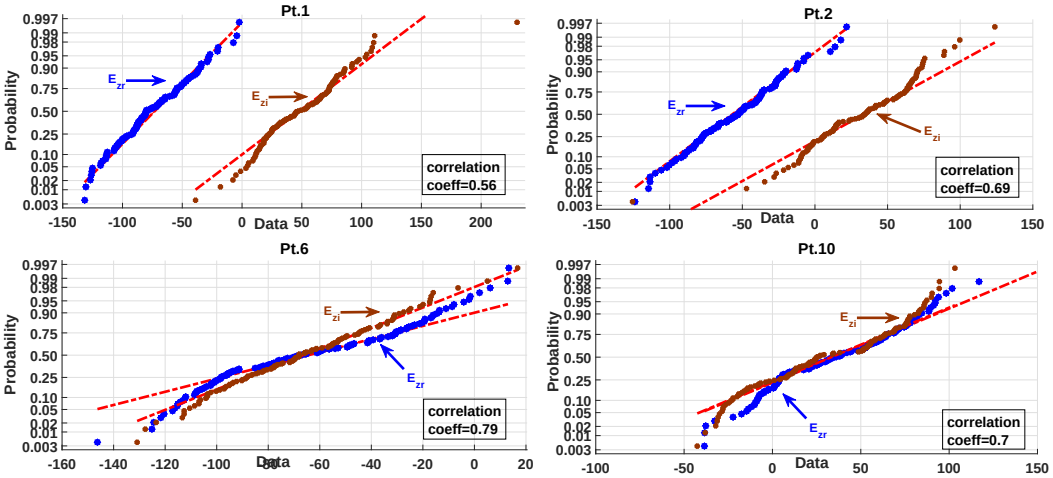

Figure 5.5 Normal probability plots for the field components along the cylindrical jet engine at excitation position 4.

are dependent with different means and variances. Fig. 5.5 also indicates the correlation coefficients between the two field components.

The statistical analysis of the jet engine environment with varying excitation location proves the concept that the jet engine environment resembles to a lossy RC [67], when the TX antenna excitation is positioned at a location other than λ distance from the center of the axis. Hence, the extended plane wave integral representation for an anisotropic RC can be used to solve the jet engine field characteristics. This technique is very useful for the analysis of the complex jet engine structures without considering their complex design geometry due to the advantages of the statistical method.

5.3 Dependency of TX antenna and RX probe location on electric field characteristics

The statistical analysis of the electric field inside the jet engine environment proves that the rotation of blades affects the characteristics of the electric field inside the jet engine cavity. The rotation of blades, or change in the TX antenna position, constitute considerable changes in the boundary conditions of the jet engine environment. At every rotational position of the blade, the distribution of the electric field inside the engine cavity will change. The distribution of the field inside the environment is due to the contribution of all the resonant modes that are available inside the jet engine environment. However, each and every mode will contribute in different style and hence, the electric field orientation at different receiving point will be different as shown in Fig. 5.6.

Figure. 5.6 shows the power of the electric field extracted from 5 different receiver locations inside the jet engine environment as a function of the blade rotation positions (120 positions by 0.125° angular increase each time) . The

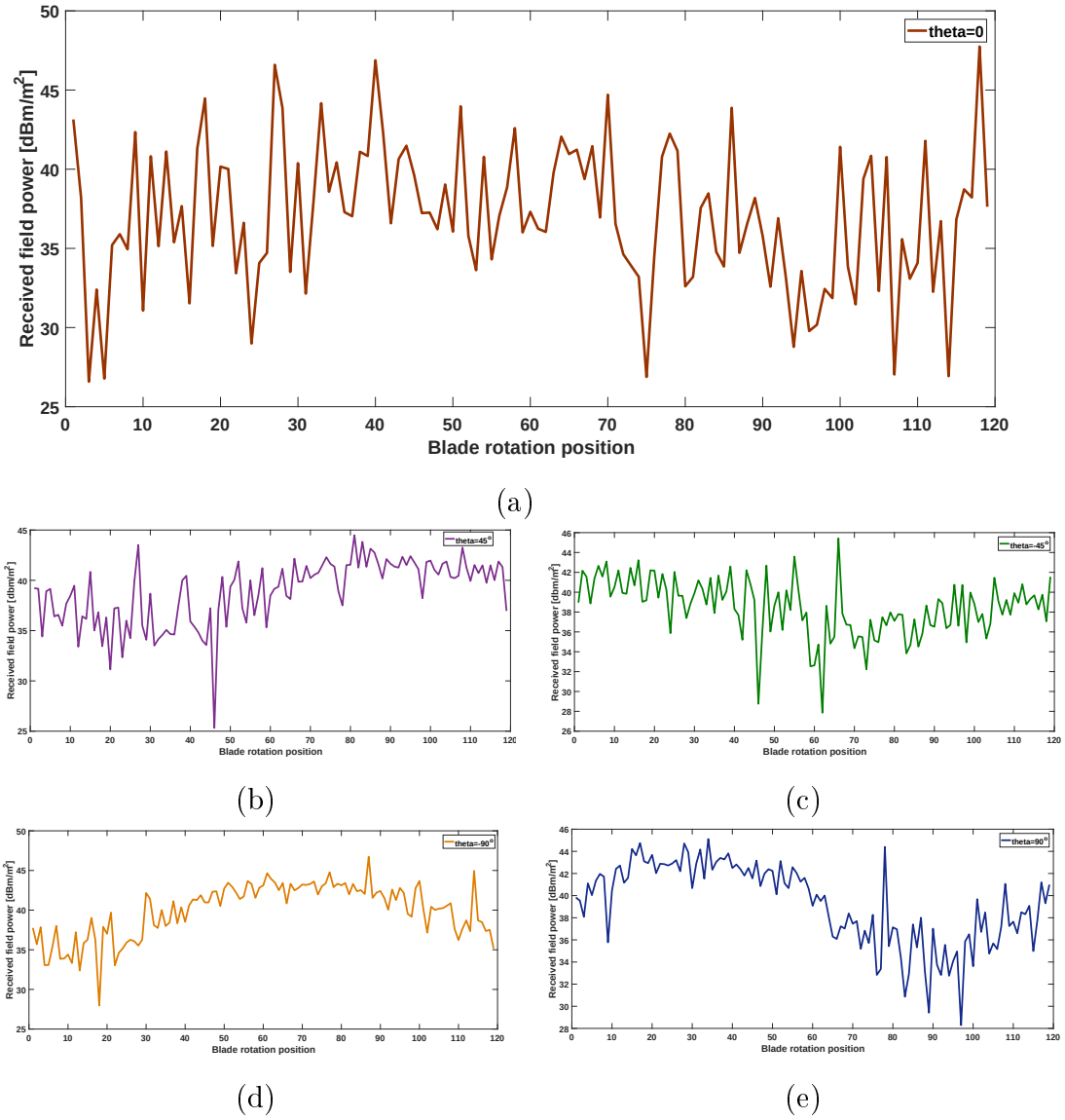

Figure 5.6 Extracted electric field strength at different receiver location (a) $\theta = 0°$ (b) $\theta = 45°$ (c) $\theta = -45°$ (d) $\theta = 90°$ (e) $\theta = -90°$.

TX antenna is positioned at $X - Z$ plane (190 mm- 45 mm) and excited continuous wave signal of frequency 5 GHz. Fig. 5.6 (b) and Fig. 5.6 (c) shows the power as a function of rotation angle at two different values of θ (clockwise and anticlockwise direction). The receiver locations are at equal distance from the TX antenna position. From the Fig. 5.6, it is clear that there is a discrepancy between the graphs even if the receivers are located at equal distance from the

TX antenna. They are obviously different from each another, but if we consider the statistical properties (μ and σ) of the average electric filed values as shown in Table 5.1, we can see that they are statistically equivalent.

Later, to check the homogeneity of the field component inside an anisotropic environment the dependency of the received electric field characteristics on different receiver locations due to different TX antenna positions is analyzed. To illustrate this study, the magnitude of the electric field component is extracted from 17 different probe locations inside the engine environment for 3 different TX antenna locations. Fig. 5.7 and Fig. 5.8 show the mean and sigma of the electric field component for those 3 TX antenna locations as a function of receiving angles. From the figure, it is clear that there is discrepancy between the curves. However, if we look at the statistical properties of the data available in table 5.1, we can see that they are statistically similar.

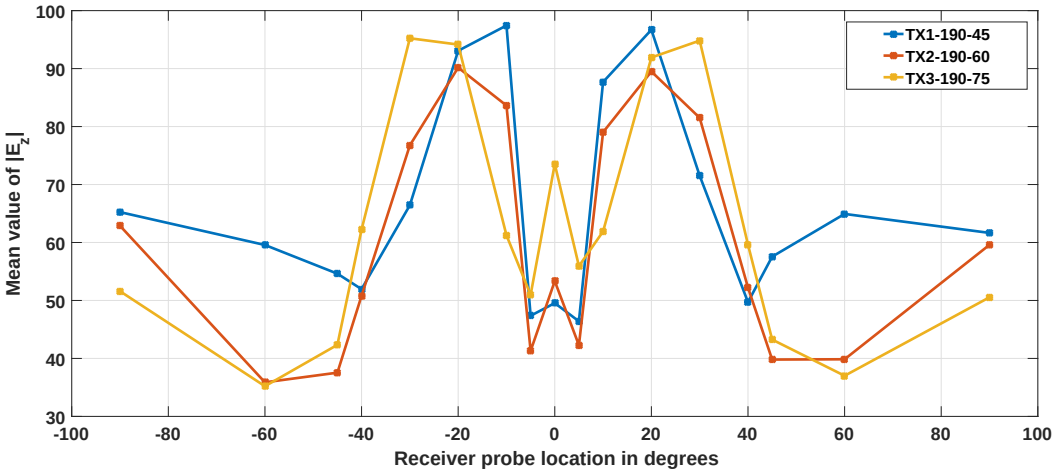

Figure 5.7 Comparison of the mean value of the $|E_z|$ component at different receiving probe due to different TX antenna position.

Table 5.1 Mean and standard deviation of $|E_z|$ at different receiver point due to 3 TX antenna location

RX	mu_TX1	mu_TX2	mu_TX3	sig_TX1	sig_TX2	sig_TX3
-90	65.2411	62.8784	51.5896	22.5074	24.3147	25.4787
-60	59.5704	35.877	35.2079	13.4795	12.4435	13.1542
-45	54.6223	37.5447	42.3481	17.051	14.6995	20.6232
-40	51.9472	50.7956	62.2283	18.6543	17.4693	18.5692
-30	66.4382	76.759	95.2315	21.8546	26.1608	32.3149
-20	93.0731	90.1769	94.1448	16.7899	20.3716	18.9715
-10	97.4321	83.6248	61.2461	22.1819	23.9682	25.69
-5	47.3631	41.3122	50.9735	26.98	25.8008	21.2933
0	49.5491	53.3384	73.5258	26.1629	30.5675	24.5119
5	46.4027	42.2759	55.9224	26.3766	25.9924	26.6964
10	87.6869	79.0241	61.9095	18.0821	23.8502	31.6079
20	96.6931	89.4953	91.9157	17.7995	16.0685	19.2289
30	71.5169	81.5034	94.8243	22.2918	27.2494	29.2449
40	49.7048	52.2285	59.6296	19.5237	18.4082	14.7605
45	57.555	39.8061	43.2535	18.6729	14.7893	17.861
60	64.929	39.8544	37.0101	16.1547	11.5316	13.3988
90	61.6533	59.6004	50.549	22.9714	24.7457	25.667

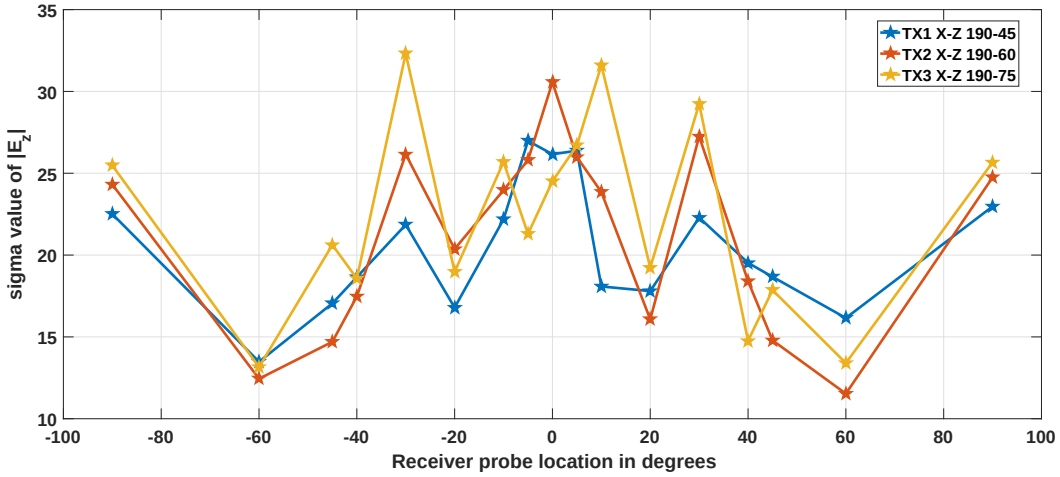

Figure 5.8 Comparison of the sigma value of the $|E_z|$ component at different receiving probe due to different TX antenna position.

5.4 Effect of Excitation Position and Number of Blades on Field Uniformity Inside Jet Engines

The DSS analysis proved that, the jet engine environment resembles a mechanically stirred RC with statistical field characteristics [13, 68]. However, the received field shows anisotropic field characteristics when the TX antenna is positioned at a position other than λ distance; hence, for the generalized statistical analysis of the jet engine environment we can adopt the theoretical formulation of the plane wave integral representation for anisotropic received fields [67]. Since, the jet engine environment shows anisotropic field characteristics, the statistical uniformity of electric field inside jet engine at particular transmitting antenna positions is investigated .

The main objective of this analysis is the investigation of the effect of excitation position and number of blades on field uniformity of electric field component inside complex anisotropic jet engine environment, which has highly correlated field characteristics.

5.4.1 Effect of Excitation Position on Field Uniformity

The maximum electric field within a complex environment is considered uniform if the standard deviation is within 3 dB above 400 MHz frequency [69]. In order to investigate the effect of excitation on field uniformity inside the jet engine, the simplified jet engine model is simulated for 120 different blade positions for two different TX antenna positions. The locations of the excitation are at 190 mm, 45 mm and 190 mm, 75 mm, referred as TX1 and TX2; respectively. The rotation of blades provide necessary randomness for the environment. The magnitude of the electric field values are extracted for each blade position at different receiving points on a circular plane **C** as shown in Fig. 4.5.

At each receiving point, the magnitude of E_z components are extracted for different 120 blade positions and then average the field values to study the field uniformity. The values of mean (μ_z) and standard deviation (σ_z) of $|E_z|$ at different receiving points are evaluated from the simulation environment. The standard deviation method is used for calculating the field uniformity inside jet engine [70]. The σ_z is expressed in dB relative to the mean by using (6.9).

$$\sigma_z(dB) = 20log((\sigma_z + \mu_z)/\mu_z) \tag{5.1}$$

Figure 5.9 shows the field uniformity limitation (3dB limit) proposed by the International Electrotechnical Commission (IEC) specification and the result of the uniformity analysis around plane **C**. It is clear from Fig. 5.9 that, the performance of the jet engine environment satisfies the field uniformity criteria for TX1 position at all the receiving points and for TX2 position the condition is not satisfying for all the receiving points. The desired field uniformity is achieved for an anisotropic jet engine environment, when the transmitting excitation is located at TX1 position. Hence, it is proved that the field unifor-

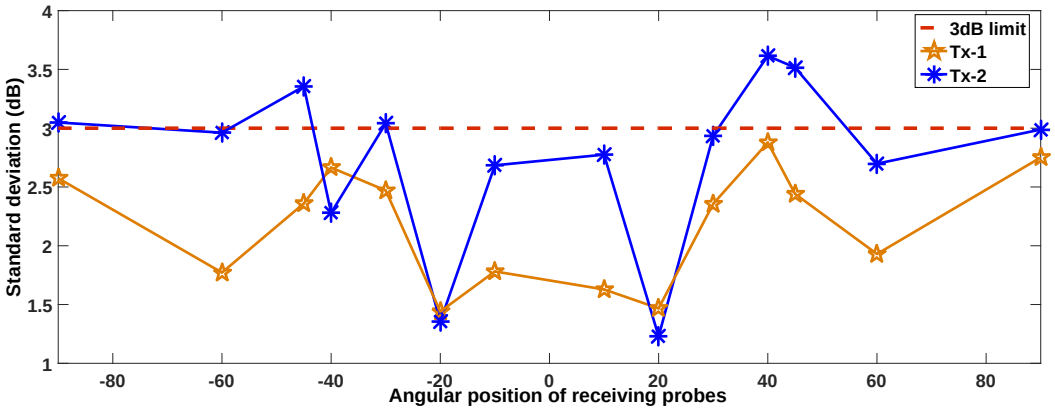

Figure 5.9 Standard Deviation with respect to receiving points for two different excitation position.

mity inside complex environment can be improved by changing the transmitting excitation position without altering the dimension of the environment.

5.4.2 Effect of Number of Blades on Field Uniformity

Later, the field uniformity with respect to the number of rotating blades inside the jet engine is analyzed. Two different jet engine models are analyzed for 120 different blade positions. Model-1 contains 1 set of 16 coplanar rotating blade and model-2 contains 1 set of 24 coplanar blades as shown in Fig. 5.10.

The electric field values are extracted for 120 blade rotations at different probe locations on plane **C**. Then the field values are averaged for statistical analysis. Figure 5.11 shows the field uniformity with respect to number of blades. The Field uniformity improved greatly, when the number of blade increased from 16 to 24 as shown in Fig. 5.11.

From the above analysis, it is clear that the field uniformity inside a complex jet engine environment depends on the position of the excitation, and the number of blades. Hence, the field uniformity can be improved by changing the excitation location or the number of blades without altering the dimension of the model.

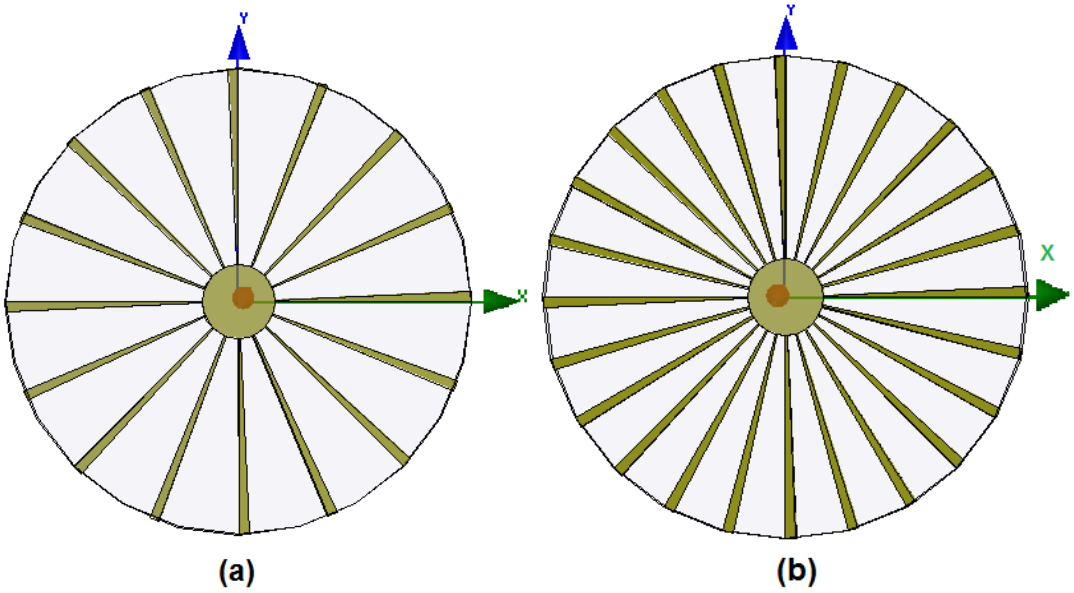

Figure 5.10 Front view of simplified jet engine model (a) 16 blade. (b) 24 blade.

In this chapter, different parameters that affect the field characteristics inside the jet engine environment is analyzed. However, the jet engine environment is extremely complex and there is a very narrow spacing between the receiving points. Hence, to model a reliable wireless communication channel inside the jet engine environment the effect of correlation between the transmitter

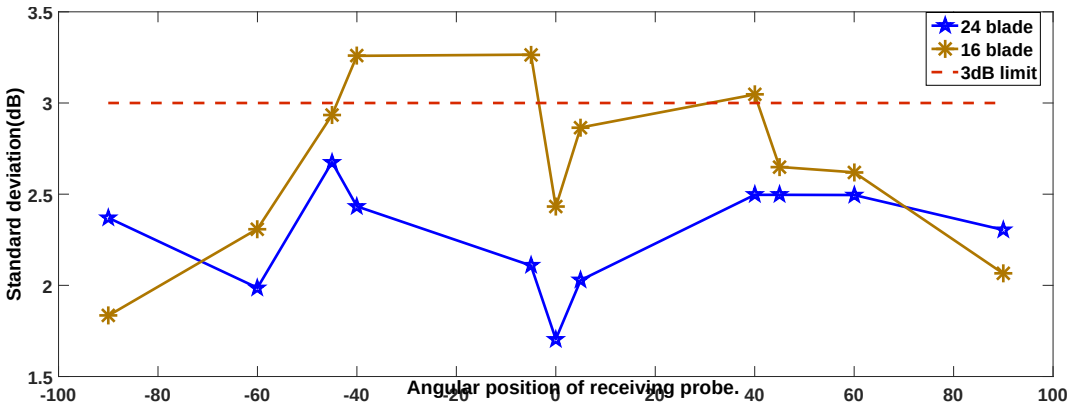

Figure 5.11 Field uniformity with different number of rotating blades.

and the receiver points should be analyzed. In the next section, a correlation based analysis is proposed to study the possibility to deploy a reliable wireless networks inside jet engines.

5.5 Effect of Excitation on Correlation Based Analysis of Electric Field Inside Jet Engines

The wireless communication facility inside the jet engine is going to operate in an environment, where a large number of reflective surfaces are present. This will affect the average power distribution of a transmitted signal to vary significantly at different locations across the jet engine environment. Jet engine environment is extremely complex with large number of metallic parts inside the environment and the receiver elements are surrounded by scatters and conductors of different size and shape. This makes Jet engine environment an RF harsh environment and its channel characteristics can be significantly different from other propagation environments. Recent studies proves that there is a possibility of wireless communication inside jet engines and also proved that the jet engine environment is a fading one [46, 71, 72]. Hence, to deploy reliable wireless networks inside jet engine, a simple channel modeling method based on correlation analysis of the electric field inside jet engine is studied. Spatial correlation of electric fields plays an important role in such wireless communication systems due to narrow spacing between the receiving points.

If the communication structure has only a single excitation, then the power variations of the transmitted signal due to harsh environment can degrade the overall system performance. In order to make the system more vigorous to these kinds of environments, different techniques can be used; one such technique is to provide the communication system with multiple excitation elements for transmitting and receiving purpose (Multiple Input Multiple Output

(MIMO)) [73, 74, 75, 76, 77, 78]. Moreover, multiple antenna system will help to increase the reliability of wireless links. If these different antennas are uncorrelated then each antenna element will experience an individual distribution of the signal strength variations as the environment changes. Hence, the receiving probes/antennas will have different received signals with difference in signal strength. Moreover, these received signals will be independent from each other. Hence, to obtain a best system performance the receiver can choose either the antenna element with strongest signal or the combination of different received signals. The correlation analysis due to single and multiple TX antennas including the geometry and design of the jet engine model is presented in the following section.

5.5.1 Correlation Analysis using Single Transmitting Antenna Excitation

In order to deploy reliable wireless networks inside jet engine, the receiving probes must be located at some optimum distance. The position of the probes inside the environment is critical in order to offer less channel correlation and optimal radio coverage. As an initial study of the channel modeling inside the jet engine, the correlation between different receiver points due to a single TX antenna is analyzed. The simulation analysis is carried out on a simplified jet engine model with 24 coplanar blades. There are 17 RX probes (as mentioned in Chapter 3) that are distributed over the plane **C** at distance 66 mm from the center along -Z axis as shown in Fig.4.5.

In this analysis, the cross correlation between the receiving probes is studied for three different antenna positions (TX1, TX2, and TX3). Initially, the TX1 antenna is positioned at 190 mm , 75 mm away from center of the axis along $X-Z$ plane. The magnitude of electric field values are extracted upon different

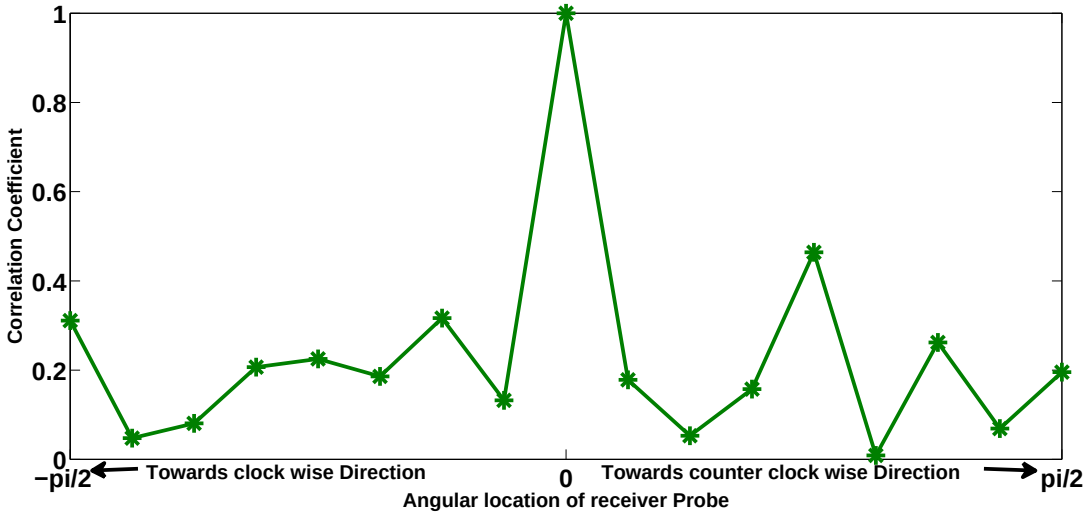

Figure 5.12 Correlation coefficient at different probe location with respect to point 1 for TX1.

probes distributed over the circular plane from $-\pi/2$ to $\pi/2$. At each probe location, the field values are extracted for 120 blade rotation. Later, average the field values to find the mean characteristics and correlation coefficient at each point. Figure 5.12 shows the cross correlation between the distributed probes due to TX1 antenna. The same procedure is repeated for TX2 antenna which is located at $X - Z$ plane (190 mm , 45 mm). The field values are analyzed using *matlab* to study the correlation between different receiver locations. Figure 5.13 represents the 4 probe locations that are highly uncorrelated and have high mean values for the average field resulting from the rotating blades. The correlation coefficient matrix between 4 probe locations for TX1 and TX2 are given in (5.2) and (5.3). The probes are located at $\phi = 0, 10°$, $60°$ in clockwise direction and $20°$ in counter clock wise direction.

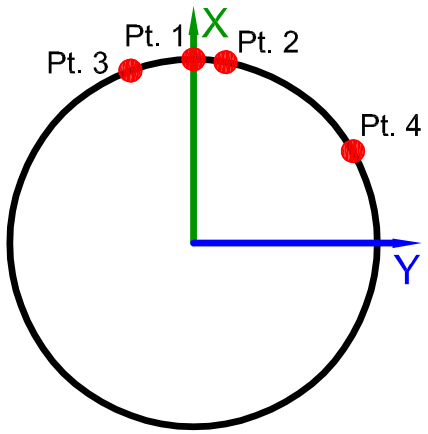

Figure 5.13 Location of 4 probes on a circular plane with less correlation.

$$\rho_{TX1} = \begin{bmatrix} 1 & 0.0529 & 0.1859 & 0.0690 \\ 0.0529 & 1 & 0.0193 & 0.0866 \\ 0.1859 & 0.0193 & 1 & 0.0656 \\ 0.0690 & 0.0866 & 0.0656 & 1 \end{bmatrix} \tag{5.2}$$

$$\rho_{TX2} = \begin{bmatrix} 1 & 0.0742 & 0.0928 & 0.0997 \\ 0.0742 & 1 & 0.0584 & 0.0795 \\ 0.0928 & 0.0584 & 1 & 0.0890 \\ 0.0997 & 0.0795 & 0.0890 & 1 \end{bmatrix} \tag{5.3}$$

However, when the transmitting antenna (TX3) is located at a distance λ from the jet engine center along $-Z$ axis, the electric field values show lowest correlation at $\phi = 0, \pi/2$ and $-\pi/2$ probe locations on the circular plane **C**. The correlation coefficient matrix is represented by (5.4). i.e. these three probe

locations are highly uncorrelated when the transmitting antenna is located at a distance λ from the center of the axis.

$$\rho_{TX3} = \begin{bmatrix} 1 & 0.0940 & 0.0788 \\ 0.0940 & 1 & 0.0535 \\ 0.0788 & 0.0535 & 1 \end{bmatrix} \tag{5.4}$$

5.5.2 Correlation Analysis Using 2 Transmitting Antenna Excitations

In this section, the cross correlation between two received signals at same probe due to 2 antennas (TX1 and TX2) located at $X-Z$ plane (TX correlation) is analyzed. TX1 and TX2 are separated by $\lambda/2$ distance and are located at (190 mm 45 mm) and (160 mm 45 mm); respectively. It is important to mention that TX1 is positioned along the radius (190 mm) of the engine environment and TX2 is positioned $\lambda/2$ distance away from TX1 vertically. The real and imaginary component of the electric field values (E_{zr} and E_{zi}) due to TX1 exhibit Gaussian distribution with particular means and variances and are dependent [68]. Similarly, the average field values of E_{zr} and E_{zi} field components resulting from TX2 antenna also have Gaussian distribution as shown in Fig. 5.14.

As an initial step, the cross correlation between the transmitting signals at a certain probe location is calculated by exciting the jet engine environment by antenna TX1 and the magnitude of the electric field values (E_{TX1}) are extracted from different probes due to 120 blade rotation. Then TX1 is replaced by TX2 and E_{TX2} is extracted due to 120 blade rotation. Figure 5.15 shows the result

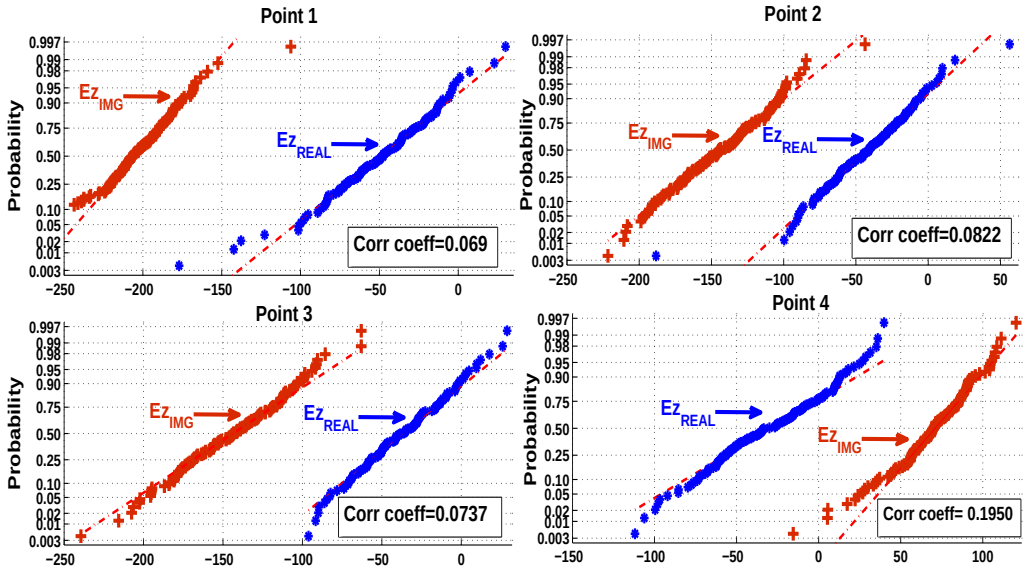

Figure 5.14 Normal probability plots for the field components along the cylindrical jet engine for TX2.

of cross correlation between E_{TX1} and E_{TX2} at different probe locations that are distributed from $\phi = -\pi/2$ to $\phi = \pi/2$, over the circular plane $\mathbf{C}$ along $-Z$ axis.

Although, various wireless technologies have been used for the analysis of EM propagation inside harsh environment, multiple input multiple output (MIMO) wireless systems have been considered as the most suitable method for characterizing propagation channel inside harsh environment such as jet engines. Moreover, multiple antenna system will help to increase the reliability of wireless links. In this model, the correlation properties of the MIMO channel are modeled by using two independent correlation matrices at the transmitter and receiver, neglects the correlation across the link between the TX and RX. A popular "Kronecker" channel modeling has been used for the MIMO performance analysis [79, 80, 81]. This particular method is proposed for this analysis due to its simplicity.

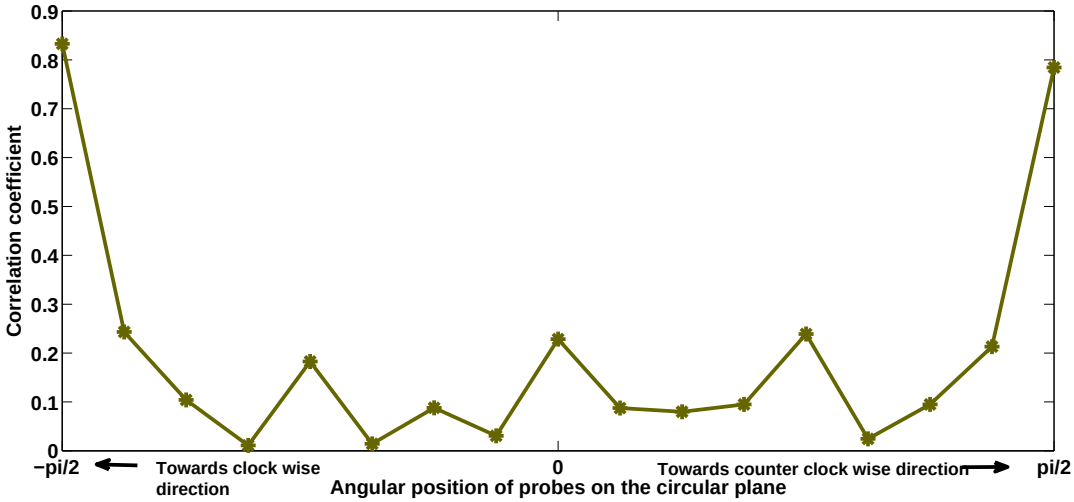

Figure 5.15 Cross correlation at receiving probes due to TX1 and TX2.

5.5.3 Correlation Analysis at the Receiver due to Antenna Array

In the initial analysis, the effect of correlation due to two different TX antennas was analyzed. As we know, the jet engine environment is highly complex with rich scattering components, antenna array over a MIMO channel can provide very high channel capacity. The capacity of MIMO channel depends on both the number of channels and on the correlation between channels. In order to generalize the correlation analysis inside the jet engine, a MIMO system of size 2×17 with an inter element spacing (dT) of $\lambda/2$ is considered as shown in Fig. 5.16. As mentioned earlier, at the receiver end we deployed 17 different RX probes to analyze the field characteristics and correlation properties as shown in Fig.4.5 and hence the size of MIMO is 2×17.

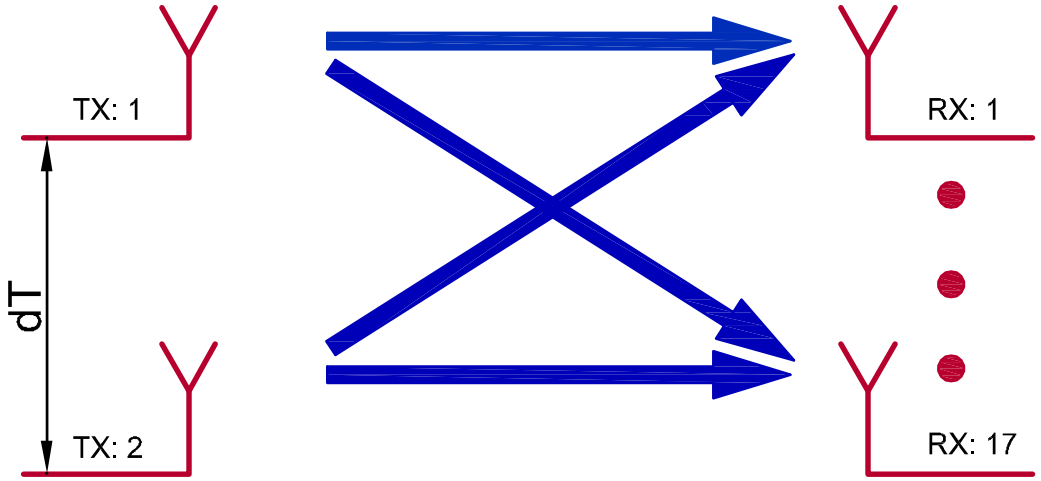

Figure 5.16 MIMO channel model.

The TX antennas are located at $X-Z$ plane; 190 mm-45 mm and 160 mm-45 mm away from the center of the axis. It is important to mention that TX1 is positioned along the radius (190 mm) of the engine environment and TX2 is positioned dT distance away from TX1 vertically. The magnitude of the electric field values (E_{z-dual}) due to 120 blade rotation and dual TX antennas are extracted at 17 probe locations and analyzed the field values statistically. Then the correlation of electric field values at those receiver probe locations are also analyzed. The probes located at $\Phi = 0, 20, -20$ and -45 degrees exhibit least correlation due to dual TX antenna excitation signal. The correlation coefficient at these 4 probe locations are given in (5.5). Those probe locations can be considered as best locations for receiving probes, when the TX antenna excitation system is separated by a distance of $\lambda/2$.

$$\rho_{TX_{dual}} = \begin{bmatrix} 1 & 0.0060 & 0.077 & 0.0236 \\ 0.0060 & 1 & 0.0287 & 0.055 \\ 0.077 & 0.0287 & 1 & 0.0123 \\ 0.0236 & 0.055 & 0.0123 & 1 \end{bmatrix} \tag{5.5}$$

Meanwhile, the transmitter and the receiver correlation analysis is studied by changing the inter element spacing of TX antennas to λ. In order to analyze the transmitter correlation, TX2 is replaced by TX3, which is located at 130 mm - 45 mm at $X - Z$ plane. The electric field values are extracted (E_{TX3}) from 17 probe locations due to TX3. The cross correlation between TX1 and TX3 is analyzed at all 17 probe locations. The receiver correlation due to dual antenna excitation system containing TX1 and TX3, separated by λ distance is also analyzed. Figure 5.17 and 5.18 shows the comparison between TX and RX correlations due to different inter element spacing (dT).

Figure 5.17 shows that the transmitter correlation is decreasing as dT has been increasing from $\lambda/2$ to λ particularly at the probes located at $\Phi = \pi/2$ and $-\pi/2$ degrees. It is very important to mention that the receiver correlation is also decreases as the inter element spacing of TX antenna excitation increases especially towards counter clockwise direction. Consequently, it is clear from the analysis that the TX antenna excitation separation has a significant effect on both the transmitter and the receiver correlation.

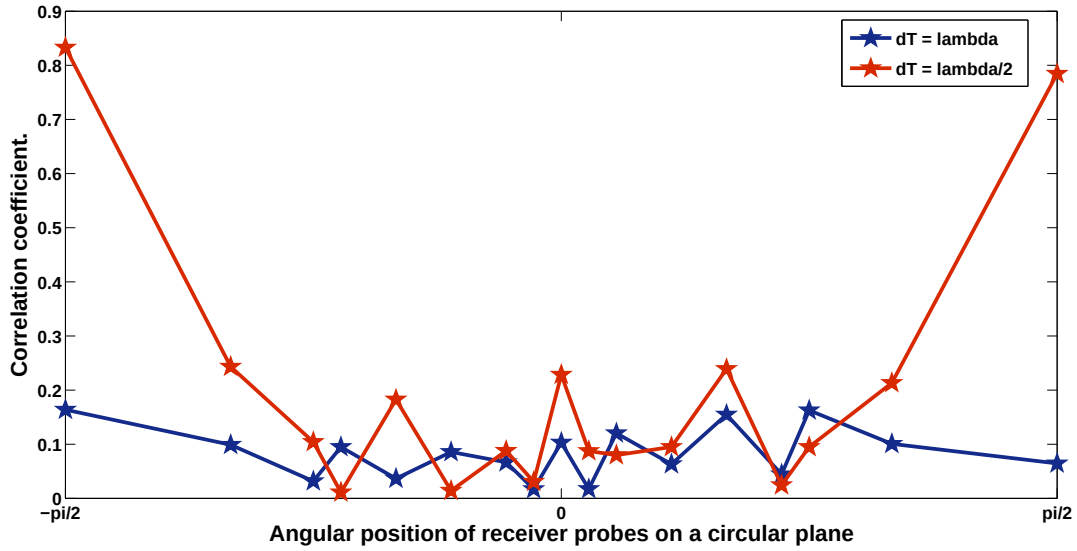

Figure 5.17 Comparison of transmitter correlation due to TX antennas separated by distance $'dT'$.

5.6 Effect of Receiver Position on Correlation Analysis

Later, the analysis of the transmitter and the receiver correlation as a function of receiver position is analyzed. To propose the best receiver location with lowest correlation characteristics, the electric field values are extracted at different planes for transmitting antennas separated by a distance of λ. These planes are set at distances from the center 60 mm(B) , 66 mm (C), and 72 mm (D) along $-Z$ axis.

In order to study about the dependency of transmitter and receiver correlation on the receiver position, the electric field values are extracted from those 3 different planes. For the initial analysis, the transmitter (TX1) is positioned at $X-Z$ plane; 190 mm - 45 mm. Then E_{TX1} is extracted and calculated the average field values at 17 probe locations around each plane (B, C and D) due to 120 blade rotations. However, it is proved that the field characteristics of electric field values ($|E_z|^2$) at plane B, C and D are exponentially distributed,

when the excitation is placed at λ distance from the center. Meanwhile, TX1 is replaced by TX3 positioned at 130 mm - 45 mm at $X - Z$ plane and extracted E_{TX3} for receiver plane B, C and D. The cross correlation between E_{TX1} and E_{TX3} is analyzed to the same receiver probes for all the three planes of extraction. Figure 5.19 shows the comparative study results of a transmitter correlation analysis at plane B, C and D when the TX antennas are separated by a distance of λ. Meanwhile, the procedure in section 5.5.3 is executed again for plane C and D with dual TX antennas separated by a distance (dT) of λ and Fig. 5.20 shows the characteristics of receiver correlation at each plane B, C and D due to dual antenna excitation system.

It is clear from the Fig. 5.19 and 5.20 that, the transmitter and receiver correlation have lowest correlation value at plane C, which is the initial plane of analysis. Plane C has least correlation compared to other two planes (B and D) and hence plane C can be considered as the best location for the receiver probes due to lowest correlation and maximum field strength.

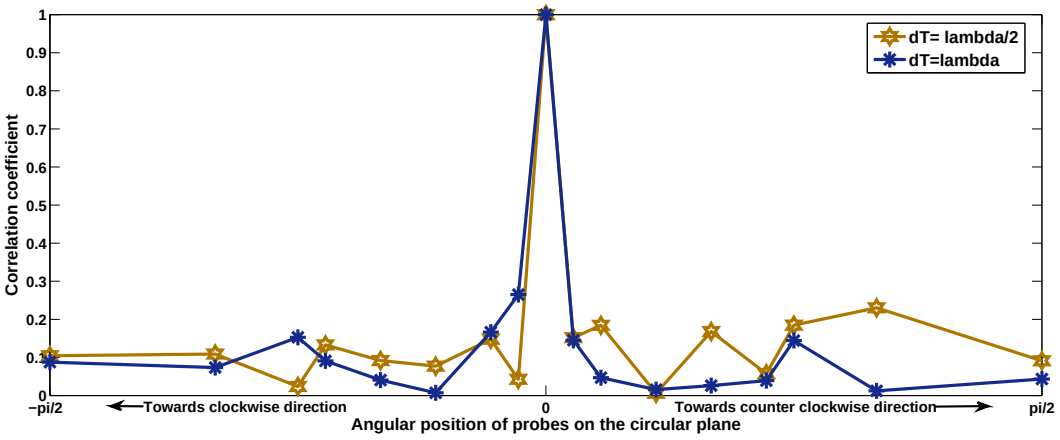

Figure 5.18 Comparison of receiver correlation due to dual TX antennas separated by distance $'dT'$.

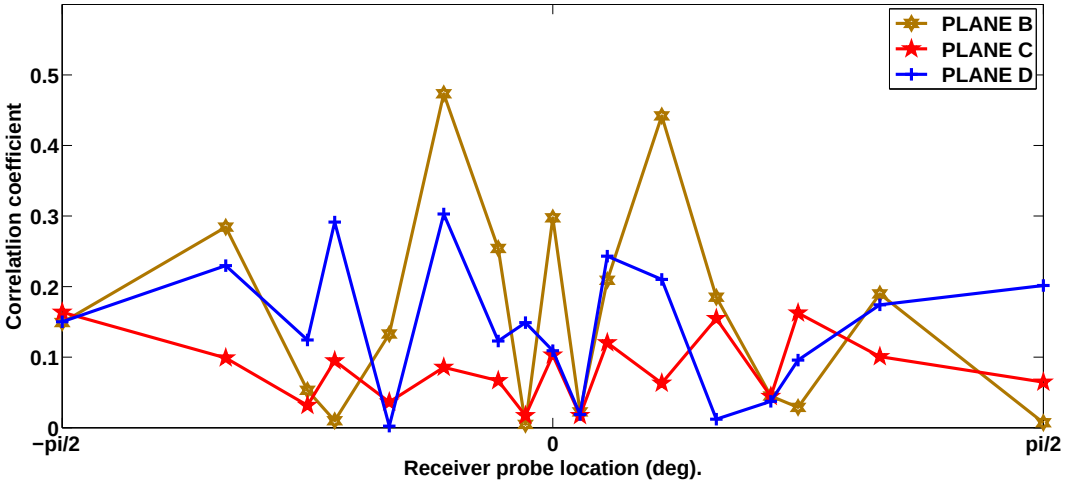

Figure 5.19 Comparison of transmitter correlation analysis of TX1 and TX2 at different planes of extraction.

5.7 Summary

In this chapter, a simplified jet engine model has been analyzed using HFSS by varying the transmitting antenna excitation position to study the effect of TX

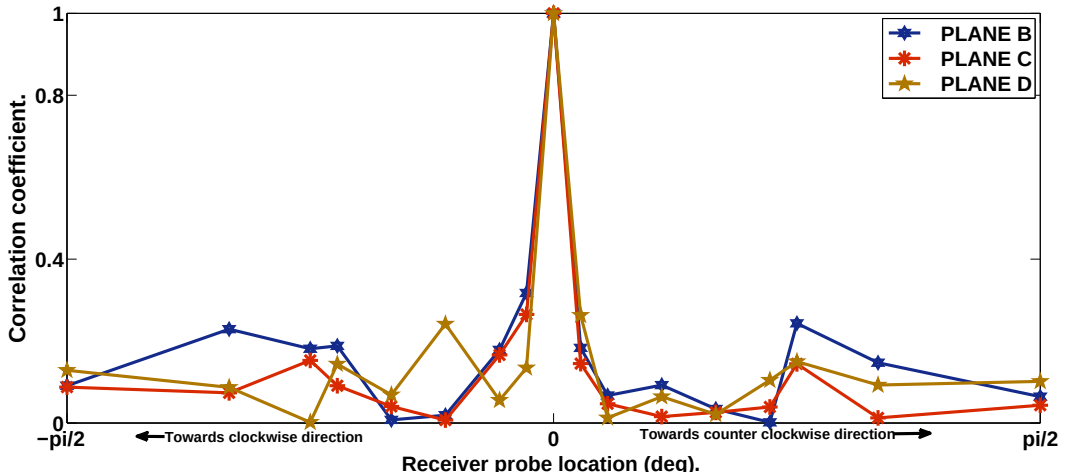

Figure 5.20 Comparison of receiver correlation analysis of dual antenna excitation at different planes of extraction.

antenna excitation location on field characteristics. The real and imaginary parts of the field values have been extracted at a particular plane and analyzed to obtain the statistical distribution. It is clear from the analysis that the empirical PDF of the simulated data are in good agreement with the theoretical Gaussian PDF and they are dependent. Later, the field uniformity inside the jet engine is analyzed with respect to transmitting antenna excitation position. The field is found to be uniform over the whole receiving positions for the transmitting antenna excitation located at a distance less than λ from the center of the axis. Meanwhile, two different jet engine model with different number of rotating blades are simulated for analyzing the effect of the field uniformity. The analysis suggest that as the number of blade increases, field uniformity is also improved. Finally, a simplified correlation based channel modeling method is studied either by using a single TX antenna excitation or by using two TX antennas, and multiple receiving probes inside jet engine. The joint correlation properties of multiple TX and RX antennas with different inter element spacing of TX antenna excitation is also analyzed. The correlation analysis showed that the TX and RX correlation decreases significantly as the inter element spacing increases. Moreover, the correlation characteristics at certain plane of extraction is also evaluated in order to choose best location for receiving antennas. The results obtained through this preliminary analysis are promising to model a reliable and simple communication path inside the jet engine environment.

Chapter 6: Static System Approach

6.1 Introduction

Static system approach (SSA) is an alternative approach to the DSA method, which introduces a novel SE method to solve the EM propagation through the entire jet engine geometry. The DSA approach which constitutes both dynamic simulation and dimension scaling approach is an effective STEM approach to solve any complex jet engine model. However, the efficiency of the dynamic system analysis requires an increased simulation positions with very small angular step size to ensure the continuous blade rotation, which means increasing the time and the complexity of the computation. Figure 6.1 shows the log file extracted from dynamic system simulation. It is clear from the files that to complete one blade rotation cycle with 0.0156° angular blade rotation, the DSS took 1 month, even with high precision system and an advanced VB script (used system is Intel(R)Xenon(R)CPU with 2.40 GHz, 2.39 GHz, 2 processors and 48GB RAM). Moreover, the dynamic simulation may cause different kind of imperfections due to the analysis of field component close to any kind of metallic components. Also, the degree of uncertainty associated with the jet engine statistical parameters should also affect the accuracy of dynamic system simulations. Hence, to reduce these system complexities a static system approach (SSA) is proposed as an alternative to the complex DSA method in this chapter.

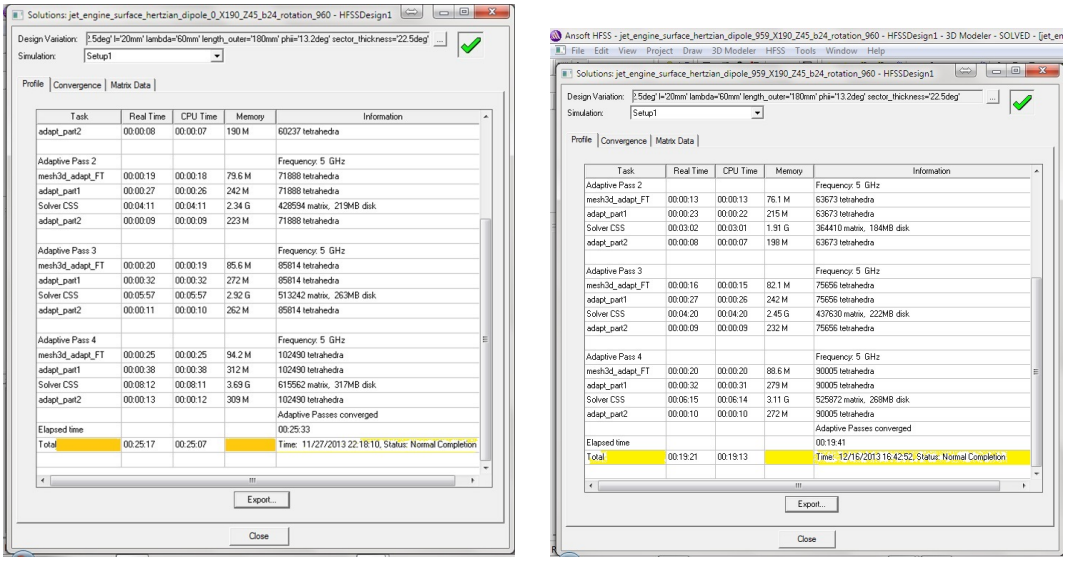

(a) (b)

Figure 6.1 Dyanmic system log file: (a) Initial simulation position. (b) Final simulation position.

6.2 Statistical Excitation Approach

In this thesis, we propose a novel approach for developing an equivalent model for the field generated inside a jet engine with rotating blades and fixed excitation. This model is represented by a fixed blade position and a random excitation inside the engine using the SA concept [15, 16, 17, 82, 83]. The concept of SA has been applied to many applications to characterize the natural randomness arising during the design or manufacturing process of large antenna excitation systems. Previously, SA theory (SAT) was used mainly to identify the influence of random antenna excitation (RA) on antenna performance [17, 18, 84, 85]. In this thesis, SA approach was used as a source of randomness of the medium instead of blade rotation. Consequently, the blade in our model is fixed, and its rotation effect is translated into the antenna excitation by using random source with predefined characteristics. Hence, it is named as statistical excitation approach.

Figure 3.3 shows, the block diagram representation of the two different system used for the statistical analysis. The aim of this analysis is to model the statistical equality between dynamic and static system. However, to analyze the statistical equality between the two systems a simple static jet engine system is modeled with static blades and random excitation. Then, the effect of random excitation on the field characteristics is analyzed to model a generalized static system which is statistically equivalent to the dynamic system.

6.2.1 Static system model

A simple static system model with a fixed blade position and random excitation is developed for the analysis. In order to randomize the environment a Gaussian distributed excitation is used to illuminate the simplified jet engine model. The inlet of the jet engine model is represented by an open cylinder with a single stage of coplanar rotating blades consisting of 24 blades as shown in Fig. 4.7. Two different excitation positions at X-Z plane are studied to analyze the effect of SE on the field characteristics. They are located at (190 mm, 45 mm) and (180 mm, 75 mm), referred as TX1 and TX2; respectively. For each excitation location, the blade is simulated statically in a fixed position and the excitation value of the Hertzian dipole is changed according to a Gaussian distribution.

We assume the excitation current to form a vector (ΔI) of independent random variables (RV) consisting of 120 observations (similar to 120 blade rotation) and these RV are Gaussian distributed with zero mean and 0.0004 variance. Fig. 6.2 represents the normal fit of Gaussian distribution of the excitation current. A Gaussian distribution has been chosen to ensure the same resulting probability distribution for the field as in the case of analyzing dynamic blades [13, 68].

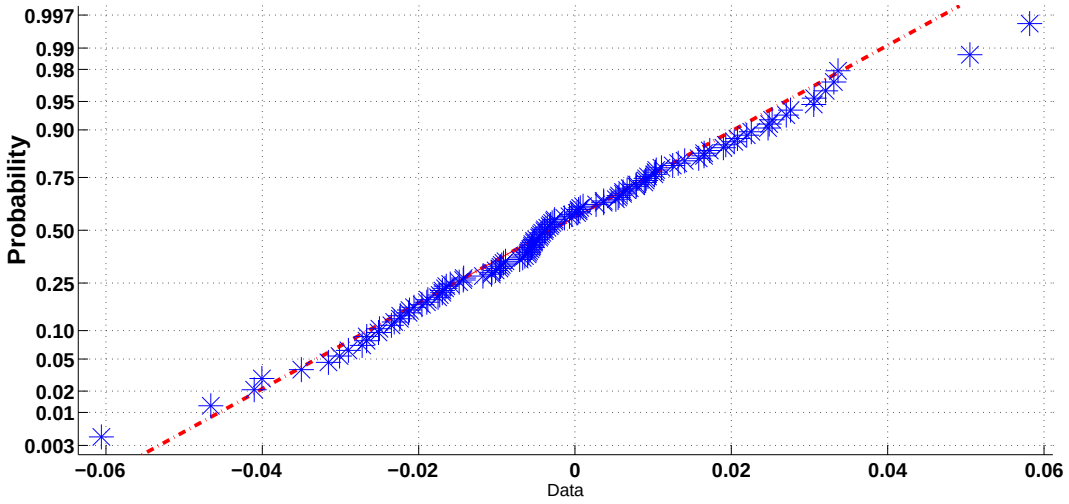

Figure 6.2 Gaussian distributed random variable used for ΔI.

In the DSA method, the Hertzian dipole excitation was characterized by constant value (a) and was equal to 0.012 Am [13, 68]. So the new excitation current; called static excitation (a_s) is obtained as shown in (6.1).

$$a_s = a + \Delta a \tag{6.1}$$

6.2.2 Statistical Analysis

In this section, the statistical analysis of the propagating field for varying excitation current is presented. For each excitation position, we study specified blade positions; namely 1, 25, 50, 75, 100 and 119, instead of analyzing the rotation effect of 120 position of the blades. The blade will be rotated from the starting position by an angle equal to the blade position multiplied by the angular step, which is equal to 0.125 degree. For each blade location we analyze the characteristics of the field propagation 120 times by feeding the varying excitation current (a_s). Later, the field values are extracted for 120 excitation vector observations for each blade locations. The electric field values

are extracted at the circular plane **C** and the field values are extracted upon 17 points distributed over the circle. At each point, we extracted the real and imaginary axial electric field values(E_{zr} and E_{zi}) for 120 different excitation values. The extracted field values are analyzed statistically. This methodology helps to analyze the jet engine without considering its dynamic nature. Moreover, this will ease the simulation processes and helps to predict the output field distribution.

6.2.3 Statistical Results of Antenna Position TX1

Using positions 1, 25, 50, 100, and 119, the E_{zr} and E_{zi} field components along the engine axis are extracted and averaged due to the input random excitation. Fig. 6.3 represents the normal plot for the extracted average field value at RX point 1 ($\theta = 0°$). Normal probability plot assess graphically whether the data could come from a normal distribution [66]. It is clear from the figure that the E_{zr} and E_{zi} field component exhibit a Gaussian field distribution. Furthermore, we analyzed the characteristics of the field component along all 16 RX locations and able to prove that the same result is applied for all other locations.

Later, the field values are analyzed statistically to study the characteristics of the statistical parameters of the field component. Figure 6.4, and Fig. 6.5 represent the mean values (μ) of the Gaussian distribution that represents the real and imaginary field components; respectively. Figure 6.6, and Fig. 6.7 represent the the standard deviation values (σ) of the Gaussian distribution that represents the real and imaginary field components; respectively.

It is clear from the above figures that the mean and standard deviation of the average field values along the engine axis follow a particular characteristics and almost don't have great changes with the different blade positions. However, at some points the graph shows some deviations. The results will be much better

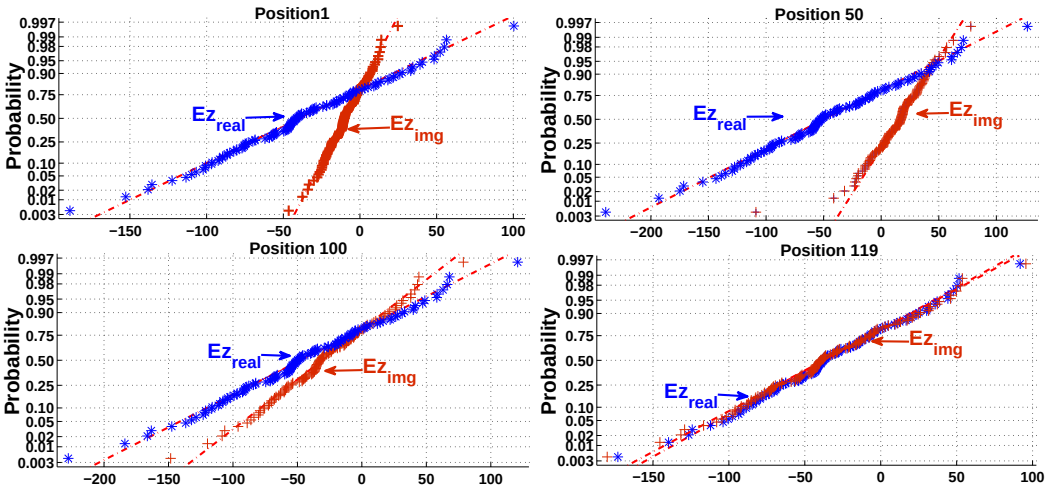

Figure 6.3 Normal probability plots for the field components at RX point 1 resulting from excitation position TX1.

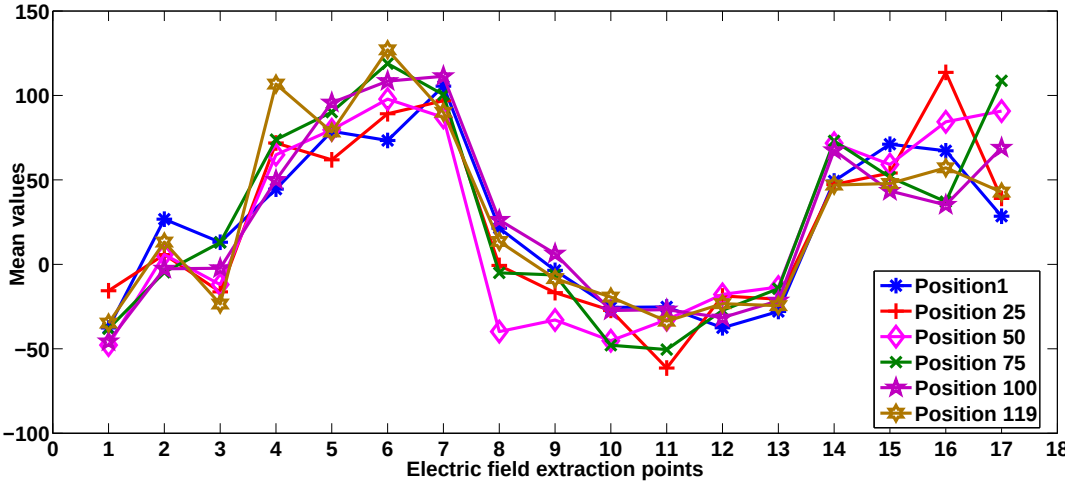

Figure 6.4 Mean values for the real field values resulting from excitation position TX1.

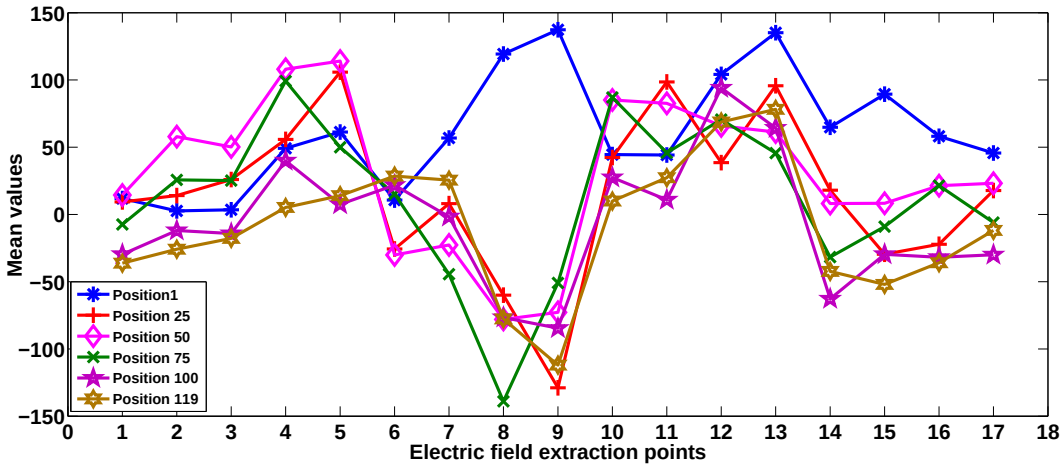

Figure 6.5 Mean values for the imaginary field values resulting from excitation position TX1.

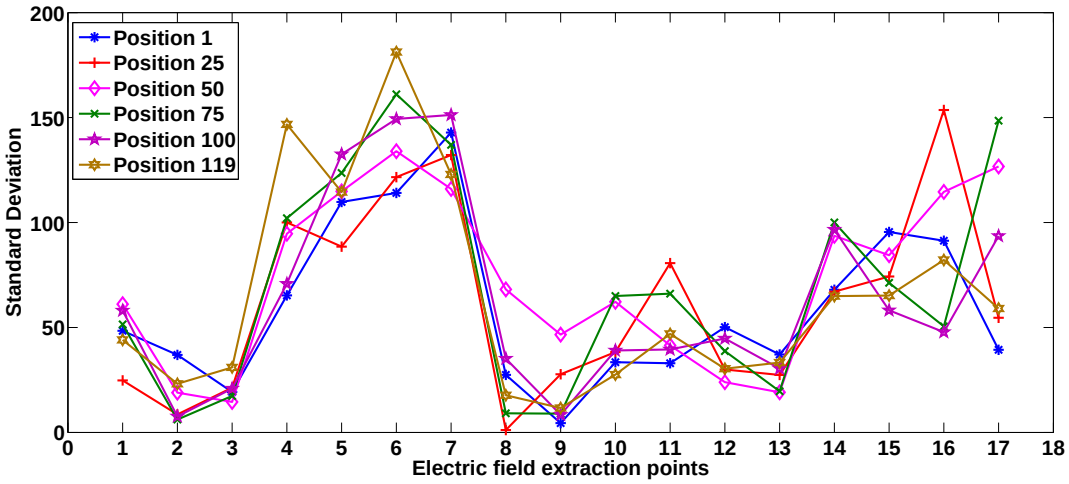

Figure 6.6 Standard deviation for real field values resulting from excitation position TX1.

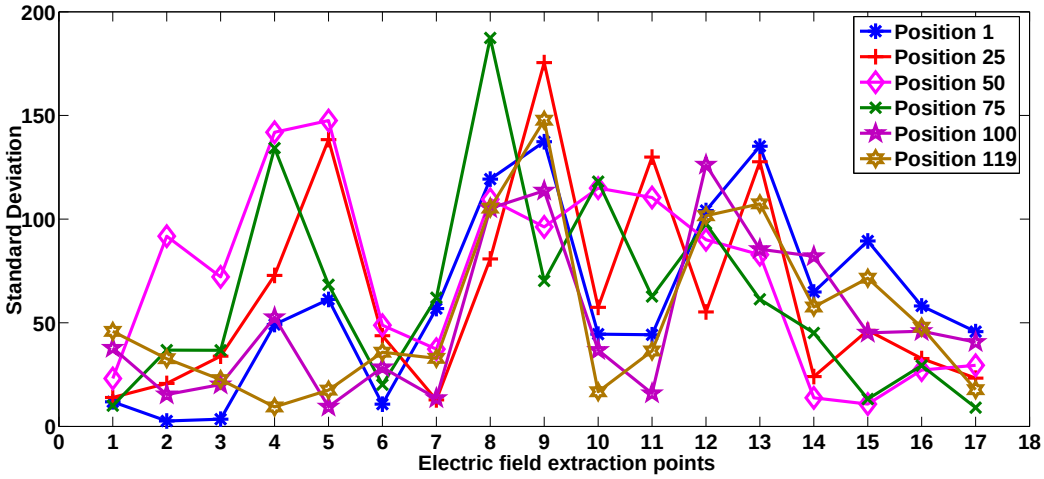

Figure 6.7 Standard deviation for imaginary field values resulting from excitation position TX1.

by increasing the number of excitation values, resulting in increasing the time of simulation.

6.2.4 Statistical Results of Antenna Position TX2

In this section, we study the analysis of the jet engine for excitation position TX2. Here, we use the same blade positions as with excitation position TX1 to extract the field values. Fig 6.8 represents the normal plot for the extracted average field value at point 1. It is clear from the figure that there is a great agreement between the field distribution and the theoretical Gaussian distribution.

Fig. 6.9, and Fig. 6.10, show the mean values of the Gaussian distribution of electric field along the 17 points for excitation position TX2. Simillarly, Fig. 6.11, and Fig. 6.12 show the distribution of standard deviation of electric field along the 17 points for excitation position TX2. It is clear from the figure that the mean values have almost same trend in all positions. However, the

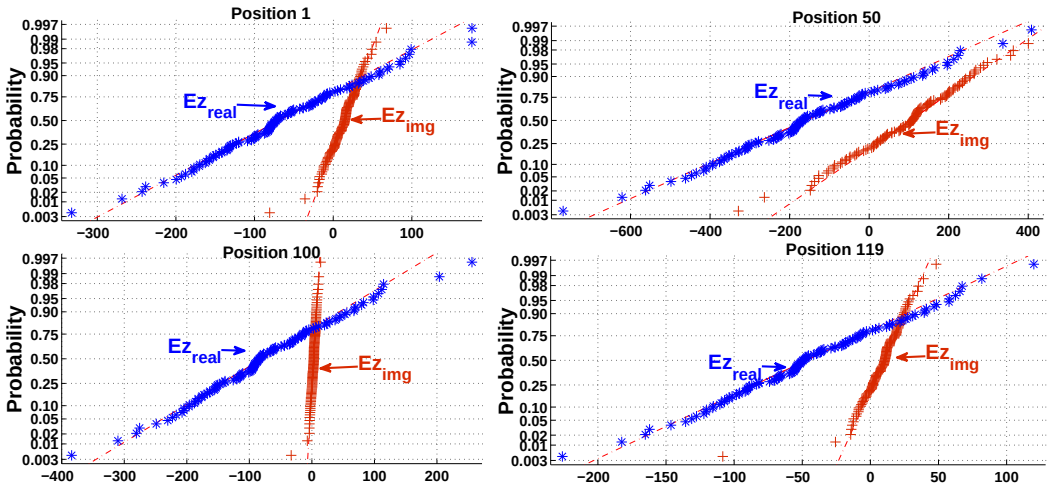

Figure 6.8 Normal probability plots for the field components at RX point 1 resulting from excitation position TX2.

standard deviation graph shows some deviations for a particular excitation position (TX2).

Hence, it is clear from the SE analysis that most of the Gaussian distributions for the field at the specified blade positions have the same μ characteristics. Consequently, independent on the positions of the blade, the Gaussian

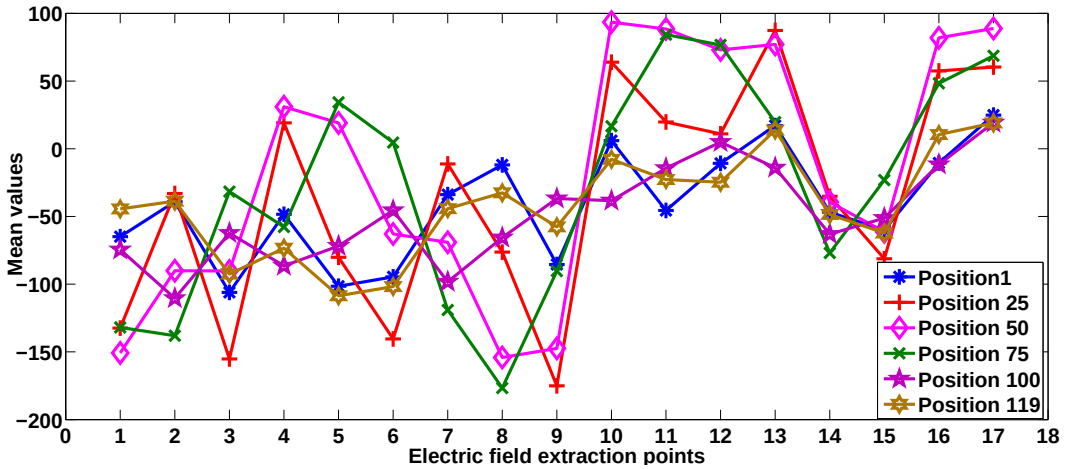

Figure 6.9 Mean values for the real field values resulting from excitation position 2.

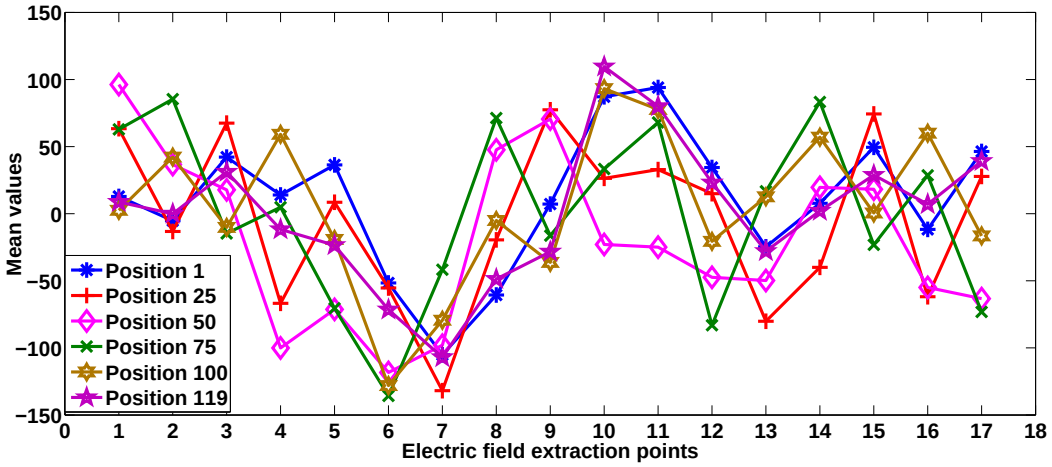

Figure 6.10 Mean values for the imaginary field values resulting from excitation position 2.

distribution of the field, resulting from the random input source will have almost the same parameter. In other words, by controlling the random current excitation parameters, we can get the same distribution for the field as if we have a rotating blade. As a result, the dynamic rotation of the blade can be translated into a statistical excitation. Only these positions are chosen to verify the idea but the same results are almost applied for other positions too. More-

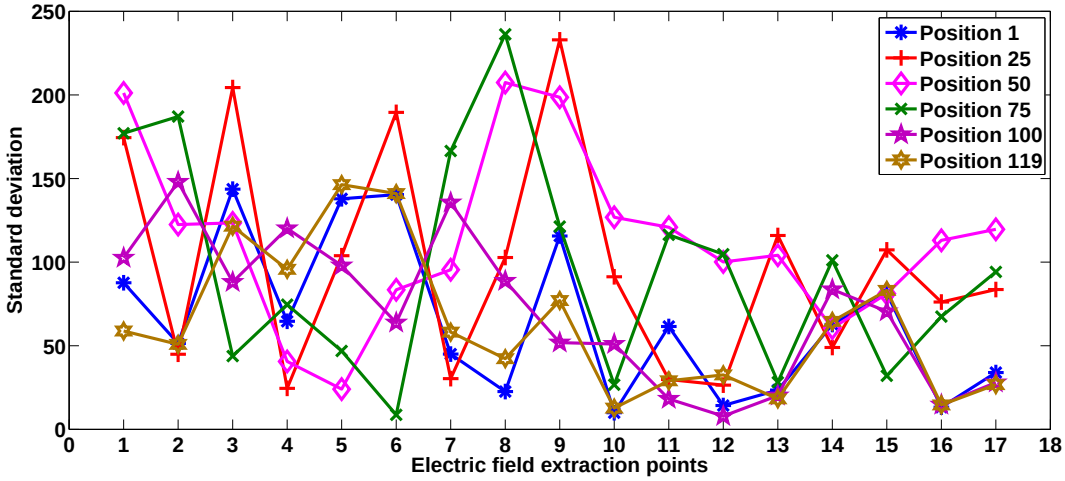

Figure 6.11 Standard deviation for real field values resulting from excitation position 2.

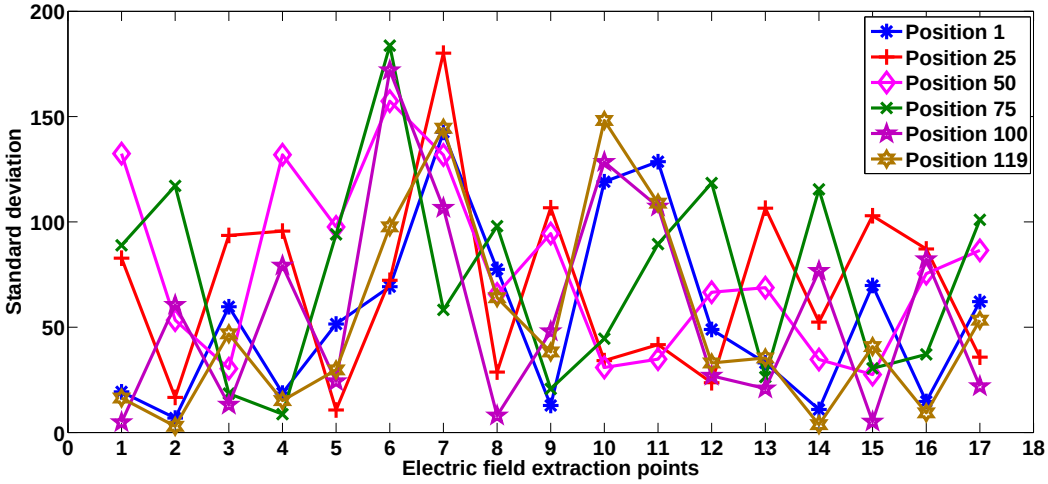

Figure 6.12 Standard deviation for imaginary field values resulting from excitation position 2.

over, by increasing the number of excitation values, the result can be much better; however, this will need much more efforts and time for simulations.

6.3 Generalized Statistical Excitation Model

In the previous section, a simple SE model is proposed to analyze the jet engine environment with out considering the complex blade rotation. The model has been considered as a static environment by using fixed blade position instead of rotating the blade. The excitation values inside the medium have been changed randomly according to a Gaussian distribution with certain characteristics. However, to generalize the SE model an analytical approach is proposed to evaluate the statistical parameters of the random excitation.

As explained before, in the dynamic system the blade rotation induce randomness and the excitation of the dynamic system is characterized by a fixed amplitude (a). In the dynamic system, $E_D(a)$ is the magnitude of the electric field resulting from the fixed antenna excitation, a. The mean and the standard deviation of the electric field in the dynamic system are represented by μ_D

and σ_D; respectively as shown in Fig. 3.3 (a). The static system represented in Fig. 3.3(b) has a random environment resulting from the random excitation (hence the use of SE) and stationary blades. The static system is excited by a constant deterministic antenna excitation, a, and another small random excitation, Δa as given in (6.1). Hence, the random excitation of the static system is characterized by the random amplitude $(a + \Delta a)$. In the static system, $E_S(a+\Delta a)$ represents the magnitude of the electric field due to the randomized excitation. The mean and the variance of the electric field in the static system is represented as, μ_S and σ_S, respectively. The SE method helps to develop an equivalent model for the fields generated from the dynamic system model.

Hence, the Δa is chosen to have the same statistical distribution as that of dynamic system model with statistical parameters; mean, μ_Δ, and standard deviation, σ_Δ. Moreover, 120 random samples of Δa have been generated in response to the 120 blade rotation in dynamic system. It is important to mention that the statistical parameters of Δa; such as mean (μ_Δ), and variance (σ_Δ^2) have to be controlled to gain statistical equality between the two systems. That means, the effect of rotation of the blades in the dynamic system can be translated into the random excitation in the static system. As a result, instead of simulating the rotation of the blades inside the engine, the engine will be considered as a static system without blades rotation but with a random excitation.

6.3.1 Derivation for the statistical parameters of Δa

Analyzing the EM propagation inside the dynamic system is extremely complex, since for each blade rotation step, a full simulation has to be carried out and the field values have to be extracted. This process is time consuming and needs powerful machines with large memory. In order to replace the dynamic system statistically by the static system, statistical parameters of Δa have to be controlled to guarantee statistical equivalency of resulting electric fields in both dynamic and static systems. Hence, μ_S and σ_S are assumed to be equal to μ_D and σ_D, respectively. The statistical parameters of Δa, i.e., μ_Δ and σ_Δ, are deduced accordingly, as shown in the following.

$$\mathbf{E}[E_D(a)] = \mathbf{E}[E_S(a + \Delta a)], \tag{6.2}$$

where $\mathbf{E}[x]$ is the expected value of x.

$$\mathbf{Var}[E_D(a)] = \mathbf{Var}[E_S(a + \Delta a)], \tag{6.3}$$

where $\mathbf{Var}[x]$ is the variance of x.

Now, applying Taylor series expansion for $E_S(a + \Delta a)$.

$$E_S(a + \Delta a) = E_S(a) + \Delta a \frac{\partial E_S(a)}{\partial a} + \frac{1}{2}(\Delta a)^2 \frac{\partial^2 E_S(a)}{\partial a^2} + O(|\Delta a|^2), \tag{6.4}$$

where $E_S(a)$ is the magnitude of the electric field for stationary blades due to the fixed excitation a. The value of Δa is assumed to be very small compared to a; hence, we can use small signal analysis utilizing first order Taylor series expansion with first derivatives only to characterize the static system.

Consequently,

$$E_S(a + \Delta a) \approx E_S(a) + \frac{\partial E_S(a)}{\partial a}\Delta a. \tag{6.5}$$

Taking the expectation of (6.5), we get;

$$\mathbf{E}\left[E_S(a + \Delta a)\right] = \mathbf{E}\left[E_S(a)\right] + E\left[\frac{\partial E_S(a)}{\partial a}\Delta a\right] \tag{6.6}$$

Since, a is a deterministic constant, $\mathbf{E}[E_S(a)] = E_S(a)$. Accordingly, (6.6) can be rewritten as

$$\mathbf{E}\left[E_S(a + \Delta a)\right] = E_S(a) + \frac{\partial E_S(a)}{\partial a}\mathbf{E}\left[\Delta a\right]. \tag{6.7}$$

From (6.2) and (6.7),

$$\mathbf{E}[\Delta a] = \frac{\mathbf{E}[E_D(a)] - E_S(a)}{(\partial E_S(a)/\partial a)} = \mu_\Delta. \tag{6.8}$$

Later, from the definition of the variance of a random variable,

$$\mathbf{Var}(X) = \mathbf{E}\left[(X - \mathbf{E}[X])^2\right] \tag{6.9}$$

Applying (6.9) in (6.3),

$$\begin{aligned}
\mathbf{Var}[E_S(a + \Delta a)] &= \mathbf{E}\left[(E_S(a + \Delta a) - \mathbf{E}[E_S(a + \Delta a)])^2\right] \\
&= \mathbf{E}\left[\left(E_S(a) + \frac{\partial E_S(a)}{\partial a}\Delta a - E_S(a) -\right.\right.
\end{aligned}$$

$$\frac{\partial E_S(a)}{\partial a}\mathbf{E}[\Delta a]\Big)^2\Big],$$

i.e.,

$$\begin{aligned}\mathbf{Var}[E_S(a+\Delta a)] &= \mathbf{E}\left[\left(\frac{\partial E_S(a)}{\partial a}\right)^2(\Delta a-\mathbf{E}[\Delta a])^2\right] \\ &= \left(\frac{\partial E_S(a)}{\partial a}\right)^2\mathbf{Var}(\Delta a). \qquad (6.10)\end{aligned}$$

Substituting $\mathbf{Var}[E_S(a+\Delta a)]$ from (6.3), we get

$$\mathbf{Var}(E_D(a)) = \left(\frac{\partial E_S(a)}{\partial a}\right)^2\mathbf{Var}(\Delta a), \qquad (6.11)$$

$$\mathbf{Var}(\Delta a) = \frac{\mathbf{Var}[E_D(a)]}{(\partial E_S(a)/\partial a)^2} = \sigma_\Delta^2. \qquad (6.12)$$

The equations (6.8) and (6.12), represents the statistical characteristics of Δa. From (6.8), and (6.12), it is clear that the mean value and the variance of the random excitation parameter depends on the mean and variance of the dynamic system electric field. Since, the jet engine environment is similar to a RC environment, the mean and the variance of the axial electric field components of the dynamic system can be analyzed using the **n** plane wave coupling method explained in [65]. Here, we consider only a particular receiver location ($\theta = 0°$) and excitation position. Then, the mean value of the amplitudes of the field rectangular components and the mean square value of the field rectangular components resulting from the sum of **n** (**n** is a free parameter) random plane waves can also be evaluated using this plane wave coupling approach as in (6.13) and (6.14) [65]. A detailed analysis is available in appendix A.

$$\langle |E_D| \rangle = E_0 \cdot \sqrt{\mathbf{n}} \cdot \sqrt{\frac{\pi}{12}} \tag{6.13}$$

$$\langle |E_D|^2 \rangle = \frac{E_0^2 \cdot \mathbf{n}}{3} \tag{6.14}$$

Later, using (6.8) and (6.12), 120 random samples of Δa is generated for a particular receiver location and this random samples are used to set up (6.1) to feed the static system model.

6.3.2 Analysis of $E_s(a + \Delta a)$

In this section, a numerical approach using the small signal analysis is used to validate the SE method. Initially, a 120 samples of Gaussian distributed random excitation; Δa for the static system is generated by using (6.8) and (6.12). Later, the small signal equation is used to generate the values of $E_s(a + \Delta a)$ as in (6.5) for all the 120 random excitation. The magnitude of the output electric field values, $E_s(a+\Delta a)$, are evaluated at a particular receiver point and are analyzed statistically. Later, the statistical characteristics of the magnitude of the electric field values are analyzed. The μ_S, and σ_S of the average electric field values are generated using numerical approach and given in Table 6.1.

Table 6.1 Statistical parameters of the dynamic and static systems computed by HFSS and MATLAB, respectively.

Point	μ_D	μ_S	σ_D	σ_S
Pt.1	49.5491	49.5400	26.1629	26.3109
Pt.2	46.4027	45.6944	26.3766	25.3916

Table 6.1 represents the comparison of the statistical parameters of the dynamic and the static system model; ie; μ_D and μ_S, σ_D and σ_S. It is important to mention that the dynamic system parameters are due to the dynamic blade rotation (DSA) inside the simulation environment where the static system parameters are evaluated using numerical approach. It is clear from Table 6.1 that the two systems almost have the same mean and variances and hence proved that the static jet engine environment is statistically equivalent to the dynamic system. Furthermore, this analysis proved that SE method can replace the complex simulation analysis method to analyze the EM characteristics inside the jet engine environment. It is important to mention that the SE method which analyze the **segment 1** numerically, helps to eliminate the complex dynamic simulations.

6.3.3 Validation Of Static System Using Simulation Approach

In this section, the characteristics of $E_s(a+\Delta a)$ of the static system evaluated using numerical approach is validated using the HFSS simulation analysis. The SE system model is simulated with a stationary blade position and a random current source as an excitation $(a+\Delta a)$. μ_Δ and σ_Δ for the receiver points are calculated using (6.8) and (6.12). 120 random samples of the Gaussian distributed Δa are generated using the calculated mean and variance corresponding to each receiver probe location. The total Gaussian distributed random excitation current for the static system is generated as in (6.1). Then, the static system is simulated for 120 random excitation. The $E_s(a+\Delta a)$ is extracted from a particular receiver location and analyzed statistically. It is found that the real and the imaginary components of the electric field along the engine axis are Gaussian distributed with different means and variances as

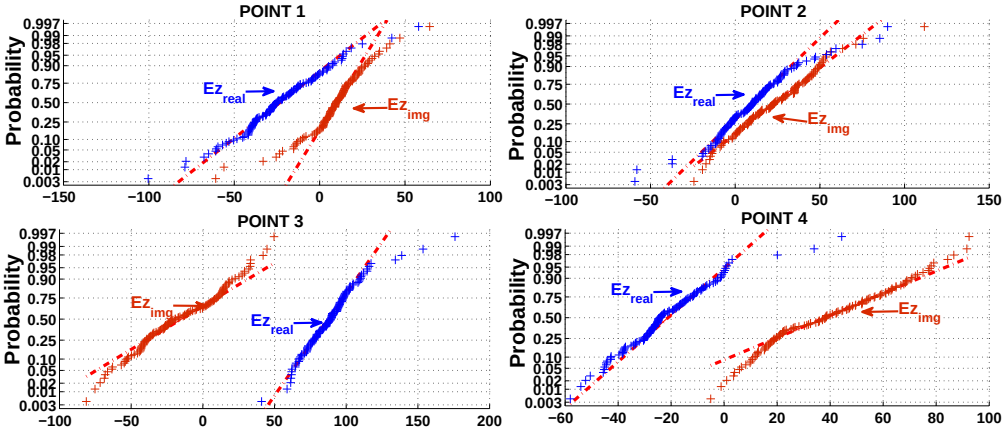

Figure 6.13 Normal probability plots of $E_s(a + \Delta a)$ along the cylindrical jet engine.

shown in Fig. 6.13, when the excitation is located at other than λ position. The normal probability plot of the extracted field components shows a strong linear pattern which justifies the Gaussian distribution [66]. The statistical parameters of the static system is also analyzed and proved that the static system model is statistically equivalent to the dynamic system model.

Table 6.2 represents verification of the numerical approach used for the evaluation of statistical parameter of the static system using FEM simulation method. The static system parameters are extracted by using FEM HFSS sim-

Table 6.2 Comparison between numerical and simulation approach statistical parameters of the static system model.

Point	μ_s (numerical)	μ_S (FEM simulation)	σ_s (numerical)	σ_S (FEM simulation)
Pt_1	49.5400	40.0100	26.3109	26.5577
Pt_2	45.6944	47.8133	25.3916	27.4004

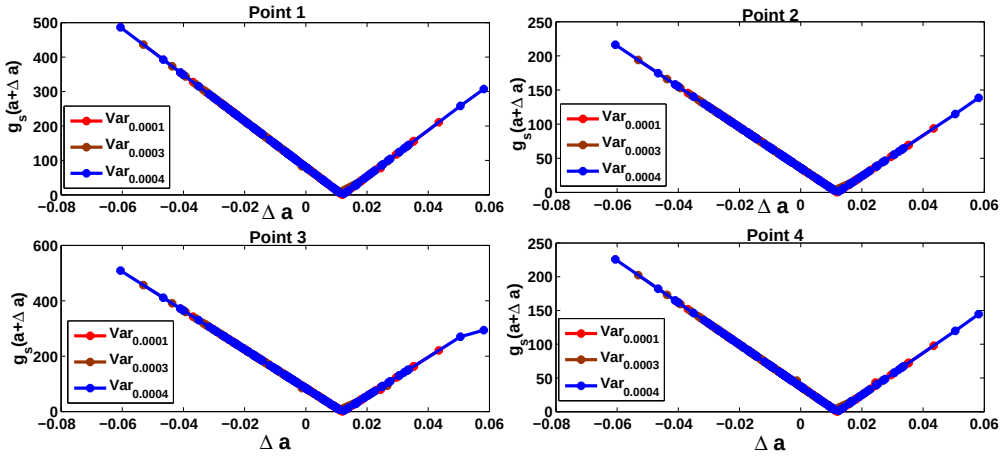

Figure 6.14 Change of $g_s(a + \Delta a)$ with respect to Δa.

ulation method is compared with the parameters evaluated using the numerical approach. From the table it is clear that both data are statistically equivalent. Hence, the numerical results are validated with the help of simulation analysis.

Later, we study the the linearity characteristics of $E_s(a + \Delta a)$. Fig. 6.14 represents a plot of $E_s(a + \Delta a)$ with the random variable Δa at different RX points. The mean value of Δa is set to zero and the simulations are done for different variances of Δa for each point. Fig. 6.14 represents the linear relationship between $E_s(a+\Delta a)$ and Δa at each point and it is independent of the value of variances of Δa . The regression analysis is then performed over the plot for every point to calculate the parameter $\partial E_S/\partial a$. The 'Regress' operation will provide the slope of the line that best predicts the values in Y axis from X axis [86]. It is clear from Fig. 6.14 that there is a linear relationship between $E_s(a + \Delta a)$ and the random excitation Δa, which proves that our assumption of ignoring higher order derivative in Taylor series expansion is valid. Moreover, at each point, the slope of the curve does not change by changing the values of Δa variances.

It is clear from the Table 6.1 and Table 6.2 that the two systems almost have the same mean and variances. However, it is proved that the numerical approach based on matlab is generally more desirable than a simulation method due to its simplicity in implementation and ability to meet the requirement of large scale complex systems.

Verification of Linearity of the Dynamic System

In this section, we tried to verify the hypothesis that the dynamic jet engine system is statistically linear and hence; to verify the linearity of statistical parameters of the electric field quantity. As explained before, the continuous wave excitation for the dynamic system is provided by a Hertzian dipole excitation, a. In order to study the linearity concept, the dynamic system is simulated using three different excitation currents ($a1$=0.075 Am, $a2$=0.012 Am, and $a3$=0.015 Am). The electric field values are analyzed statistically and Table 6.3 represents the statistical properties of the dynamic system, μ_D and σ_D, at different receiving locations.

Table 6.3 Dynamic system parameters when excitation is located at (190 mm, 75 mm).

	$a1$		$a2$		$a3$	
Point	μ_D	σ_D	μ_D	σ_D	μ_D	σ_D
Pt.1	30.9682	16.3518	49.5491	26.1629	61.9363	32.7037
Pt.2	29.0017	16.4854	46.4027	26.3766	58.0034	32.9708
Pt.4	54.8043	11.3013	87.6869	18.0821	109.6086	22.6026
Pt.6	60.4332	11.1247	96.6931	17.7995	120.8664	22.2494

In order to verify the linearity, the multiplicative property for μ_D and σ_D can be easily verified from Table 6.3 by verifying that $\mu_D(\text{a1})/\mu_D(\text{a3}) \approx 1/2$. Next, to verify the additive property, the simulation is repeated for a new condition of $(a1 + a2)$. The newly evaluated μ_D and σ_D are compared with the sum of the corresponding parameters from Table 6.3. It is clear from the Table 6.3, Table 6.4 and Table 6.5 that μ_D, and σ_D are statistically linear in input excitation and able to verify the linearity hypothesis of dynamic system.

Table 6.4 Dynamic system characteristics when excitation is located at (190 mm, 75 mm).

	Using $(a1 + a2)$		From Table 6.3	
Point	$\mu_D(a1 + a2)$	$\sigma_D(a1 + a2)$	$\mu_D(a1) + \mu_D(a2)$	$\sigma_D(a1) + \sigma_D(a2)$
Pt.1	80.5173	42.5147	80.5173	42.5147
Pt.2	75.4044	42.862	75.4044	42.862
Pt.4	142.4912	29.3833	142.4912	29.3834
Pt.6	157.1263	28.9243	157.1263	28.9242

Table 6.5 Dynamic system characteristics when excitation is located at 190 mm, 75 mm.

	Using $(a1 + a3)$		From Table 6.3	
Point	$\mu_D(a1 + a3)$	$\sigma_D(a1 + a3)$	$\mu_D(a1) + \mu_D(a3)$	$\sigma_D(a1) + \sigma_D(a3)$
Pt.1	92.9045	49.0555	92.9045	49.0555
Pt.2	87.0051	49.4561	87.0051	49.4562
Pt.4	164.4129	33.9038	164.4129	33.9039
Pt.6	181.2995	33.3741	181.2995	33.3741

Table 6.6, Table 6.7 and Table 6.8 represents the statistical characteristics of electric field due to TX antenna excitation located at 190 mm, 75 mm from the center of the axis. This analysis also proves the dynamic system is statistically linear in input excitation and able to verify the linearity hypothesis of dynamic system.

Table 6.6 Dynamic system parameters when excitation is located at (190 mm, 45 mm).

	$a1$		$a2$		$a3$	
Point	μ_D	σ_D	μ_D	σ_D	μ_D	σ_D
Pt.1	45.9536	15.3199	73.5258	24.5119	91.9072	30.6399
Pt.2	34.9515	16.6853	55.9224	26.6964	69.903	33.3705
Pt.4	38.6934	19.7549	61.9095	31.6079	77.3868	39.5099
Pt.6	57.4473	12.0181	91.9157	19.2289	114.8947	24.0361

Table 6.7 Dynamic system characteristics when excitation is located at (190 mm, 75 mm).

	Using $(a1 + a2)$		From Table 6.3	
Point	$\mu_D(a1 + a2)$	$\sigma_D(a1 + a2)$	$\mu_D(a1) + \mu_D(a2)$	$\sigma_D(a1) + \sigma_D(a2)$
Pt.1	80.5173	42.5147	80.5173	42.5147
Pt.2	75.4044	42.862	75.4044	42.862
Pt.4	142.4912	29.3833	142.4912	29.3834
Pt.6	157.1263	28.9243	157.1263	28.9242

Table 6.8 Dynamic system characteristics when excitation is located at 190 mm, 75 mm.

	Using $(a1 + a3)$		From Table 6.3	
Point	$\mu_D(a1 + a3)$	$\sigma_D(a1 + a3)$	$\mu_D(a1) + \mu_D(a3)$	$\sigma_D(a1) + \sigma_D(a3)$
Pt.1	92.9045	49.0555	92.9045	49.0555
Pt.2	87.0051	49.4561	87.0051	49.4562
Pt.4	164.4129	33.9038	164.4129	33.9039
Pt.6	181.2995	33.3741	181.2995	33.3741

6.4 Summary

In this chapter, we analyzed propagation characteristics of EM field inside the jet engine environment using SE approach. The magnitude of the electric field has been extracted and analyzed to obtain the statistical parameters of the dynamic system which are used to set the parameters of the static system in order to establish statistical equivalence between the two systems. The static system model is represented by a fixed blade position while the excitation is randomized. The effect of excitation on the field characteristics of the dynamic and static systems has been analyzed and verified that both the systems are statistically linear with respect to input excitation. The result of numerical analysis of the static system model agrees well with the result of FEM simulation results. Numerical results demonstrate the reliability of the proposed SE technique. The statistical equivalence between the two systems has been verified. Since the static system is significantly computationally simpler, the proposed static approach will help in analyzing complex dynamic systems such as jet engines without the need for repeated complex simulations stemming from blades ro-

tations. It is important to mention that this method is sufficiently accurate yet simple enough to describe the fields inside the complex and dynamic cavity environments compared to the classical deterministic perspective.

Chapter 7: Doppler Effect in Jet Engine Analysis

7.1 Introduction

As explained in previous chapters, analysis of EM propagation inside jet engine turbines and hence to extract the field values from arbitrarily shaped dynamic model geometry having large sizes, blade rotation, complex terminations, and cross-section variations is extremely difficult. The dynamic jet engine environment is generally characterized as a multipath fading environment, because of the movement of the transmitter, receiver or the rotational movement of the blades [87]. The rotation of the blades in the dynamic jet engine system introduces a Doppler effect which introduces phase noise in the received signal of the dynamic system. Consequently, the frequency spectrum of the received signal will be widen and hence, a frequency shift between the transmitted and the received signal will be produced. Hence, to model the statistical characteristics of the electric field inside the dynamic system, the phase deviation of the electric field value due to Doppler shift should be evaluated.

Moreover, the analysis of the amplitude and phase distortion characteristics of EM signals inside the jet engine environment due to the Doppler frequency shift is essential to define the communication channel characteristics of micro size wireless sensors, attached to the turbine blades that measure parameters such as strain, temperature, and pressure. This will introduce an

extra challenge for modeling the communication channel inside the engine environment. Different approaches were available in literature for analyzing the effect of Doppler spectrum inside RC environment [88, 89, 90, 91, 92] . The Doppler effect inside RC has been analyzed either by observing the power variation by sweeping intermediate frequency or by assumed stirrer speed estimation [89, 90]. However, in this thesis the effect of frequency spread on the electric field characteristics inside the jet engine environment is analyzed. In this novel approach, the Doppler spread inside the jet engine environment is evaluated for an assumed stirrer speed. Later, this Doppler spread is emulated inside the engine environment to study the effect of Doppler spread on field characteristics.

7.2 Jet engine Model

To simplify the complexity of jet turbine geometry, a simplified jet engine system segment is considered for the analysis as shown in Fig. 7.1. The simplified segment is modeled with Ansyst HFSS FEM software. The inlet of the jet engine model is represented by an open cylinder with a single stage of coplanar rotating blades consisting of 24 blades, mounted on a central shaft and extended to the wall of the cylinder as shown in Fig. 4.7. The scaled frequency (F_0) used for modeling the system is 5 GHz. The system has a Hertzian-dipole excitation (a) as a simple transmitting excitation that radiates continuous wave fields and is located at a distance λ from the center of the axis. The receiving probes are located at different positions on a circular plane **C** as shown in Fig. 4.7 (c). As mentioned before, Plane **C** is a circular plane and is located at a distance 6.6 cm away from the central axis along the $-Z$ axis.

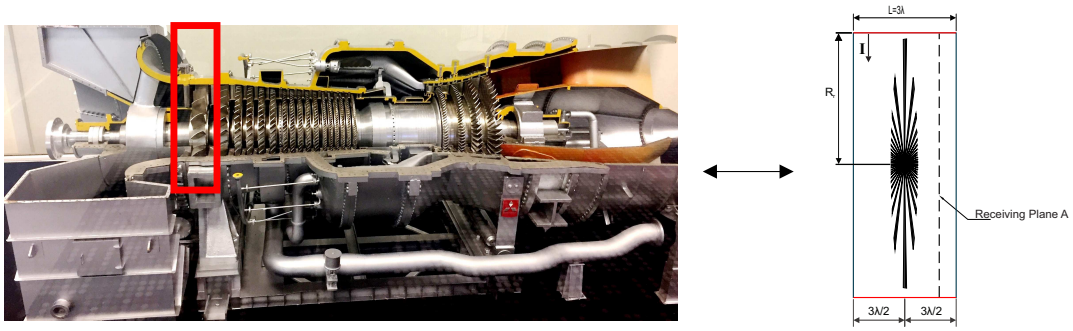

Figure 7.1 Segmentation of complex jet engine turbine.

7.3 Analysis

As explained before, a Doppler frequency shift is existing inside the jet engine environment as a result of the blade rotation or the movement of the transmitting and the receiving antennas. In this thesis, both the transmitting antenna excitation and the receiving probes are made stationary; hence, the randomness inside the medium is only due to the rotational movement of blades in the environment. In this analysis, a stepwise rotation (mode stirred) of the blades are used to generate randomness inside the environment. It is worth to mention that the Doppler frequency spread inside a complex cavity can be analyzed efficiently for a fictitious stirrer rotational movement although the measurements are done when the stirrers are stationary [90]. Hence, it is assumed that the blades inside the jet engine are stirred at the rate of 20,000 Revolutions Per Minute (RPM)[?, 72]. Then, the Doppler shift inside the jet engine is set according to the engine RPM using (7.1) [90].

$$F_D = 2piR_r\omega/\lambda \text{ [90]} \tag{7.1}$$

Where, F_D is the Doppler frequency shift due to the blade rotation , λ is the wavelength, r is the radius and ω is the angular velocity of the blade rotation. The Doppler spectrum (F_S) extends over the range (F_0 - F_D) to (F_0 + F_D), where F_0 is the center frequency. For a used jet engine RPM of 20,000 and by using 7.1, (F_S) will extend over the range (5GHz $\pm$ 6632 Hz) and the Doppler frequency range is distributed over a frequency axis (F_{5^-}, F_{4^-}, F_{3^-}, F_{2^-}, F_{1^-}, F_{5^-}, F_0, F_{1^+}, F_{2^+},F_{3^+},F_{4^+},F_{5^+}).

7.4 Simulation Analysis and Results

As a primary analysis to evaluate the effect of emulated Doppler frequency shift on the amplitude of the electric field, the dynamic jet engine structure has been simulated over F_S. For each frequency of the spectrum, the jet engine model is simulated for 240 distinct positions of the blade rotation with 0.0625° angular increase to ensure the randomness inside the medium. The magnitude and phase of the electric field component along the Z axis is extracted from the receiving probes for each frequency to analyze the statistical characteristics. Then, the electric field values (E_z) are averaged at each receiving location to study the effect of frequency deviation on the field magnitude and phase.

Fig. 7.2 shows the behavior of the magnitude of the $|E_z|^2$ electric field component at different receiving locations in the used frequency range, represented as; $E_{F_{5^-}}$, $E_{F_{4^-}}$, etc;. Fig. 7.2 indicates the statistical analysis of the extracted field values along θ from 0° to 90° only, due to the symmetry inside the environment. From Fig. 7.2, it is clear that the electric field strength at different probe location is varying due to the blade rotation and the random environment.

Later, the phase variation of the electric field due to the jet engine blade rotation is analyzed statistically as shown in Fig. 7.3.

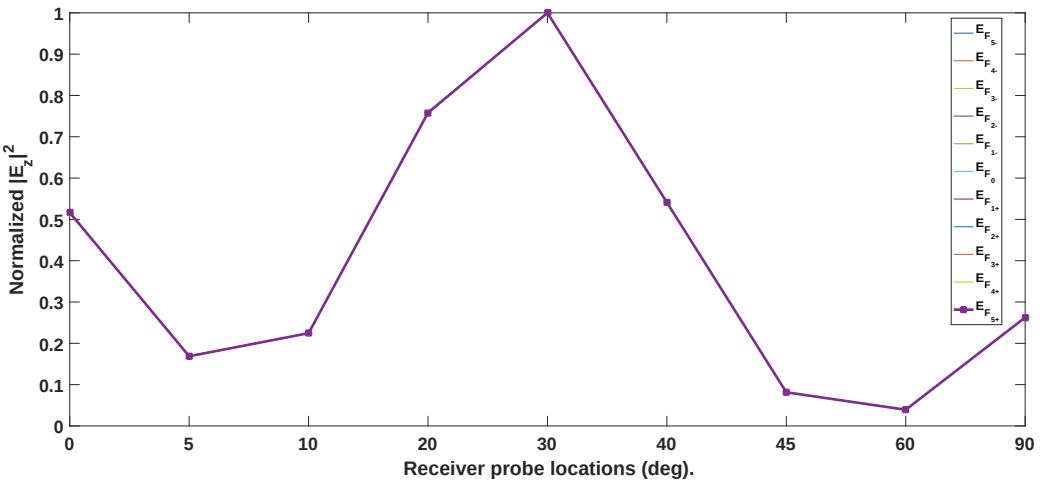

Figure 7.2 Effect of frequency on electric field values.

From Fig. 7.3, it is clear that the phase of the received signal is varying inside the jet engine environment. Figure. 7.4 shows the comparison of the phase deviation at two different receiving locations inside the jet engine environment. It is clear from the analysis that at $\theta = 90°$, the phase deviation (0.08 rad) is very small compared to other receiver location (-2.76 rad) and is less affected by the Doppler frequency shift. Hence, $\theta = 90°$ probe location can be considered

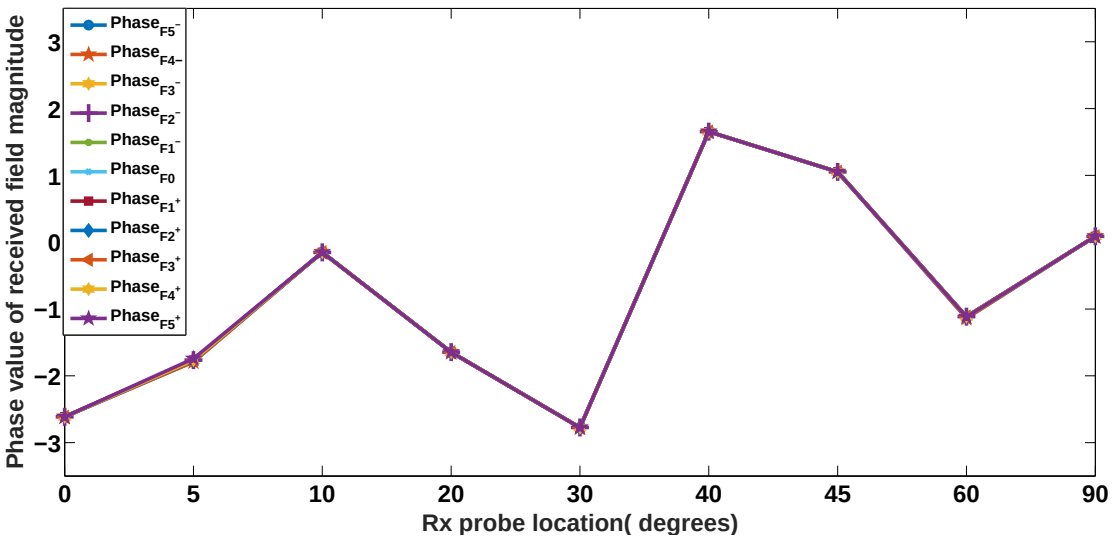

Figure 7.3 Phase deviation as a function of receiver location.

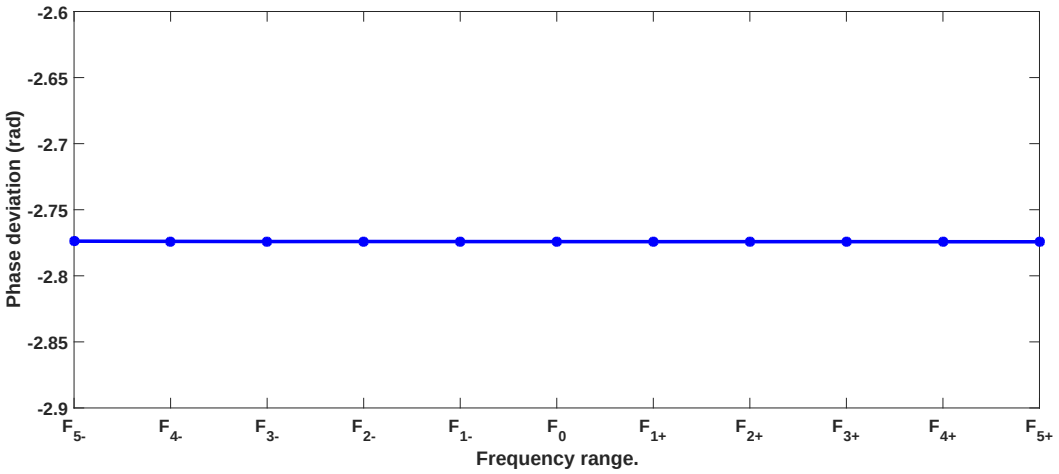

(a)

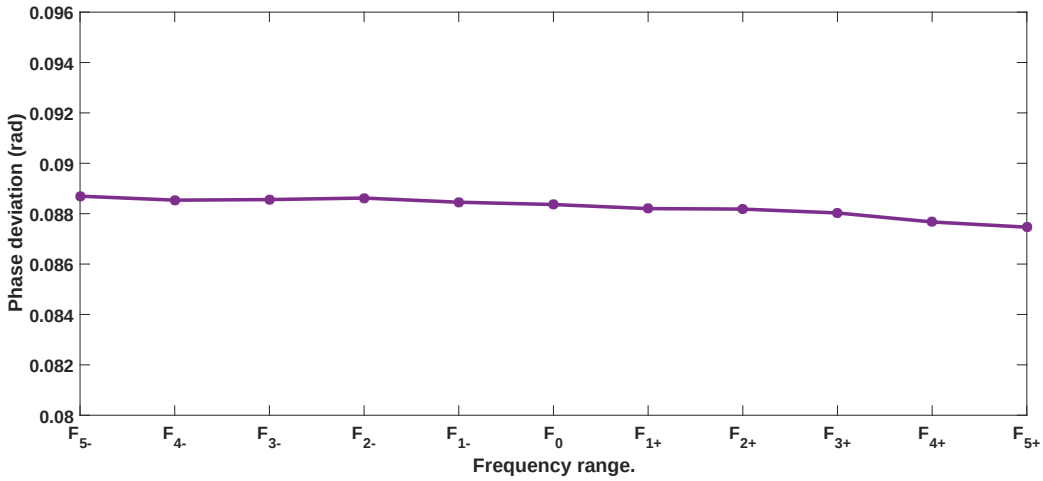

(b)

Figure 7.4 Phase of the electric field component at (a) θ =30° (b) θ =90°.

as the best location for the receiving antenna because of very small phase shift in the received signal. Furthermore, this analysis helps to model a generalized static jet engine system by emulating the magnitude and phase time variations of the field due to the blade rotation into the random excitation inside the engine by using the SE concept.

The results are promising for the future mathematical modeling of the communication channel inside static jet engine environment by varying the magnitude and phase of the random excitation. Moreover, by considering the time

derivative of the phase(ϕ), the Doppler frequency shift induced by the jet engine rotational motion can be evaluated without considering the dynamic rotational speed of the engine blade by using (7.2).

$$f_D = \frac{1}{2\pi}\frac{d\phi}{dt} \tag{7.2}$$

7.5 Summary

A simplified jet engine model is analyzed to study the effect of frequency shift due to the blade rotation on the magnitude and phase of the received electric field inside the jet engine environment. The analysis is based on the theoretical Doppler spectrum method, where the Doppler frequency shift is calculated for a particular RPM. The results show that the amplitude deviation due to frequency shift is negligible at some particular receiving probe location. Later, the effect of the blade rotation on the phase deviation of the field value is analyzed. This analysis plays a great role in choosing the best receiving location inside the jet engine environment, where the propagation of the EM field is less affected by the complex blade rotation. The results are promising for the future statical excitation based jet engine system development by emulating the phase and magnitude deviation due to blade rotation into random excitation and hence the jet engine can be considered as a static system without blade rotation. Moreover, the results can guide the future Doppler spectrum analysis by using phase time variation of the transmitting and receiving signal inside the jet engine without considering the dynamic rotational speed of the blades.

Chapter 8: Conformal Antenna Design for Jet Engine Application

8.1 Introduction

The jet engine environment has extremely high temperature and pressure which affect the rotating parts of the engine turbine. Condition monitoring of such parts of an aircraft is necessary to avoid engine failures and in the case of in-service engines, the need for wireless sensors in rotating equipment is self-explanatory. The sensors and accompanying electronic devices must be able to make sure that the variations in engine attributes like temperature and pressure abnormalities are reliably captured and transmitted. This will enhance the possibility to enable better planning for maintaining the attributes up to an allowable limit. In order to set up a decisive wireless network to extract different engine parameters from the high-temperature metallic cavity, we need to consider different constraints that will affect the performance of the antenna system.

The antenna should be low profile with extremely thin substrate to fit the environment which has many complex components. Moreover, the proposed antenna should be resistant to chemicals and high moisture conditions. It is also important to mention that the antenna should radiate conical beams since they may be attached to the surface of the environment. Hence, we choose microstrip patch antenna for this particular application. Microstrip patch an-

tennas have been widely used in wireless system applications because of their attractive features such as compact structure, light weight due to the absence of heavy metal stamped and ease of fabrication because of printed circuit technology. Moreover, the radiation pattern and the polarization characteristics of the microstrip antennas depends on the excitation of modes and the shape of the patch. Various shapes of the patches are proposed for these types of antennas, such as circular, square, triangular, elliptical, ring etc; [93].

It is important to mention that some particular antenna applications require high antenna directivity, while maintaining the low-profile structure. This requirement leads to the development of patch antenna arrays. Patch antenna arrays exhibit low weight and low profile with conformability. Moreover, the manufacturing cost of patch array is less compared to other commercial antenna array systems. Because of these advantages, in this thesis we mainly focused on the analysis and design of patch antenna arrays that can be used inside harsh environment. We analyzed characteristics of circular, half circular and rectangular patch antenna model to design a novel antenna system for jet engine environment.

8.1.1 Circular Patch Antenna

The circular patch antenna (CPA) geometry is the simplest geometry, since it requires only one parameter (radius) to describe the antenna characteristics and hence there is only one degree of freedom to control the dimension of the patch as shown in Fig. 8.1. The change in the radius of the patch affect the resonant frequency (fr) as shown in (8.1), where m, n represents the mode number, R_{eff} is represented as the effective radius of the patch antenna which is higher than the actual patch radius (R) due to the effect of fringing. The resonant frequency (f_r) of the TM_{nm} mode in the CP antenna can be evaluated

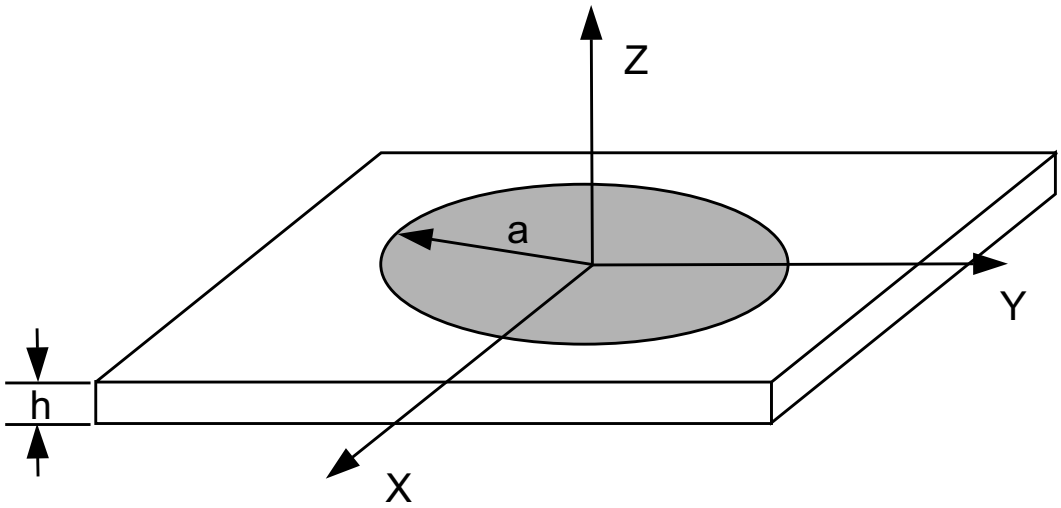

Figure 8.1 Circular patch antenna.

also using (8.2), and R_{eff} can be found from (8.3), where χ_{nm} is the root of the Bessel function equation $J_n(x)$, $K_1 = \kappa_0\epsilon_r$ and κ_0 is the free space wave number, h is the height of the substrate, ϵ_r is the dielectric constant and R is the physical radius of the patch.

$$(f_r)_{mn0} = \frac{\chi'_{mn}C}{2\pi R_{eff}\sqrt{\epsilon_r}} \tag{8.1}$$

$$K_1 R_{eff} = \chi_{nm} \tag{8.2}$$

$$R_{eff} = R\sqrt{1 + \frac{2h}{\pi R\epsilon_r}\left[ln\left(\frac{\pi R}{2h}\right) + 1.7726\right]} \tag{8.3}$$

From (8.3), it is clear that the size of the radiating patch depends on the height of the substrate, dielectric constant of the substrate and the order of particular excitation mode. The parameter, χ'_{mn} will determine the order of the

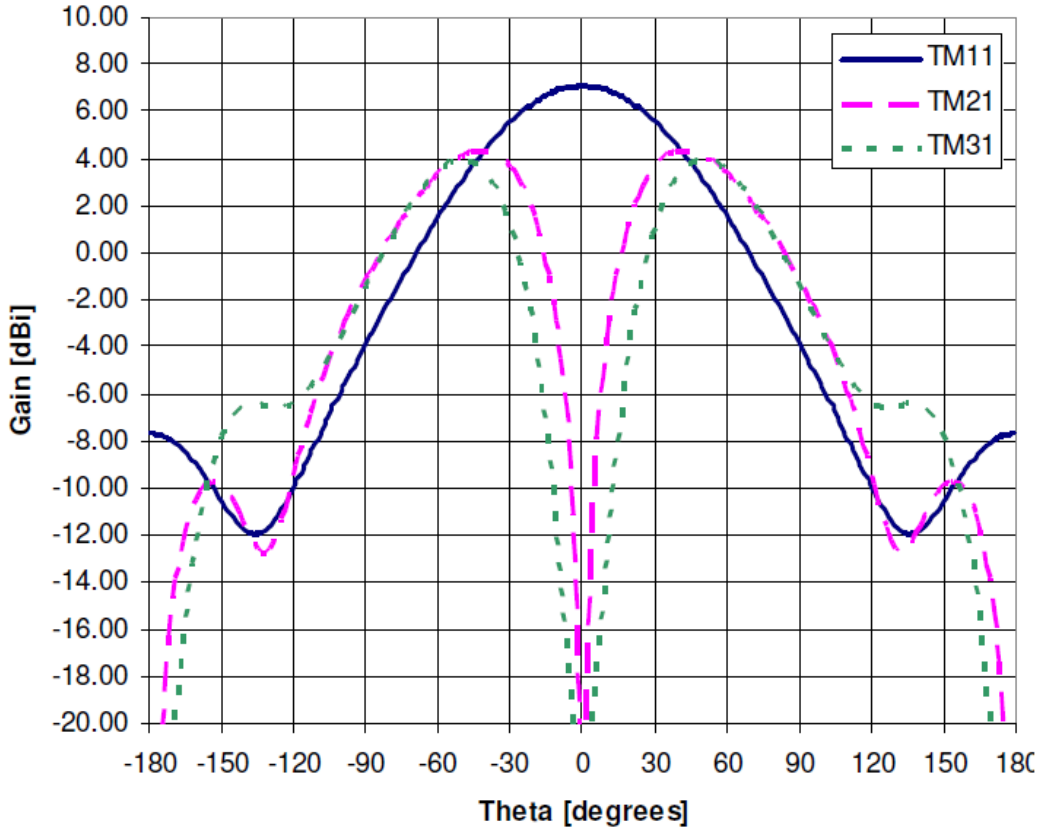

Figure 8.2 Radiation characteristics of different modes in circular patch antenna.

resonant mode and frequency. The microstrip antenna has different radiation pattern according to the resonant mode. The primary mode that support the circular patch antenna is TM_{11} mode and has a pattern broadside to the antenna. However, the higher order modes like TM_{12}, TM_{20} have a null along the Z-axis and two main lobes symmetric along Z-axis as shown in Fig. 8.2.

The circular patch antenna is proposed for the harsh jet engine application, because of its ability to reject the harmonics coincide with its excited modes. Normally, the harmonics are the multiples of the fundamental frequency and the resonance frequency of the CPA is expressed in terms of the root of the derivative of Bessel function. As a result, the harmonics produced by the jet engine environment will not be able to excite the higher order modes of

CPA [94]. It is also important to understand how the characteristics of a patch antenna can model by varying the fundamental parameters of the patch antenna design. Hence, in the following section we analyzed the effect of various parameters on antenna characteristics.

8.1.2 Effect of substrate characteristics

The different substrate parameters that affect the antenna characteristics are the substrate permittivity (ϵ_r) and the thickness of the substrate (h). It is important to mention that increasing ϵ_r reduces the size of the patch and hence the radiation pattern gets broaden. However, small ϵ_r provides a symmetric radiation patterns and as ϵ_r increases the pattern symmetry gets deteriorates and will increase the antenna cross polarization.

Moreover, the substrate height of the antenna has a great effect on the bandwidth of microstrip antennas. Bandwidth of the patch antenna increases as the substrate height increases. As thickness of the substrate increases, the zone of the fringing fields get extended and hence results a broad radiation pattern.

8.1.3 Effect of Feed location

The location of the feeding point is important to maintain a good impedance matching between the antenna and the load during the design process. Moreover, the feeding location has significant effect on the excitation of different modes. That means, by choosing an appropriate feeding location the resonant mode can easily excited above the adjacent modes [55].

8.1.4 Effect of central shorting pin

It is important to mention that the central shorting pin which connects the upper patch to the ground plane will improve the purity of resonant mode. The shorting pin will act as an additional parameter to control different mode excitations. However, the pin radius should be optimized accordingly to minimize the non-resonant mode excitation.

8.1.5 Effect of ground plane

The radiation characteristics of various modes depends on both size and thickness of the ground plane. The thickness of the ground plane affects the reflection coefficients of various modes and hence affects the excitation efficiency of the non-resonant modes [55]. As the thickness of the ground plane increases, the excitation efficiency of higher order modes reduces. Hence, it is important to mention that the thickness of the ground plane can be used as an additional parameter to modify the excitation of different order modes. Thus, while designing a microstrip antenna with a high degree of mode excitation, it is important to optimize not only the patch dimension but also the size and thickness of the ground plane.

As explained before, in wireless communication applications the size of the conventional patch antenna becomes a major constraint and hence, researchers are being focused on the miniaturization of the patch antenna over the years with out affecting the performance of the antenna. There are many effective size reduction methods are available without altering the physical dimension of the antenna, which includes the use of shorting pins, resistor load, use of high dielectric constant materials, and introduction of slots, and modification of the original patch geometry etc; [55, 95, 96]. Hence, a brief analysis of effect

of different size reduction methods on the CP antenna is analyzed using circuit model analysis.

8.2 Model Analysis

8.2.1 Analysis of Circular Patch Antenna Loaded with Via and Notch

In this section, a simple CPA geometry with notch and via as shown in Fig. 8.3 is analyzed using circuit theory concept. The simple CPA consists of two vertical notches (L_n X W_n) and the antenna is shorted with a via at the center of the patch. The notches are introduced on the curved surface of the CPA as shown in Fig. 8.3 (a). The side view of the antenna is shown in Fig. 8.3 (b). The via and notches are introduced on the patch to minimize the antenna size and hence, to study its effect on the antenna characteristics. As mentioned before, the designed antenna needs to have a canonical beam pattern to satisfy the jet engine requirement. Hence, if only one via is used to short the circular patch antenna then it should be positioned at the center of the patch as shown in Fig. 8.3 (a) to obtain the particular radiation pattern [97].

The lumped element equivalent circuit of a normal patch antenna geometry consist of a parallel combination of capacitance (C_c), inductance (L_c) and resistance (R_c) can be represented as shown in Fig. 8.4 and its values can be evaluated using the same method used in [98, 99].

When a via is introduced on a patch antenna, a parallel inductance (L_v) will be added to the patch geometry and its value can be evaluated using (8.4). The probe-feed of the antenna also exhibits an inductive characteristic at high frequencies as in (8.4), where R_v and $\mathbf{h}$ are the radius and height of via hole or the probe feed [100]. It is important to mention that the effect of via

resistance is avoided in the equivalent circuit model since it is extremely small in comparison to the via reactance at high frequencies [101].

$$L_v = \quad 0.2\left[h - ln\left(\frac{h+\sqrt{R_v^2+h^2}}{R_v}\right) + \frac{3}{2}\left(R_v - \sqrt{R_v^2+h^2}\right)\right] \tag{8.4}$$

The equivalent circuit of a via loaded patch geometry is represented in Fig. 8.5(a) and hence the impedance of the via loaded patch can be evaluated using (8.5).

$$Z_v = \frac{1}{\frac{1}{R_c} + \frac{1}{j\omega L_c} + \frac{1}{j\omega L_v} + j\omega C_c} \tag{8.5}$$

When notches are introduced on the curved surface of the circular patch antenna, it will affect the flow of the electric current and hence, the initial antenna resonance characteristics will change. The change in the antenna characteristics is due to the flow of two different currents of varying direction (one normal to the patch and other around the notches). Therefore, an extra inductance (L_s)

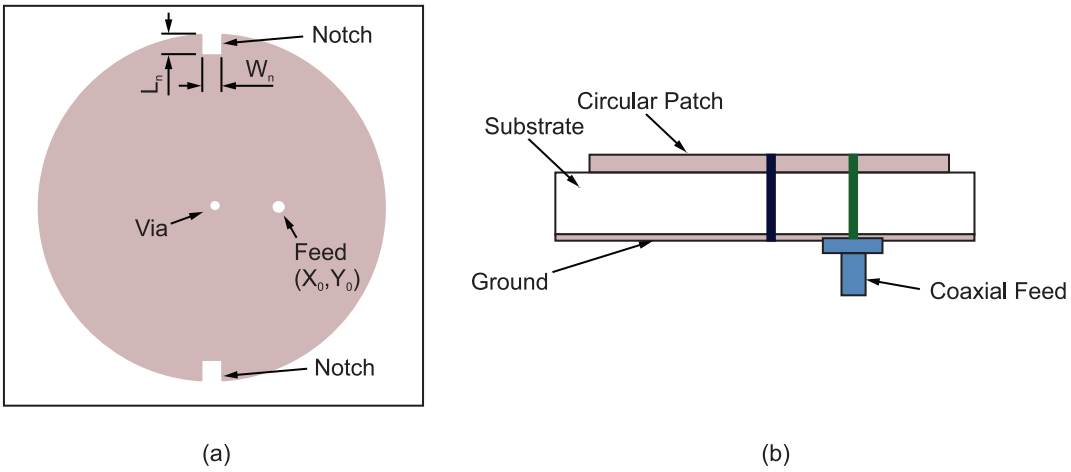

Figure 8.3 Circular patch antenna geometry with notches and via: (a) Top view (b) side view.

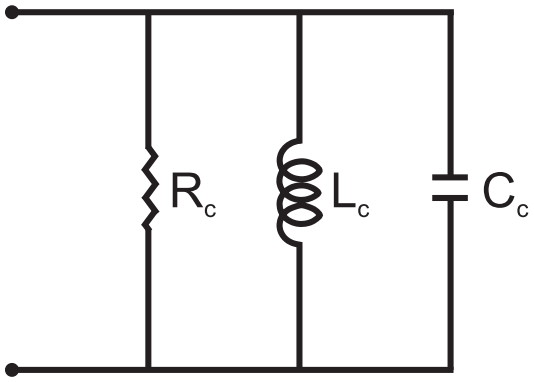

Figure 8.4 Equivalent circuit diagram of a simple circular patch antenna geometry.

and capacitance (C_s) due to the notch will be added with the initial patch antenna equivalent circuit. The equivalent lumped circuit of notch loaded patch antenna is shown in Fig. 8.5 (b). The L_s and C_s can be calculated using (8.6), and (8.7); where, L_n is the depth of the slot, C_g is the gap capacitance and μ_0 is the permittivity of free space [102, 103].

$$L_s = \frac{h\mu_0\pi}{8}\left(\frac{L_n}{W_r}\right)^2 \tag{8.6}$$

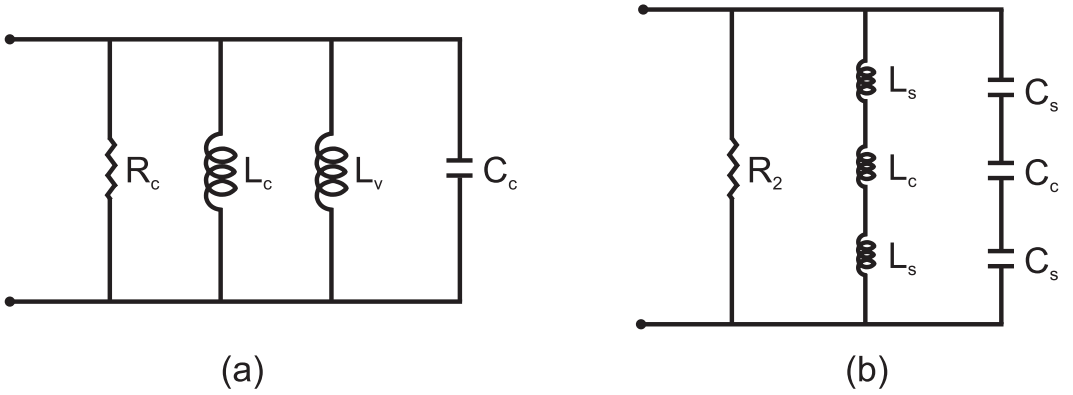

Figure 8.5 Equivalent circuit diagram of a circular patch antenna geometry: (a) with via. (b) with notch.

$$C_s = \left(\frac{L_n}{W_r}\right) C_g \tag{8.7}$$

Then, the equivalent impedance of the patch due to notch can be represented as in (8.8), where R_2, C_2 and L_2 can be evaluated using the method used in [99] and given below in (8.9) and (8.10).

$$Z_n = \frac{1}{\frac{1}{R_2} + \frac{1}{j\omega L_2} + + j\omega C_2} \tag{8.8}$$

$$C_2 = \frac{C_c C_s}{2C_c + C_s'} \tag{8.9}$$

$$L_2 = L_c + 2L_s \tag{8.10}$$

Hence, the equivalent circuit of the proposed simple CPA geometry loaded with notch and via can be represented as in Fig. 8.6. The total impedance of the proposed antenna can be evaluated as shown in (8.11), where Z_m is the mutual impedance due to mutual inductance (L_m) and capacitance (C_m) between the resonators [99].

$$Z_{total} = Z_n + \left(\frac{Z_m Z_v}{Z_m + Z_v}\right) \tag{8.11}$$

$$Z_m = \frac{1}{j\omega C_m} + j\omega L_m \tag{8.12}$$

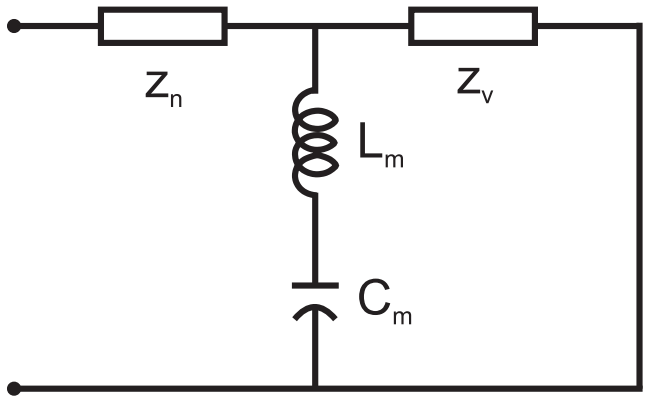

Figure 8.6 Equivalent circuit diagram of the proposed circular patch antenna geometry.

It is important to mention that, these analytical model analysis helps to model different antenna parameters such as; reflection coefficient (Γ), return loss, and VSWR as in (8.14).

$$\Gamma = \frac{Z_0 - Z_{total}}{Z_0 + Z_{total}} \tag{8.13}$$

$$VSWR = \frac{1+\Gamma}{1-\Gamma} \tag{8.14}$$

The radiation pattern of the proposed circular patch antenna can be evaluated using (8.15) and (8.16), where V_0 is the radiating edge voltage, $\mathbf{R}$ is the radius of the patch antenna, $\mathbf{r}$ is the distance to far field point [104]. In the circular patch antenna, when $\mathbf{n = 1}$ the radiation pattern becomes normal to the patch and other values of $\mathbf{n}$ produce a null in the radiation pattern normal to the patch.

$$E_\theta = -j^n k_0 \frac{V_0\ R}{2} \frac{e^{-jk_0 r}}{r} \left[J_{n-1}(k_0 R sin\theta) - J_{n+1}(k_0 R sin\theta)\right] cos(n\phi); \tag{8.15}$$

where $(0 \leq \theta \leq \pi/2)$

$$E_\phi = j^n k_0 \frac{V_0}{2} \frac{R}{r} e^{-jk_0 r} \left[J_{n-1}(k_0 R sin\theta) + J_{n+1}(k_0 R sin\theta) \right] cos\theta sin(n\phi); \quad (8.16)$$

where $(0 \leq \phi \leq \pi/2)$

In this section, a brief analysis of the effect of via and notch on CPA is given. The analysis proves that as the number of via increases the inductive reactance increases and hence, the number of via (N_v) have a great effect on controlling the resonant frequencies of the patch antenna geometry. Moreover, the position of vias and the separation between the via (d) influences the antenna impedance and radiation characteristics. Hence, by using a careful optimization method of N_v and d on CPA geometry, the required radiation characteristic can be obtained.

8.2.2 Analysis of HCPA

The analysis of a half circle patch antenna (HCPA) is relatively same as that of a circular patch antenna. However, the effective radius (R_{heff}) of the HCPA changes due to the change in overall patch dimension. Also, it is assumed that HCPA is identical to an extended rectangular patch antenna design and hence, the effective radius of HCPA (R_{heff}) can be calculated by equating its area to that of the expanded rectangular patch antenna by using (8.17), where L_e and W_e are the length and width of extended rectangular patch antenna [94]. The resonance frequency of HCPA can be evaluated as in (8.18); where, C is the velocity of light, ϵ_{reff} is the effective dielectric constant.

$$R_{heff} = \sqrt{\frac{L_e W_e}{\pi}} \quad (8.17)$$

$$f_r = \frac{\chi_{nm} C}{2\pi R_{eff} \epsilon_{reff}} \tag{8.18}$$

Analysis of Notch Loaded HCPA

A single half circular patch antenna geometry as shown in Fig. 8.7, can be analyzed using same method explained in section 8.2.1. Figure 8.8(a) and (b) shows the current distribution and radiation pattern for a single HCPA and notch loaded HCPA. The introduction of notch change the direction of the current in the patch as shown in Fig. 8.8 and hence there will be a change in antenna resonance characteristics. The radiation pattern of the proposed HCPA can be evaluated as in (8.15) and (8.16), where V_0 is the radiating edge voltage, **R** is the radius of the patch antenna, **r** is the distance to far field point [104]. However, it is clear from the simulation that both the antenna has broadside pattern.

Normally, the fundamental mode and higher order mode of HCP antenna generates a broadside radiation pattern as shown in Fig. 8.8, similar to that of the fundamental mode of a CPA [94]. However, this particular application requires a radiation pattern that has a null in the broadside direction and the main beam pointed towards the fan blade to implement a strong communication

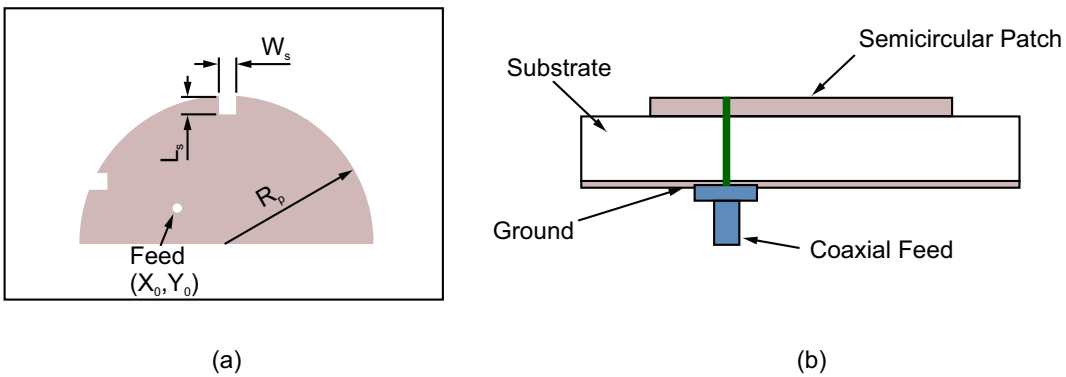

Figure 8.7 Geometry of HCPA (a) top view and side view.

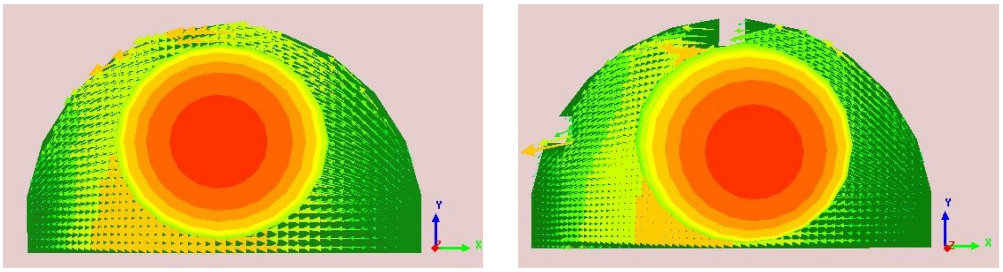

(a) (b)

Figure 8.8 Current distribution at 2.44 GHz: (a) normal HCPA (b) NLHCPA.

link between the sensors and the receiver. Hence, two radiating patches are connected in series to obtain a radiation pattern that has null at broadside direction.

8.2.3 Analysis of Slot Loaded Rectangular Patch Antenna

A slot loaded rectangular patch antenna as shown in Fig. 8.9 is analyzed to study the effect of narrow slots on rectangular patch antenna radiation characteristics. A narrow symmetrical slot with dimension L_s X W_s is introduced parallel to the radiating edges of the antenna and the antenna is fed through a 50 Ω coaxial probe as shown in Fig. 8.9. The dimension of the slot is very small compared to the dimensions of the patch geometry. The position of the slot with respect to the patch is an important parameter to adjust the antenna resonance characteristics. A brief analysis of slot loaded rectangular patch antenna is shown here.

The rectangular patch with out slot can be represented as a parallel combination of capacitance (C_c), inductance (L_c) and resistance(R_c) as shown in Fig. 8.4. The value of equivalent lumped elements can be calculated using (8.19), (8.20), and (8.21), where L_e, and W_e are the effective length and width

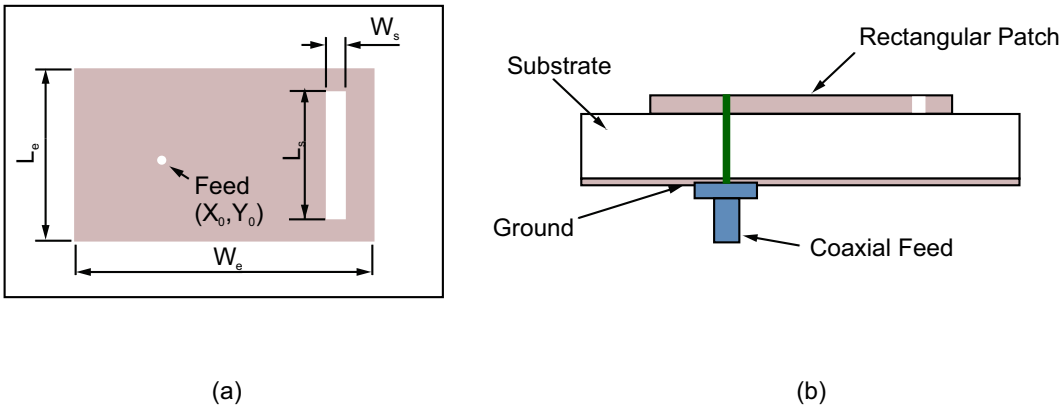

Figure 8.9 Rectangular patch antenna geometry: (a) Top view (b) side view.

of the rectangular patch antenna and can also be represented as L_e=2R, and W_e=π R/2; R is the radius of the circular patch antenna, Q is the quality factor, $\omega_r = 2\pi f_r$, x_0 is the feed point location along the length of the patch [94]. Then, the equivalent patch impedance can be evaluated using (8.22).

$$C_c = \frac{L_e W_e \epsilon_0 \epsilon_e}{2h} cos^{-2}(\pi x_0/L) \tag{8.19}$$

$$R_c = \frac{Q}{\omega_r^2 C_c} \tag{8.20}$$

$$L_c = \frac{1}{\omega_r^2 C_c} \tag{8.21}$$

$$Z_{pr} = \frac{1}{\frac{1}{R_c} + \frac{1}{j\omega L_c} + j\omega C_c} \tag{8.22}$$

To analyze the slot loaded rectangular patch antenna, the duality concept between the slot and patch can be considered. The input impedance of the thin slot can be calculated using *Babinet's* principle as in (8.23) [105].

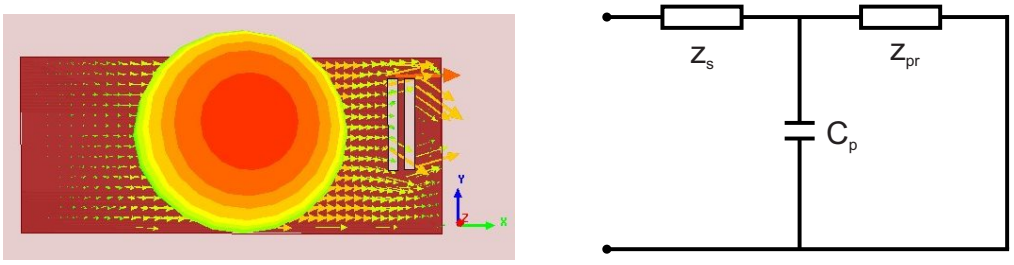

(a) (b)

Figure 8.10 (a) Current distribution on notch loaded rectangular patch antenna (b) equivalent circuit diagram of the proposed slot loaded rectangular patch antenna geometry

$$Z_s = \frac{\eta_0^2}{4Z_{cy}} \tag{8.23}$$

where, $\eta_0 = 120\pi$ represents the intrinsic impedance of free space,

$$Z_{cy} = R_r(KL_s) - j\left[120\left(ln(\frac{L_s}{W_s} - 1\right)cot\left(\frac{KL_s}{2}\right) - X_r\left(KL_s\right)\right] \tag{8.24}$$

where, R_r represents the radiation resistance of the slot and X_r is the input reactance of the slot [105, 106]. The equivalent circuit of the slot loaded rectangular patch geometry can be represented as in Fig. 8.10(b). Then, the input impedance of the design can be evaluated using (8.25), where Z_p is the reactance due to the coupling capacitance C_p.

$$Z_T = Z_s + \frac{Z_{pr}Z_p}{Z_{pr}+Z_p} \tag{8.25}$$

By using (8.25), different antenna parameters can be calculated as shown in (8.14). The radiation pattern of the proposed slot loaded rectangular

patch antenna can be evaluated using (8.26) and (8.27), where k=$k_0\sqrt{\epsilon_e}$ and $x = \frac{k_0 W}{2} sin\theta sin\phi$.

$$E_\theta = \frac{-Jk_0V_0\ We^{-jk_0r}}{\pi r} cos(khcos\theta)\frac{sinx}{x} cos(\frac{K_0L}{2} sin\theta sin\phi) cos\phi; \qquad (8.26)$$

where $(0 \leq \theta \leq \pi/2)$

$$E_\phi = \frac{-Jk_0V_0\ We^{-jk_0r}}{\pi r} cos(khcos\theta)\frac{sinx}{x} cos(\frac{K_0L}{2} sin\theta sin\phi) cos\phi sin\phi; \quad (8.27)$$

where $(0 \leq \phi \leq \pi/2)$

From the above analysis and simulation, it is clear that the narrow slots that are located near to the antenna radiating edges may introduce minor perturbations to the excited modes. The current through the patch should rotate around the slot and this will change resonance characteristics as shown in Fig. 8.10 (a). The length (L_s) and the position of the slot plays a significant role in the deformation of antenna radiation characteristics. Moreover, the previous analysis proved that, by changing the length and position of L_s, the radiation pattern characteristics of the higher order mode of the rectangular patch antenna can be controlled [107].

8.3 Antenna Design For Harsh Environment Application

The radiation characteristics of an antenna for a wireless communication inside jet engine environment is important especially in implementing a strong communication link between the sensors and receivers. In order to extract the attributes of jet engine parameters, the transmitting antennas and the sensor nodes will be installed on the fan blades and the proposed receiving antenna

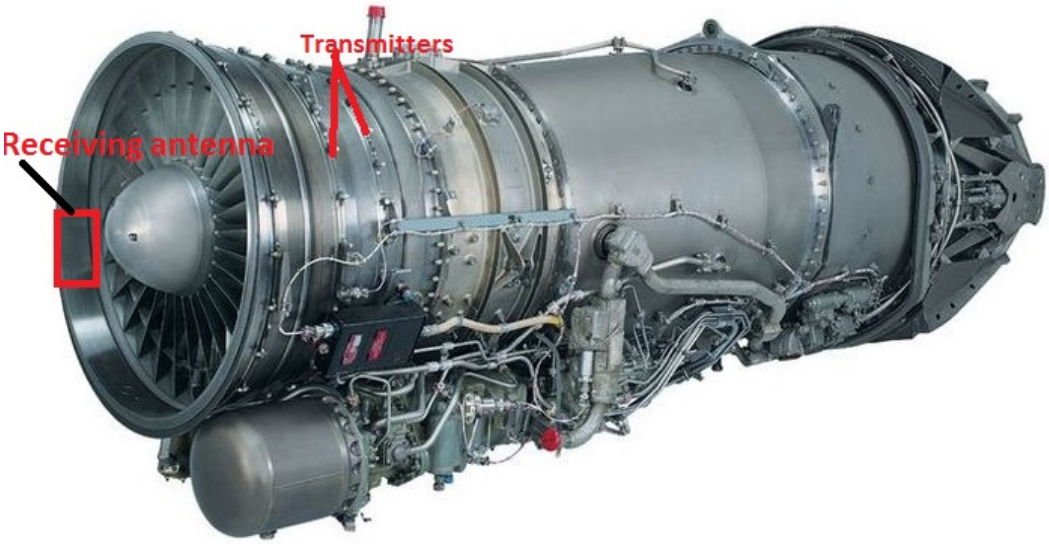

Figure 8.11 Location of transmitter and receiver inside jet engine.

will be placed on the surface of the environment as shown in Fig.8.11. Hence, to constitute an excellent communication channel inside the environment, an antenna is recommended to have a radiation pattern, that has null in broadside direction (similar to those of a vertical monopole antenna). Hence, if some of the required radiation parameters are not produced with a single radiating patch, we can arrange radiating elements in a geometric and electrical configuration. Thus, the design specifications of three new antennas formed by two radiating elements are proposed in the next sections. The array geometry helps to obtain a higher level of directivity compared to a single microstrip antenna.

8.4 Proposed Antenna Design Specifications

In this thesis, a circular patch antenna geometry, a half circular patch antenna geometry, and a hybrid rectangular circular patch antenna geometry is proposed for the harsh metallic environment application. The receiver antenna for wireless communication application inside the harsh metallic environment

is required to be with low footprint and flexible to avoid interfering with the aerodynamic design. In addition to this the small size of the antenna enable flat installation as shown in Fig. 8.11, without violating the conformity requirement. Also, the performance of the antenna is expected to have a center frequency at 2.45 GHz (ISM band) to enable license free deployment and avoid interfering with aviation equipment.

8.4.1 Circular Patch Antenna Array Design

A CPA array structure with compact size is proposed and designed for the WSN application inside the jet engine as shown in Fig. 8.12. In order to make the designed antenna conformal to the jet engine environment, an extremely thin substrate with low weight (low density) and thickness has been considered. The thickness of the substrate is very small compared to the free space wavelength

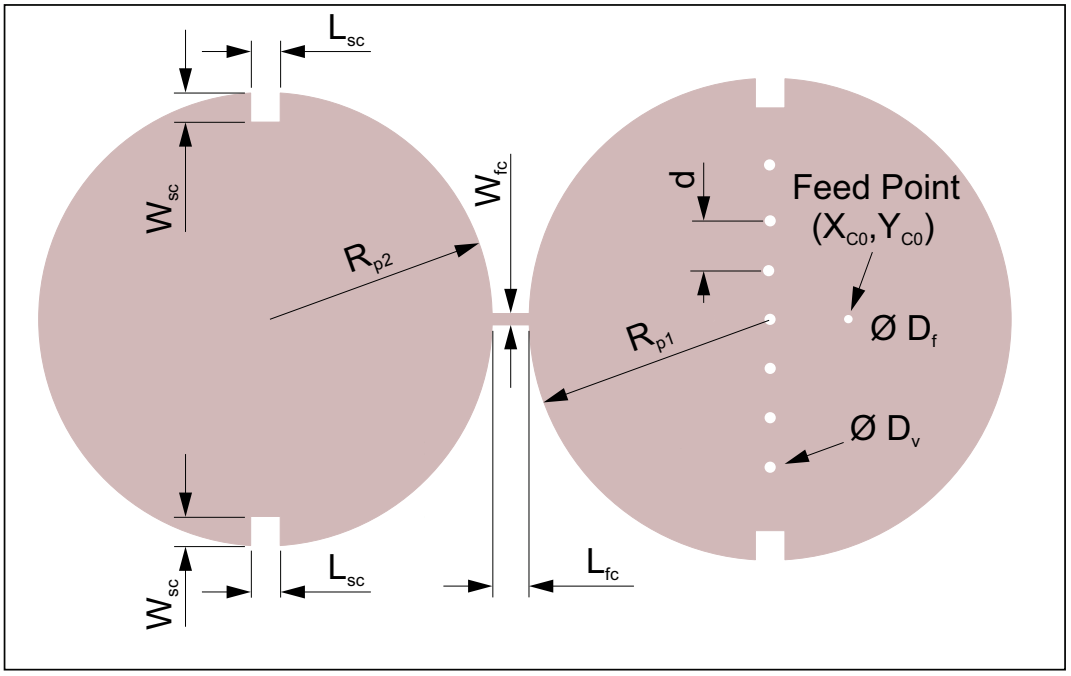

Figure 8.12 Geometry of proposed circular patch array antenna (all dimensions are in *mm*).

and the patch radius. The circular patches have a radius of R_{p1} and R_{p2} for patch 1 and patch 2 respectively. The electrical size of the antenna is varied by two symmetric square notches (L_{sc} X W_{sc}) that are cut on the patch area and then the circular patches are connected in series as in Fig. 8.14. The parameters related to the CPA geometry is designed and optimized using 'Ansys® Designer 2014' as follows (all dimensions are in mm); $R_{p1} = 24.44$, $R_{p2} = 23$, $L_{fc} = 3.9$, $W_{fc} = 1.15$, $L_{sc} = W_{sc} = 3$ and the dimension of the designed coaxial pin is ϕD_f =0.5 mm .

The patch array is fed by a coaxial feed and the feeding location is optimized carefully to have an impedance matching with the connector. The real part of the input impedance is 50 Ω and this makes the design easy to match the impedance by appropriately altering the feeding location (X_{c0}, Y_{c0}) along the patch radius. Since the antenna radiation pattern is affected by the location of the feeds, the selection of the relevant feed location is necessary to obtain the dual beam pattern. Moreover, the notches and the vias in the proposed design makes these process more complicated. Hence, the simulation software is used to optimize the suitable feed position. Thus, in this particular design the feed is located at (8.5, 0) mm from the center of patch 1.

The square notches and identical vias are introduced to change the characteristics of the array antenna system. Each via has a diameter of ϕD_v =0.5 mm and are separated by a distance of $d = 5\,mm$. The position and dimension of vias and notches are optimized using the simulation software. The number of vias plays a significant role in changing the designed resonant frequency for the patch antenna and also the radiation characteristics as explained in section 8.2.1. The total dimension of the antenna system is $0.49\lambda_0$ X $0.8\lambda_0$ mm^2 and the height of the substrate is $0.0031\lambda_0$ mm, where λ_0 is the free space wavelength. The proposed antennas have been fabricated, measured and compared to the simulation results. The simulated CP antenna geometry is shown

in Fig.8.13 (a), and the distribution current and far field pattern is shown in Fig.8.13 (b).

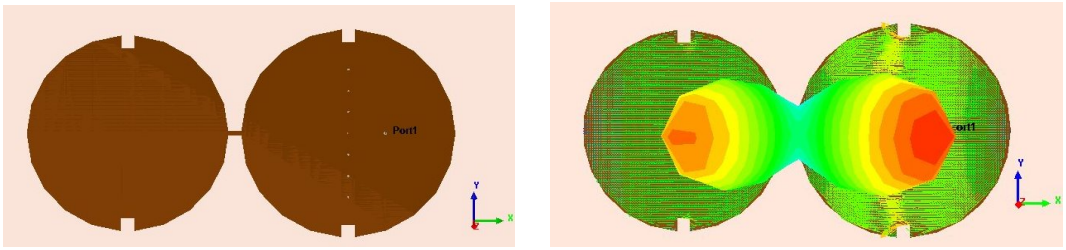

(a) (b)

Figure 8.13 Proposed antenna model: (a) Simulated CPA array.(b) Current distribution of CPA array.

However, the proposed antennas needs to be small and compact to achieve the jet engine environmental constraints. Hence, a modified half circle antenna and modified rectangular patch antenna design with rectangular slots are proposed in next sections and compare their results with the CP antenna design.

8.4.2 Modified Half Circle Patch Antenna Design

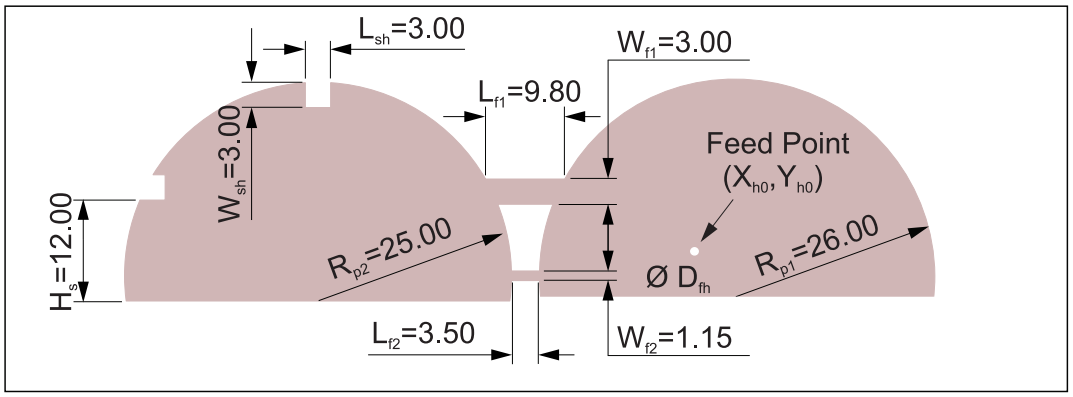

Figure 8.14 Geometry of the proposed half circular patch array antenna (all dimensions are in mm).

The proposed antenna consists of two radiating patches connected in series with dual feed line as shown in Fig. 8.14. The antenna is fed with coaxial feeding technique and is situated on Patch 1. The electrical size of patch 2 is varied by two identical notches of dimension (L_{sh} X W_{sh}), that are cut on the patch area. Notch 1 is introduced along the center of the patch (perpendicular to the diameter edge), while notch 2 is positioned parallel to the edge of the diameter of that patch. The notches help in changing the characteristics of the current distribution of the antenna system [101]. A brief simulation analysis and comparison of flow of current on the normal HCPA and the NLHCPA are shown in Fig. 8.8. The notches introduced on the patch discontinue the path of the electrical current flow on the patch and hence, the current has to circulate around the notch as shown in Fig. 8.8 (b). Thus, the antenna resonant characteristics will change due to the influence of the equivalent series inductance introduced due to the effect of notches on actual patch antenna equivalent LCR circuit [98, 99]. The narrow notch on the patch surface also plays a significant role in controlling the impedance bandwidth of the antenna [108].

From Fig. 8.8, it is clear that the single HCPA geometry generates a broadside radiation pattern. However, our particular antenna design changes the broadside radiation pattern into a pattern that has a null in the broadside direction as shown in Fig. 8.15(a). Figure 8.15(b) shows the simulation model of the proposed antenna geometry. Furthermore, the two narrow notches on the patch introduce dual frequency band and hence the location of the notches should be designed carefully to diminish the effect of the higher resonant frequency and increase the antenna bandwidth.

The HCP array is fed by a coaxial feed with a 50 Ω SMA connector and the feeding location on patch 1 (X_{h0}, Y_{h0}) is optimized carefully to have an impedance matching. In this particular design, it is (-5.898, 5.987) mm from the center of the axis which is located at the center of the diameter edge of

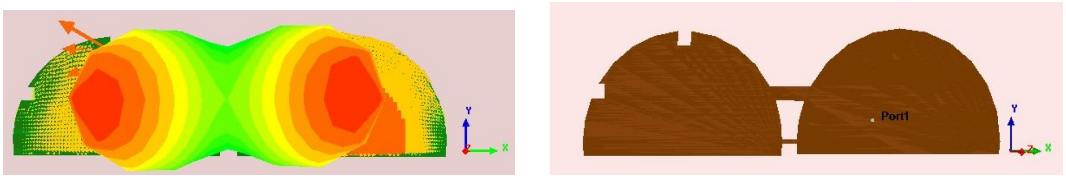

(a) (b)

Figure 8.15 Proposed antenna model: (a) Simulated proposed HCPA. (b) Current distribution of proposed HCPA at 2.44 GHz .

patch 1. The small feed line between the patches is designed for 50 Ω and the diameter of the probe feed (ϕD_{fh}) is optimized to have a value of 0.6 mm. A small perturbation (connector) between the two patches act as an additional feed line between the patches and helps to increase the gain and bandwidth of the proposed antenna.

8.4.3 Hybrid Rectangular Circular Model

Figure 8.16 shows the design of the hybrid antenna model that is going to be used on the surface of the jet engine inlet wall. The proposed antenna design

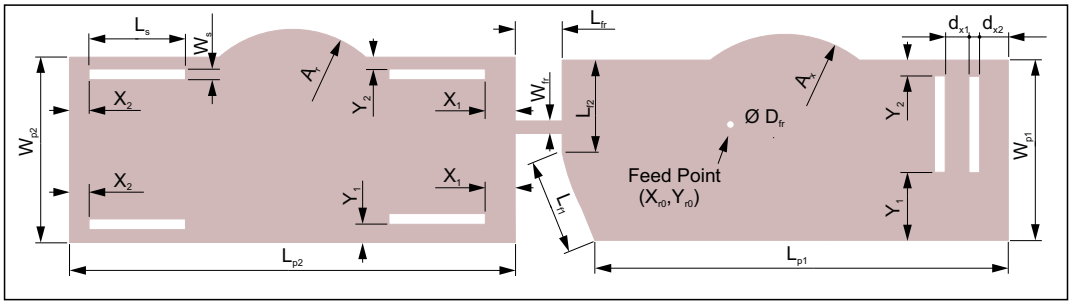

Figure 8.16 Geometry of proposed HRCP design (all dimensions are in mm).

has a unique shape with upper curvature and rectangular slots. The upper

curvature helps to achieve the radiation characteristics of the star microstrip patch antenna. The star microstrip patch antenna has an ability to provide an excitation symmetry, where a single feed excitation can generate the desirable mode excitation. The circumference of a star microstrip patch is an important parameter in defining its resonant frequency, and the resonant frequency is inversely related to the total arc length. The analysis also proved that the bandwidth of the antenna decreases with decreasing the arc dimension [109]. Hence, by using this particular curvature shape, the antenna resonance can be adjusted by adjusting the height of the curvature. The height of the curvature is adjusted carefully to adjust the operating frequency with the required radiation characteristics.

The rectangular slots are introduced on both patches to change the electrical length of the array antenna system. The slots on both the patches have equal dimensions (L_s X W_s) and the antenna resonance frequency can be altered by changing the slot length, while keeping the width of the slot constant. Also, the bandwidth and the radiation characteristics of the antenna is related to the dimension of the slot. Hence, the slot dimensions and its position on each patch are designed by careful iteration by using the simulation software. The height of the curvature is adjusted carefully to adjust the operating frequency with the required radiation characteristics.

The proposed antenna is fed through a coaxial probe feeding method and the feed is located on patch 1 ($HRCP_1$). It is easy to obtain the input matching by adjusting the feed position. The feeding location has a significant effect on the excitation of different order modes. Hence, by choosing an appropriate feeding location (X_{r0}, Y_{r0}) the resonant mode can easily excited above the adjacent modes [55]. The feed point location is optimized carefully to obtain the best match between the antenna input impedance and the generator impedance.

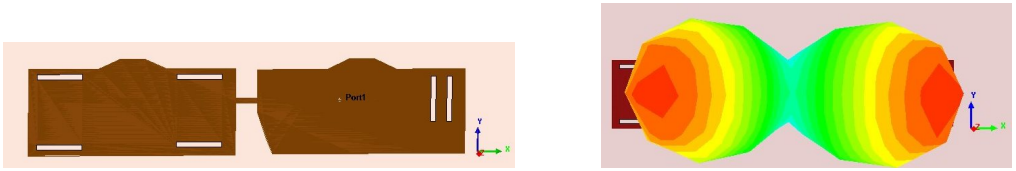

(a) (b)

Figure 8.17 Proposed HRCP antenna model: (a) Simulated antenna. (b) Simulated current distribution.

The feed line between the patches is designed for 50 Ω and is numerically optimized to have a width of 1.15 mm.

The parameters related to the HRCP geometry is designed and optimized using 'Ansys® Designer 2014' as follows (all dimensions are in mm); $L_{p1} = 38.6$, $L_{p2} = 41.62$, $W_{p1} = 16.83$, $W_{p2} = 17$, $L_s = 9$, $W_s = 1$, $L_{f1} = 8.8$, $L_{f2} = 8.86$, $L_{fr} = 4.3$, $W_{fr} = 1.15$, $d_{x1} = 2.2$, $d_{x2} = 2.6$, $d_{y1} = 6.2$, $d_{y2} = 1.45$, $Y_1 = 1.7$, $Y_2 = 1$, $X_1 = 2.8$, $X_2 = 1.82$, $A_r = 2.6$, $A_x = 2.4$, $\phi D_{fr} = 0.6$. The simulated antenna model and the current distribution is shown in Fig. 8.17.

8.5 Simulation and Measurement Analysis

The proposed antennas are simulated using 'Ansys® Designer 2014'. The designed antennas should be mounted on a metallic plane and hence the antennas are simulated with an infinite ground plane. The proposed antennas are low profile and hence, the substrate chosen for this particular application is RT/duroid 5880 with a thickness (h) of 0.381 mm ($0.0031\lambda_0$), dielectric constant (ϵ_r)= 2.2 and loss tangent is 0.0009. The substrate is extremely flexible due to its small thickness and substrate material properties. This allows the material to be bent and mounted on curved surfaces like the wall of the jet en-

gine[1]. The thermal coefficient of dielectric constant (TCDK) of this particular material is very low and hence the dielectric constant of this material remains stable even when it is exposed to a wide range of temperature. Moreover, RT/-duroid 5880 possess extremely low water absorption characteristics and hence this material is ideal for jet engine applications where the proposed antenna is going to expose in high moisture conditions. The patch geometries are fed by a coaxial feed with a 50 Ω SMA connector and the feeding location is optimized carefully to have an impedance matching with the connector.

In the fabrication of the antenna PCB screen printing method is adopted. This method consists of a photo resist application, printing the model on the PCB and then the development process. All measurements are carried out with Agilent E8363B Network Analyzer. The measurement of the radiation pattern of the proposed antenna is conducted in an Anechoic Chamber. A standard antenna test facility is used to study the radiation characteristics of the proposed antenna. A detailed explanation of the used techniques are available in Appendix B. The measurement results of the proposed antennas are available in the following section.

8.5.1 Measurement Results

The proposed CPA has been fabricated, measured and compared to the simulation results. Photographs of the fabricated CPA geometry is shown in Fig.8.18(a) and the antenna test facility is shown in Fig.8.18(b).

The measured and simulated S_{11} parameter of the CPA is shown in Fig. 8.19 (a), which describes the relationship between the input power and reflected power to the system for a two port network and is measured using network analyzer. From the simulation S-parameter results in Fig. 8.19 (a), it is clear

[1]It must, however, be noted that due to the very small size of the designed antennas and very large curvature of jet engines, practically, no bending will happen.

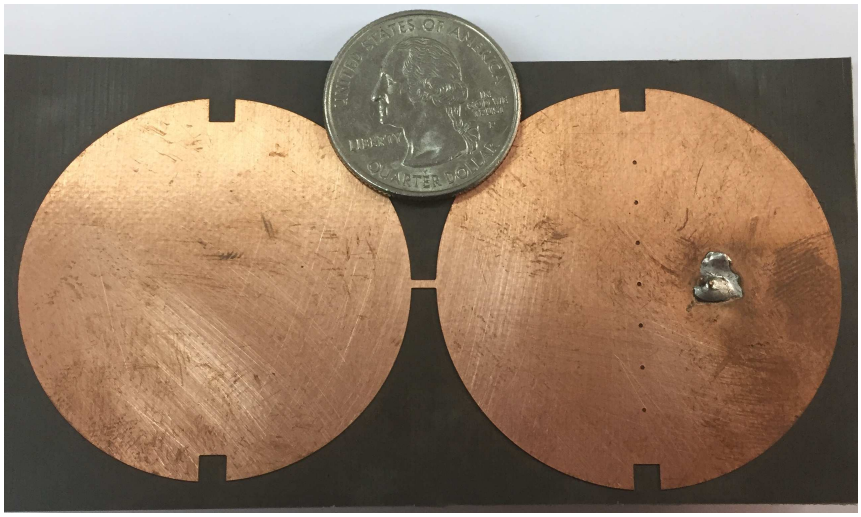

(a)

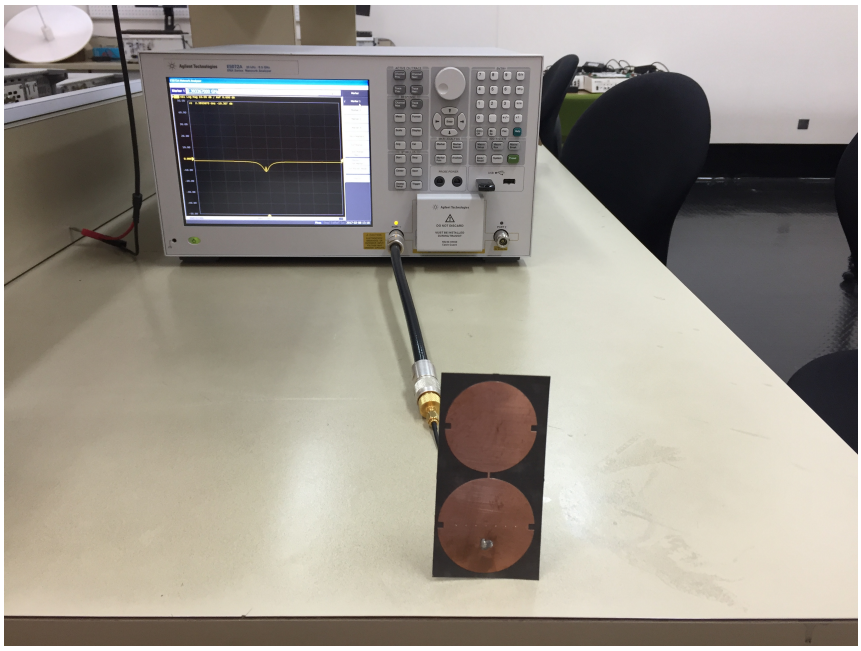

(b)

Figure 8.18 Proposed antenna model: (a) Fabricated circular patch antenna array (b) Testing of CPA.

that the proposed antenna is resonating exactly at 2.47 GHz with the return loss value of -25.82 dB. However, the measurement result shows a shift to 2.42 GHz which may be due to fabrication errors. The VSWR of the simulated antenna at 2.47 GHz is 1.18 as shown in Fig. 8.19(b). From Fig. 8.19, it is clear that there is

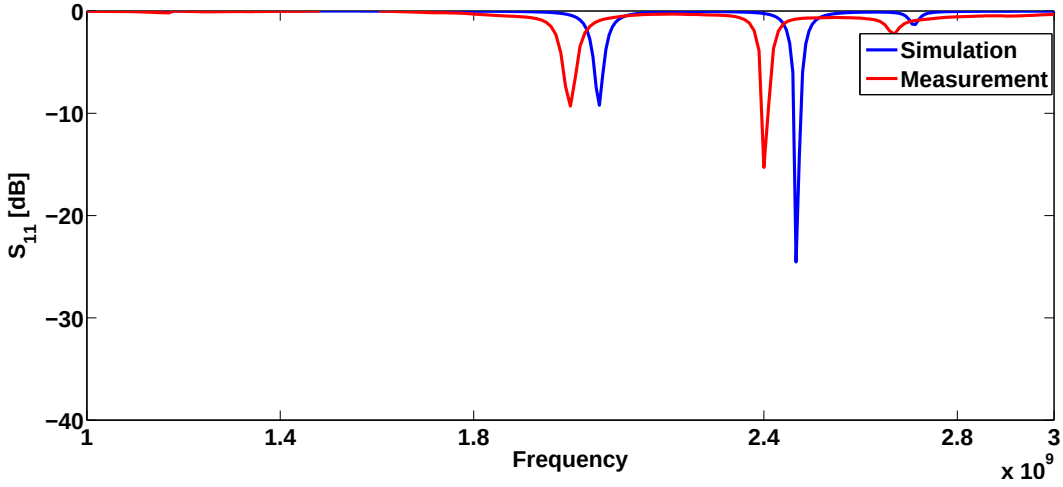

(a)

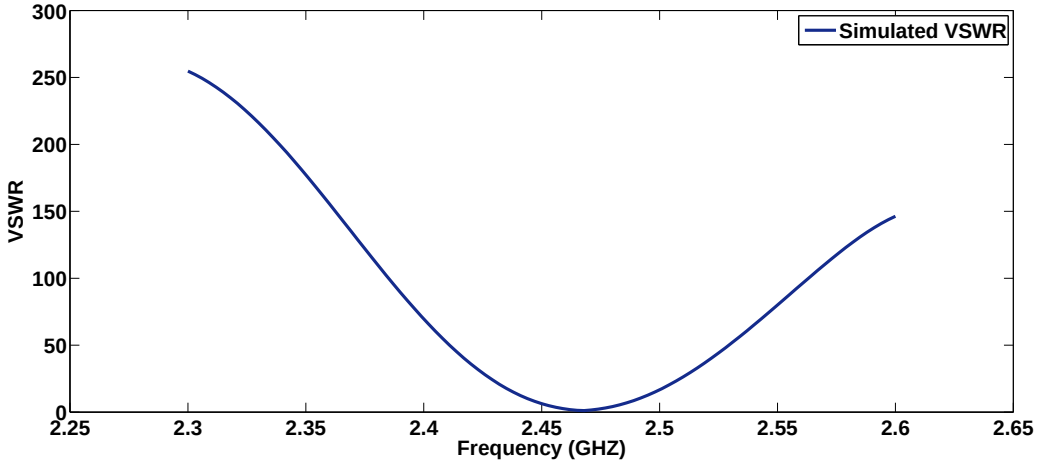

(b)

Figure 8.19 Simulated and measured reflection characteristics of the circular patch antenna array: (a) S_{11} parameter. (b) VSWR.

a small discrepancy between the simulated and measured frequency values and is due to the variation of the value of the substrate relative permittivity during fabrication process[2]. It is important to mention that, the input impedance of a coaxial probe fed antenna is extremely sensitive to the distance between the via and the feeding probe location. Furthermore, the size of the via and

[2]It is worth mentioning that other possibilities such as etching imperfections and fabrication specification errors have been eliminated by incorporating them into the simulation and noticing no effect on frequency. Moreover, the effect of ϵ_r error was verified by simulation to cause a similar frequency shift with in the $\pm$ 0.02 value stated in the material data sheet.

the probe dimension also have an effect on antenna input impedance. Hence, to match the impedance of the antenna careful optimization of dimension and the position of vias and feed location is important. A very small shift in the probe location during the fabrication can account a remarkable variation in the antenna reflection coefficient. This may be another important reason for the discrepancy. From the analysis, it is clear that the impedance matching of

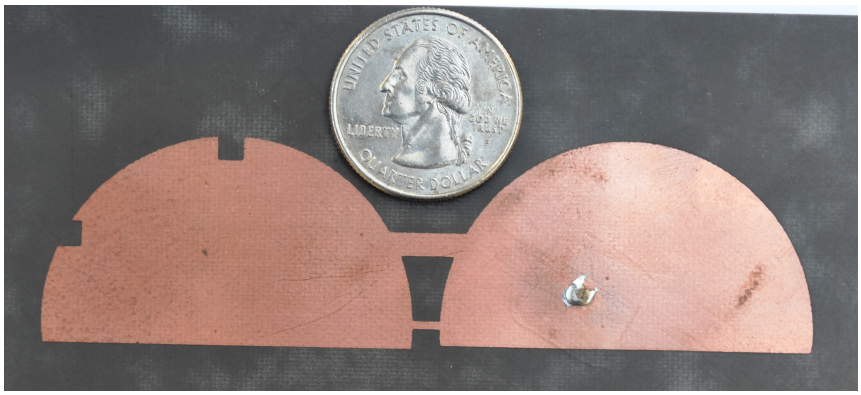

(a)

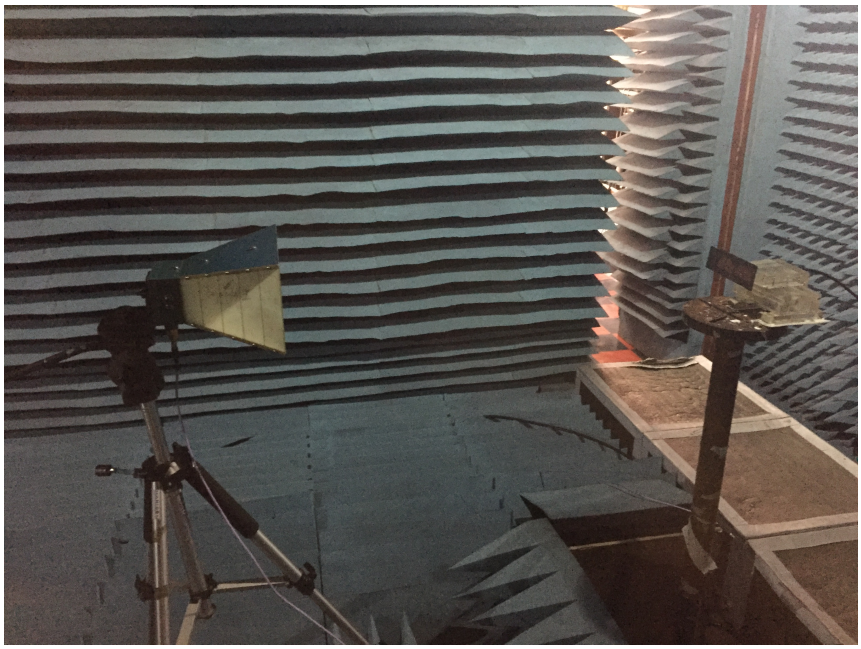

(b)

Figure 8.20 Proposed antenna model: (a) Fabricated HCPA geometry. (b) Testing of HCPA in anechoic chamber.

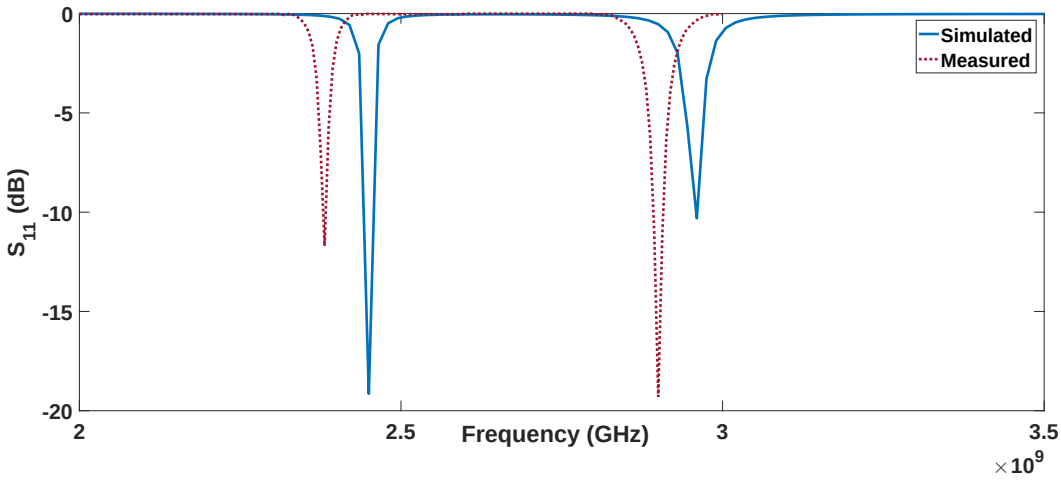

(a)

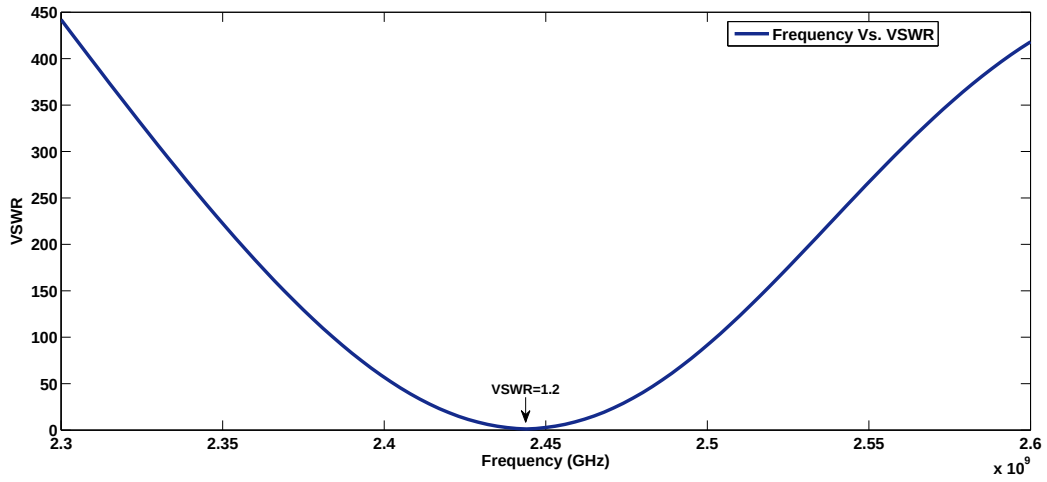

(b)

Figure 8.21 Simulated and measured reflection characteristics of the half circular patch antenna array: (a) S_{11} parameter. (b) simulated VSWR.

a CP antenna operating at a single mode is very difficult and its impedance bandwidth will be narrow [97, 110].

Figure.8.20 shows the fabricated HCP antenna model and the test facility set up. The measured and simulated S_{11} parameter of the HCPA are shown in Fig. 8.21 (a), and is measured using the network analyzer. It should be men-

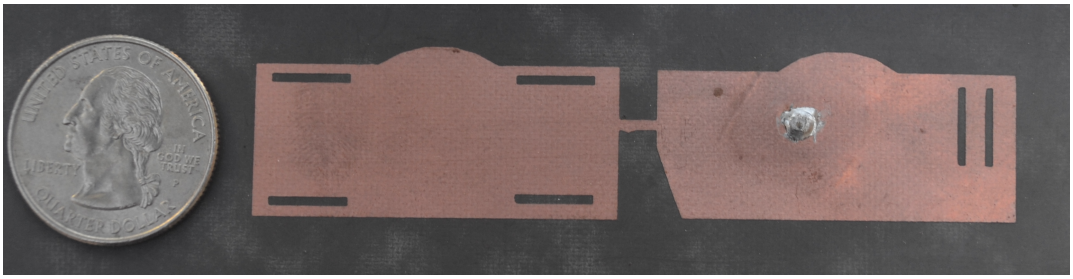

Figure 8.22: Fabricated HRCP antenna.

tioned that the simulated antenna has a return loss value of -19 dB at 2.44 GHz as shown in Fig. 8.21. However, the measurement result shows a resonance shift to 2.4 GHz (lower end of ISM band). There is a small discrepancy between the simulated and measured results which may be due to the etching tolerances and the variation of the value of the substrate relative permittivity during fabrication process. Figure 8.21 shows that the proposed antenna has a dual frequency band due to the effect of notches and hence the location of the notches should be designed carefully to diminish the effect of the higher resonant frequency and increase the antenna bandwidth.

The fabricated HRCP antenna is shown in Fig. 8.22 and have been tested and compared to the simulation results. The measured and simulated S_{11} parameter of the HRCPA is shown in Fig. 8.23. From Fig. 8.23 (a), it is clear that the proposed HRCP antenna is resonating at 2.47 GHz with the return loss value of -20 dB and the VSWR of the simulated antenna is shown in Fig. 8.23 (b). The discrepancy in the measured S_{11} characteristics of HRCP antenna is mainly due to the effect of probe diameter. The proposed antennas have extremely small thickness and hence the feed connector diameter (D_{fr}) was designed to be very small (0.5 mm) to get better antenna performance. How-

ever, the lack of availability of off-the-shelf SMA connector with such small diameter, leads to the use of another connector with bigger probe dimension (D_{fr} = 1.6 mm). Thus, the measured reflection coefficient shows a remarkable change compared to the simulation result. However, the effect of probe dimension on the return loss is verified with the help of new simulation incorporating the new feeding diameter as shown in Fig. 8.23 (a). From the analysis, it is

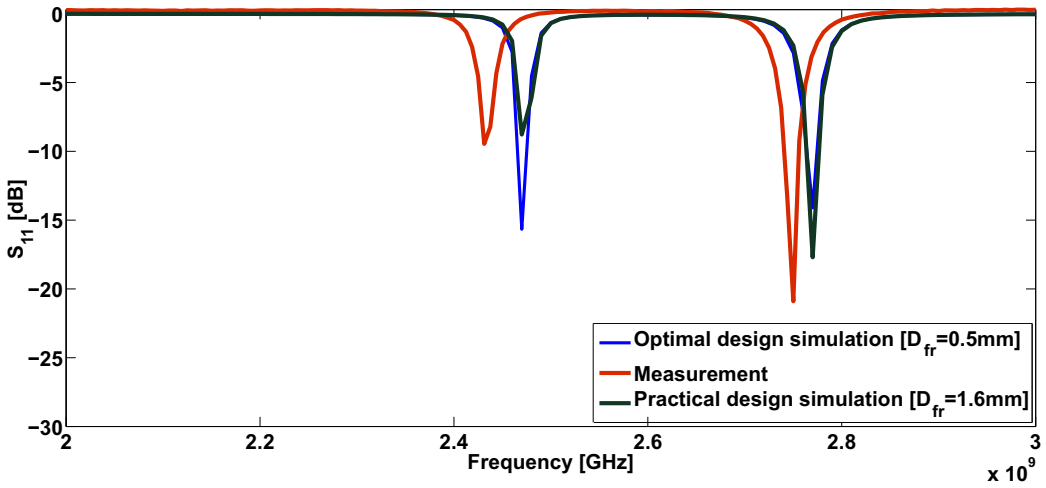

(a)

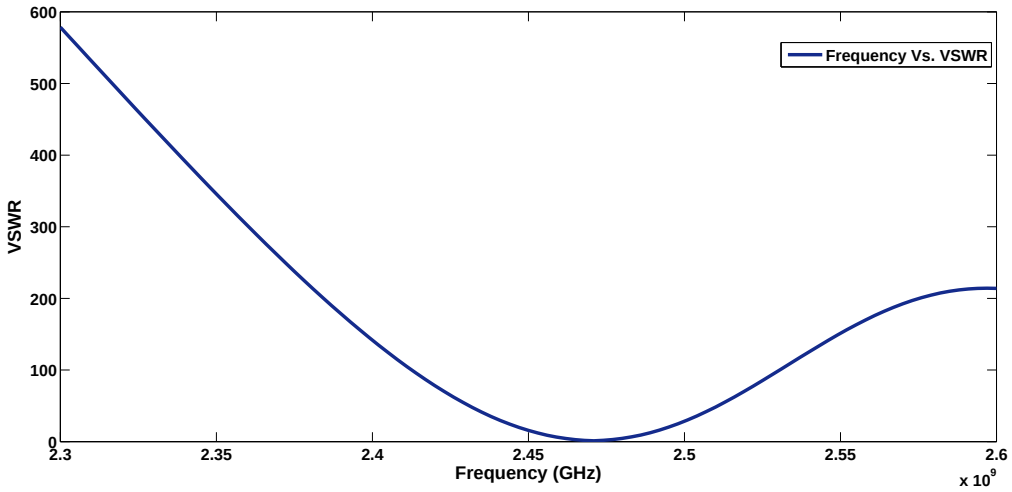

(b)

Figure 8.23 Simulated and measured reflection characteristics of the HRCP antenna array: (a) S_{11} parameter. (b) VSWR.

clear that the probe dimension has an effect on the antenna characteristics and the use of custom made SMA connector can eliminate the measurement discrepancy.

From the analysis of the antennas, it is clear that the discrepancies between the simulated and measured results may come various factors such as; connectors discontinuities, fabrication errors and high substrate losses. Also, the characteristics of SMA connectors have an important effect on measurement results. It is also important to mention that, the input impedance of a coaxial probe fed antenna is extremely sensitive to the distance between the via and the feeding probe location. Furthermore, the size of the via and the probe dimension also have an effect on antenna input impedance. Hence, to match the impedance of the antenna careful optimization of dimension and the position of vias and feed location is important.

8.5.2 Radiation Characteristics

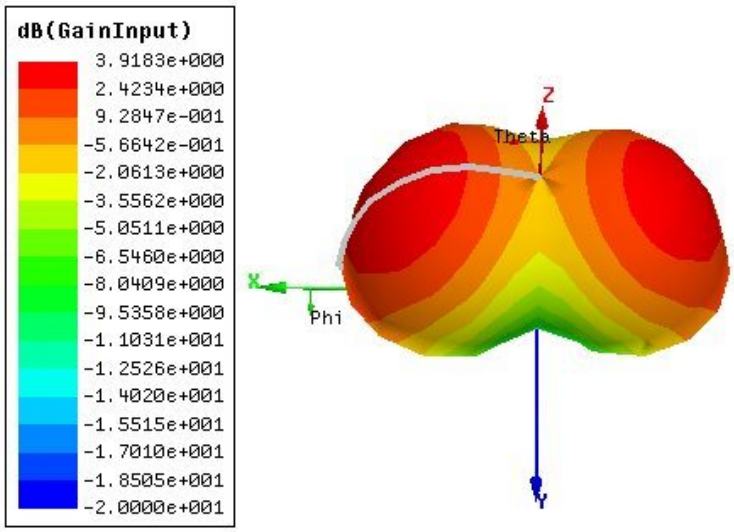

Figure 8.24 Simulated 3-D radiation pattern of the circular patch antenna array.

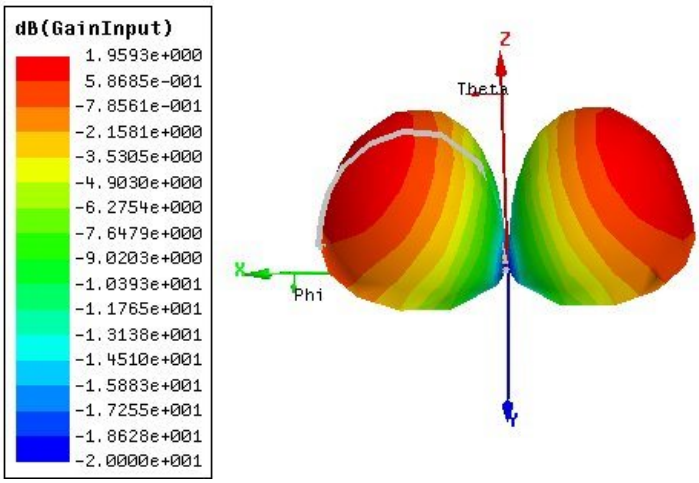

Figure 8.25 Simulated 3-D radiation pattern of the HCP antenna array.

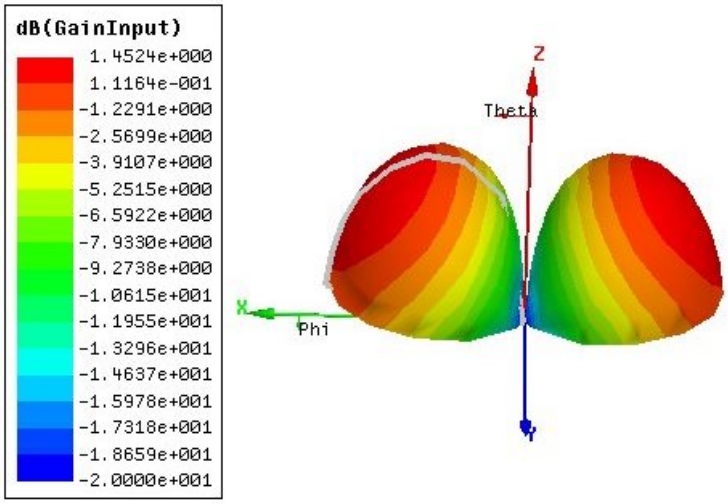

Figure 8.26 Simulated 3-D radiation pattern of the HRCP antenna array.

The three dimensional representation of radiation pattern of CP antenna is shown in Fig. 8.24. With 7 vias along the center of the feeding patch, the behavior of the patch antenna changed drastically. The antenna gain is 3.58 dB and the radiation pattern has two directions of strong radiation, one normal to the vias and one away from the coaxial feeding point as shown in Fig. 8.24. This

means that the maximum radiation will be towards the engine environment, if the receiver is positioned at the intake of the jet engine.

As explained before, the normal HCP antenna has a broadside radiation pattern. However, the antenna array geometry, alignment of notches and the dual feed line between the two patches changes the HCP antenna radiation pattern from a pattern that has its major lobe broadside to the ground plane, into a pattern that is pointing towards the engine and other lobe pointing outwards. Figure. 8.25 shows the 3-D radiation pattern of the simulated HCP antenna and the radiation pattern has two directions of strong radiation as shown in Fig. 8.25. The proposed antenna has a gain of 1.95 dB as shown in figure. This means that the maximum radiation will be towards the engine environment if the receiver is positioned at the intake of the jet engine. These results arise because of the careful iteration of the dimensions. Figure 8.26 shows the 3-D radiation pattern of the simulated HRCP antenna. The gain of the modified antenna is reduced to 1.42 dB because of the deformations introduced on the patch to reduce the size of the antenna design.

2-D Radiation Characteristics

In order to compare the simulation radiation characteristics with the measured results, the two dimensional representation of the radiation characteristics is evaluated. Figure 8.27 shows the simulated 2D radiation pattern (RP) of the CPAA geometry. The simulated and measured co-polarization radiation patterns of HCP array is shown in Fig. 8.28. The measured results agree well with the simulated results and the measured cross polarization is about 20 dB below the co-polarization level. Figure 8.29 shows the simulated and measured radiation characteristics of HRCP antenna. From Fig. 8.29, it is clear that the proposed antennas exhibits a dual radiation pattern with a null in the bore-sight direction of typically about $-20\,dB$. The measured results agrees very

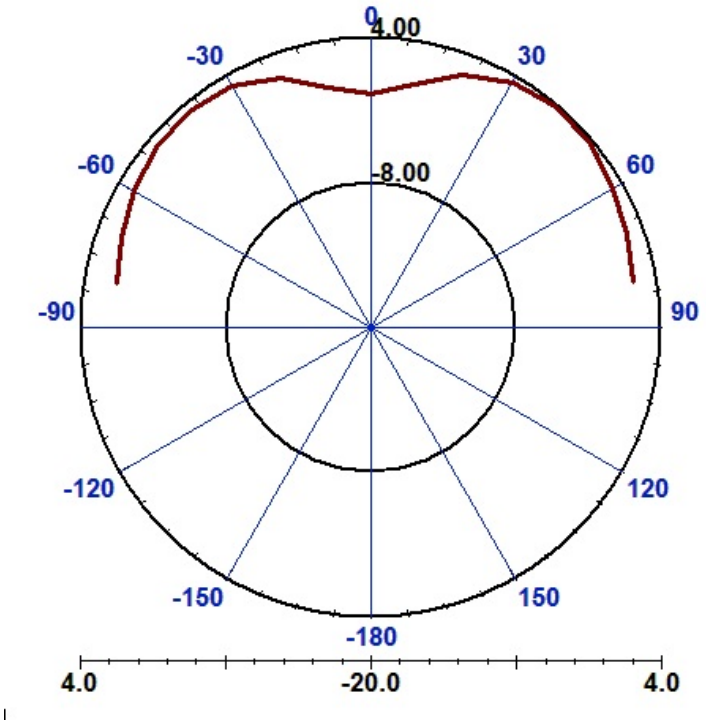

Figure 8.27 Simulated radiation characteristics of circular patch antenna array.

well with the simulated results and the measured cross polarization is about 19 dB below the co-polarization level

The measured radiation characteristics of all three antennas agrees very well with the simulated results. However, the small discrepancy may be due to the misalignment of the antenna during the measurement. All simulation results provided above have been achieved using infinite ground plane assumption because of our particular application. However, during fabrication and measurement process a finite ground plane is used and hence, the antenna input impedance will change slightly during measurement. This will affect the radiation characteristics of the antenna.

The proposed HRCP antenna shows low efficiency because of the extremely thin substrate thickness. Since the thickness is very small, the E-fields between the microstrip lines and ground plane will be extremely strong and this will de-

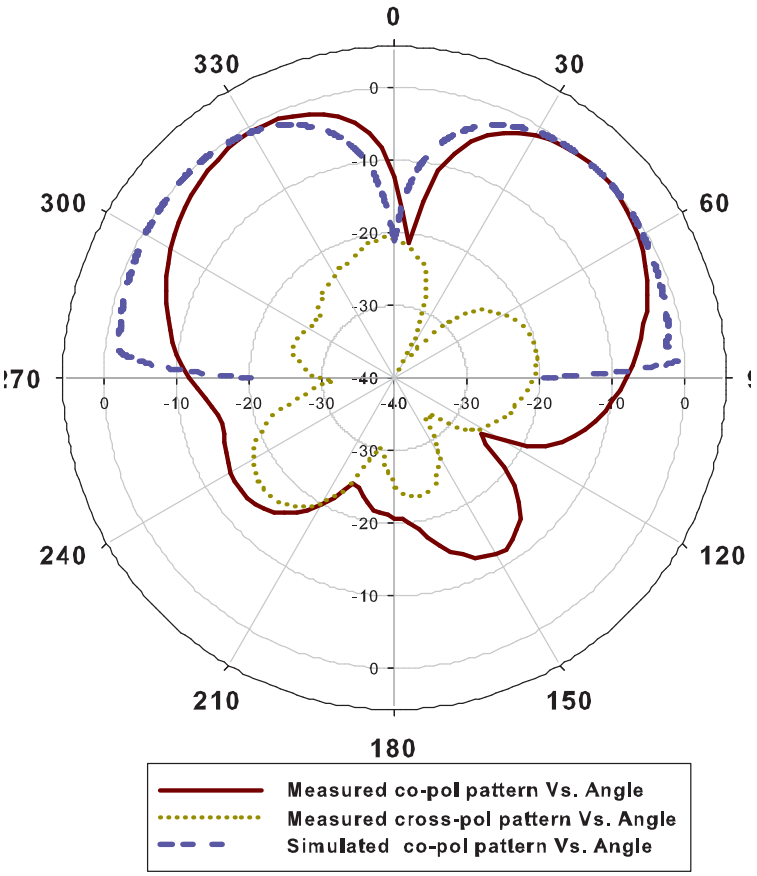

Figure 8.28 2-D Radiation pattern of proposed HCP antenna array.

crease the efficiency of the antenna [55]. However, for the jet engine application the distance between the sensor and the receiving antenna is very short and hence the low efficiency does not affect the system performance. The results are very promising for the future antenna measurements in real environment.

The radiation pattern of the HRCP design is very useful, if the antenna is positioned at the inlet of the jet engine. The main lobe of the radiation pattern is pointed towards the fan blade, where the sensors will be located. Also the total area of the radiating element is reduced considerably compared to CP antenna but still able to produce the required radiation pattern.

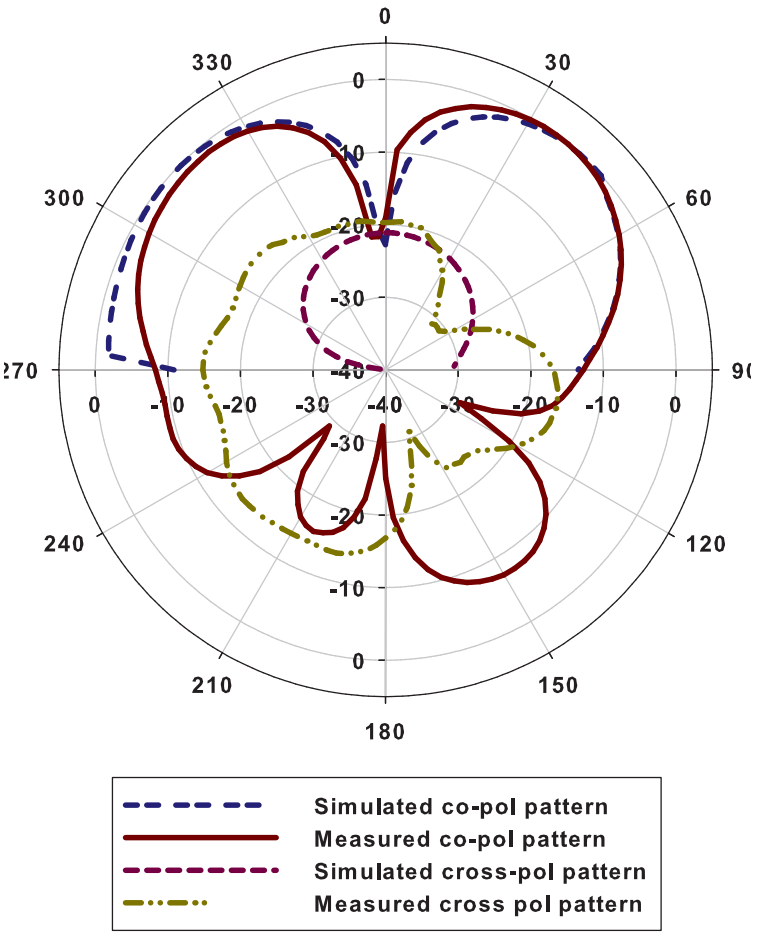

Figure 8.29 2-D Radiation pattern of proposed HRCP antenna array.

8.6 Discussion

This thesis propose three new antenna models for wireless communication application inside harsh metallic environment. A detailed analysis of the impedance characteristics and the radiation behavior of all three recommended antenna models are also provided. A two element circular patch antenna, modified half circle antenna and a hybrid rectangular circular patch antenna is analyzed. The overall dimension of the HRCP and HCP antenna is reduced significantly compared to the CP antenna model, still able to maintain the required dual

Table 8.1 Specification of substrate material.

Model	Material	ϵ_r	tanδ	h (mm)
Rectangular [57]	Rogers ULTRALAM 3850	2.9	0.0025	0.1
CP, HCP and HRCP	Rogers duroid 5880	2.2	0.0009	0.381

beam pattern. The area of half circle is almost half the area of CP antenna. It is clear from the analysis that, the impedance bandwidth of HCP antenna is smaller than that of CP geometry due to reduced overall patch dimension. All simulation results provided above have been achieved using infinite ground plane assumption because of our particular application. However, during fabrication and measurement process a finite ground plane is used and hence, the antenna input impedance will change slightly during the measurement. The measured and simulated radiation characteristics of all three antenna geometry agrees very well. However, it should be noted that the gain of the HCP antenna is marginally smaller than that of the CP geometry due the fact that the straight edge of HCP antenna also radiates. The gain of HRCP antenna is reduced slightly compared to the HCP, however the overall dimension of HRCP is significantly smaller than HCP geometry. The Table 8.1 shows a comparison of used substrate material and their characteristics.

The Table 8.2 shows a comparison 4 different antenna models proposed to use inside harsh environment. From the Table 8.2, it is clear that the area of the HRCP model is reduced significantly compared to the CP antenna model and the rectangular patch antenna, and still able to maintain the required characteristics. Since, the size of the proposed HRCP model is very small it can even mounted on the large jet engine environment without violating the conformity principle. That means, when there is an environmental constraint

Table 8.2 Comparison of various antenna model for harsh environment application.

Model	Length (mm)	Height (mm)	Area(mm^2)	F (GHz)	RL (dB)	G (dB)
Rectangular [57]	120	16	1920	2.48	-13	not available
CP	99	49	4851	2.47	-26.12	3.92
HCP	96	27	2592	2.44	-19.8	1.95
HRCP	88	20	1760	2.47	-15.83	1.45

on the size of the antenna, the slot loaded HRCP geometry has been proved as an effective and adaptable antenna system for the jet engine application. If there is no restriction on the size of the antenna, the more efficient CPA geometry can be adapted to harsh metallic fading environment applications.

8.7 Summary

The thesis presents the design and analysis of two element linear array of circular , modified half circle, and a hybrid rectangular patch array antenna that can be used for wireless communication application inside jet engines. In order to deal with harsh environment, the physical dimensions of the antenna is designed on an extremely thin and flexible substrate. The proposed design has an interesting low profile configuration with 0.381mm substrate height only. Hence, the antenna can be conformal to the jet engine environment. Moreover, the antennas are designed to have a canonical radiation characteristics. The designed antenna system is simulated, fabricated and tested using anechoic chamber. The simulation results and the measurement results shows some discrepancy due to fabrication error. The effect probe diameter on the measurement re-

sults are analyzed with the help of simulation and able to prove the reason for small discrepancy. The measured radiation pattern is really promising for the jet engine applications since the strongest radiation field of the antenna is pointed towards the engine blade. The proposed antennas have better performance compared to already existing model. The extremely small thickness of the substrate makes the manufacturing process of the antenna tedious. Since the antennas are going to be placed on a curved metallic environment, the manufactured antenna will be tested in such Harsh environment. The jet environment has large number of scatters and reflectors which distributed around the sensors; hence, a dual circular polarized patch antenna will be designed in future for better results.

Chapter 9: Conclusion

The contribution of this thesis is distinctive to the analysis of EM propagation inside complex jet engine geometries and design of a low profile antenna model. The ideas proposed in this thesis are not limited to the cases of jet engines and gas turbines because these problems can be generalized for the study of EM propagation inside any large, complex geometries containing rotating metallic objects. It was shown that none of the existing methods (deterministic and numerical) are ultimately successful in explaining the behavior of EM propagation inside the complex environment. Hence, the STEM is introduced as an exceptional tool that can capture the time-dynamic effects of the jet engine environment while providing feasible and accurate results compared to the traditional deterministic approach. The statistical based analysis proposed to model the EM propagation inside a complex jet engine environment is sufficiently accurate yet simple enough to describe the fields inside the complex and dynamic cavity environments.

- Two new system models and two different hypothesis are proposed to model the EM propagation inside jet engine by assuming that the environment is similar to a mechanically stirred reverberation chamber. A full wave FEM simulation software is used for modeling and analyzing the EM propagation inside the complex jet engine environment. When the excitation was at λ distance, $|E_z|^2$ was proven to have an exponential distribution function similar to a mechanically stirred RC. However,

when the excitation was other than λ position the real and the imaginary field components along the engine axis have Gaussian distributions. The effect of the dimension of the jet engine on the standard deviation of the electric field inside the jet engine is analyzed and proved that the σ of the electric field is linearly related to the radius of the jet engine.

- A novel SE concept was introduced as a method to translate the source of randomness inside the dynamic jet engine resulting from the blade rotation into a randomness resulting from varying the excitation current randomly. It is worth to mention that SE method is used for jet engine application for the first time. In order to deal with SE analysis the simplified static jet engine model has been considered as a static environment by using fixed blade position instead of rotating the blades. The excitation values inside the medium have been changed randomly according to a Gaussian distribution with certain characteristics. These analyzes suggested that analyzing a complex jet engine environment can be accomplished in a simplified yet accurate manner without the need to consider the dynamic rotation of the blades through multiple rotation simulation runs. The effect of excitation on the field characteristics of the dynamic and static systems has been analyzed and verified that both the systems are statistically linear with respect to input excitation. The result of numerical analysis of the static system model agrees well with the result of FEM simulation results. Numerical results demonstrate the reliability of the proposed SE technique. The statistical equivalence between the two systems has been verified. Moreover, the static system model analysis is more efficient compared to the dynamic system because of the ease of analysis and reduced computational complexity.

- Later, simplified jet engine model is analyzed to study the effect of frequency shift due to the blade rotation on the magnitude and phase of the received electric field inside the jet engine environment. The analysis is based on the theoretical Doppler spectrum method, where the Doppler frequency shift is calculated for a particular RPM. This analysis help to choose a best receiving location inside the jet engine environment, where the propagation of the EM field is less affected by the complex blade rotation and frequency shift. The results are promising for the statical excitation based jet engine system development by emulating the phase and magnitude deviation due to blade rotation into random excitation and hence the jet engine can be considered as a static system without blade rotation. Moreover, the results can guide the future Doppler spectrum analysis by using phase time variation of the transmitting and receiving signal inside the jet engine without considering the dynamic rotational speed of the blades.

- Finally, the design and analysis of two element linear array of circular , modified half circle, and a hybrid rectangular patch array antenna that can be used for wireless communication application inside jet engines was proposed. In order to deal with harsh environment, the physical dimensions of the antenna was designed on an extremely thin and flexible substrate. Moreover, the antennas are designed to have a dual beam radiation characteristics. The measured and simulated data shows some variations because of the losses arises due to the extremely thin substrate. As the height of the substrate is very small, the electric field exist between the patch and the ground plane will be extremely strong. This will reduce the efficiency of the antenna. However, to deal with the particular application the substrate should be extremely thin, not to affect the

airflow through the engine environment. The measured radiation pattern is really promising for the jet engine applications since the strongest radiation field of the antenna is pointed towards the engine blade. The extremely small thickness of the substrate makes the manufacturing process of the antenna tedious. However, the proposed HRCP geometry has been proved as an effective and adaptable antenna system for the jet engine application compared to existing models in the literature.

9.1 Future Scope

One of the main objective of this thesis was to analyze the characteristics of the EM propagation inside the jet engine environment to establish a wireless network inside the jet engine environment. The outcome of this thesis is very much useful for the analysis of the complex jet engine structures without considering their complex design geometry due to the advantages of the statistical method. However, a more detailed analysis is required to model the excitation parameters with respect to the dimension of the jet engine cavity. Furthermore, a detailed mathematical analysis is required to model the relation between the TX and the RX antenna location with the statistical parameters of the electric field propagation and hence, to control the characteristics of the statistical excitation parameters.

In this thesis, a Doppler frequency shift is emulated to study its effect on the electric field characteristics. The analysis proved that the magnitude and phase of the electric field at different receiving locations inside the jet engine environment have different characteristics. Consequently, to verify this result a real and complex jet engine set up with experimental measurements are required. Hence, in the near future a simple prototype of the real jet engine system will be used to validate our simulation results. Moreover, the

effect of phase deviation due to the blade rotation should account to model the statistical parameters of random excitation inside the static system approach.

The outcome of the conformal antenna design and analysis is really promising for modeling a modern harsh environment communication system model. However, a more detailed analysis is required to achieve the major constraints, such as size reduction, increased efficiency, and low manufacturing errors. A detailed study is required in this field to achieve the above mention criteria. Then, the designed antenna should be tested in the real harsh jet engine environment to analyze the effect of harsh environment on the antenna systems. The proposed antenna is designed for receiving purpose and hence it will be positioned on the outer casing of the inlet. However, the same proposed antenna can be used as a transmitter antenna, because of the particular dual beam radiation pattern it has. This need a detailed investigation in the future to identify a more suitable circularly polarized antenna array that can have the above mention criteria. Also, metamaterial substrate can be designed to reduce the size and to increase the efficiency of the proposed antenna model for the wireless communication application inside the harsh environment. A detailed study is required in this field to achieve the above mention criteria.

Bibliography

[1] G.Studor, "" fly-by-wireless": A revolution in aerospace vehicle architecture for instrumentation and control," 2007.

[2] R. K. Yedavalli and R. K. Belapurkar, "Application of wireless sensor networks to aircraft control and health management systems," *Journal of Control Theory and Applications*, vol. 9, no. 1, pp. 28–33, 2011.

[3] D.-K. Dang, A. Mifdaoui, and T. Gayraud, "Fly-by-wireless for next generation aircraft: Challenges and potential solutions," in *2012 IFIP Wireless Days*, Nov 2012, pp. 1–8.

[4] C. Zhang, J. Xiao, and L. Zhao, "Wireless asynchronous transfer mode based fly-by-wireless avionics network," in *2013 IEEE/AIAA 32nd Digital Avionics Systems Conference (DASC)*, Oct 2013, pp. 4C5–1–4C5–9.

[5] T. W. Johnson and D. L. Moffatt, "Electromagnetic scattering by open circular waveguides," *Radio Science*, vol. 17, no. 6, pp. 1547–1556, 1982.

[6] C. C. Huang, "Simple formula for the rcs of a finite hollow circular cylinder," *Electronics Letters*, vol. 19, no. 20, pp. 854–856, 1983.

[7] G. Crabtree, W. Huegle, and D. Salisbury, "RCS compact range test results for a set of simplified engine face models," *GE Aircraft Engines, Cincinnati, OH, Tech. Rep. TM94226*, 1994.

[8] H. Anastassiu, J. Volakis, and D. Ross, DCand Andersh, "Electromagnetic scattering from simple jet engine models," *IEEE Transactions on Antennas and Propagation,*, vol. 44, no. 3, pp. 420–421, 1996.

[9] K. K. Chan, R. Martin, and F. Tremblay, "Scattering from a cylinder with two sets of rotating blades," *IEEE International Symposium on Antennas and Propagation Digest, Montreal PQ, Canda*, pp. 274–277, July 1997.

[10] J. Liu, E. Dunn, P. Baldensperger, and J. Jin, "Computation of radar cross section of jet engine inlets," *Microwave and optical technology letters*, vol. 33, no. 5, pp. 322–325,, 2002.

[11] H. T. Anastassiu, "A review of electromagnetic scattering analysis for inlets, cavities, and open ducts," *IEEE trans.on Antennas and Propagation Magazine*, vol. 45, pp. 27–40, Dec., 2003.

[12] H. Anastassiu, J. Volakis, and D. Ross, "The mode matching technique for electromagnetic scattering by cylindrical waveguides with canonical terminations," *Journal of Electromagnetic Waves and Applications,*, vol. 11, no. 12, pp. 1363–1391, 1995.

[13] A. Abdelaziz, D. Trinchero, and T. Khattab, "Statistical analysis of electromagnetic field inside a jet engine using reverberation chamber approach," *PIERM*, vol. 24, pp. 157–165, 2012.

[14] A. Krishna, T. Khattab, A. F. Abdelaziz, and M. Guizani, "Applying statistical antenna approach in jet engine electromagnetics field analysis," *2013 Loughborough Antennas and Propagation Conference, Lougborough, UK*, 2013.

[15] Y. S. Shifrin, "Pioneer award: Statistical antenna theory: Formation and extension," *IEEE Aerospace and Electronic Systems Magazine*, vol. 31, no. 8, pp. 24–36, 2016.

[16] ——, "On history of occurrence of statistical antenna theory (sat). peculiarities of sat compared to usual antenna theory," *Telecommunications and Radio Engineering*, vol. 73, no. 19, 2014.

[17] ——, "Forty years experience in development of statistical antenna theory: A review," *Telecommunications and Radio Engineering*, vol. 69, no. 18, pp. 1591–1614, 2010.

[18] A. Sibille, "A small signal analysis of statistical antenna modelling," in *3rd European Conference on Antennas and Propagation.* IEEE, 2009, pp. 2102–2106.

[19] J. Liu and J. Jin, "A special higher order finite-element method for scattering by deep cavities," *IEEE Transactions on Antennas and Propagation,*, vol. 48, no. 5, pp. 694–703, 2000.

[20] H. Ling, R. Chou, and S. Lee, "Shooting and bouncing rays: Calculating the RCS of an arbitrarily shaped cavity," *IEEE Transactions on Antennas and Propagation,*, vol. 37, no. 2, pp. 194–205, 1989.

[21] R. Burkholder, R. Chou, and P. Pathak, "Two ray shooting methods for computing the EM scattering by large open-ended cavities," *Computer physics communications*, vol. 68, no. 1-3, pp. 353–365, 1991.

[22] P. Baldensperger, J. Liu, and J. Jin, "A hybrid SBR/FE-BI technique for computing the RCS of electrically large objects with deep cavities," in *IEEE Antennas and Propagation Society International Symposium*, vol. 4, 2001, pp. 726–729.

[23] J. Odendaal and D. Grygier, "RCS measurements and results of an engine-inlet system design optimization," *IEEE Antennas and Propagation Magazine,*, vol. 42, no. 6, pp. 16–23, 2000.

[24] S. Wong, E. Riseborough, G. Duff, and K. Chan, "Radar cross-section measurements of a full-scale aircraft duct/engine structure," *IEEE Transactions on Antennas and Propagation,*, vol. 54, no. 8, pp. 2436–2441, 2006.

[25] H. W. Naus, "Statistical electromagnetics: Complex cavities," *IEEE Transactions on Electromagnetic Compatibility*, vol. 50, pp. 316–324, May, 2008.

[26] A. Panaretos, C. Balanis, and C. Birtcher, "Shielding effectiveness and statistical analysis of cylinderical scale fuselage model," *IEEE Transactions on Electromagnetic Compatibility*, vol. 42, pp. 361–366, May, 2005.

[27] T. Panaretos, C. Balanis, and C. Birtcher, "HIRF penetration into simplified fuselage using a reverberation chamber approach," *IEEE Transactions on Electromagnetic Compatibility*, vol. 47, pp. 667–670, August, 2005.

[28] R. Vaughn and J. Anderson, *Channels, Propagation, and Antennas for Mobile Communications.* London: IEE Press, 2003.

[29] Y. Kim, H. Lim, J.-H. Han, W.-Y. Song, and N.-H. Myung, "Rcs reduction of open-ended circular waveguide cavity with corrugations using mode matching and scattering matrix analysis," *Progress In Electromagnetics Research*, vol. 146, pp. 57–69, 2014.

[30] J. Jin, S. Ni, and S. Lee, "Hybridization of SBR and FEM for scattering by large bodies with cracks and cavities," *IEEE Transactions on Antennas and Propagation,*, vol. 43, no. 10, pp. 1130–1139, 1995.

[31] T. T. Chia, R. J. Burkholder, and R. Lee, "The application of FDTD in hybrid methods for cavity scattering analysis," *IEEE International Symposium on Antennas and Propagation Digest, Montereal PQ, Canda*, pp. 274–277, July 1997.

[32] J. Jin, F. Ling, S. Carolan, J. Song, W. Gibson, W. Chew, C. Lu, and R. Kipp, "A hybrid SBR/MOM technique for analysis of scattering from small protrusions on a large conducting body," *IEEE Transactions on Antennas and Propagation,*, vol. 46, no. 9, pp. 1349–1357, 1998.

[33] H. Lim and N. H. Myung, "A novel hybrid aipo-mom technique for jet engine modulation analysis," *Progress in Electromagnetic Research, PIER*, vol. 45, pp. 27–40, Dec. 2003.

[34] R. Burkholder and T. Lundin, "Forward-backward iterative physical optics algorithm for computing the rcs of open-ended cavities," *IEEE Transactions on Antennas and Propagation*, vol. 53, no. 2, pp. 793–799, 2005.

[35] F. Obelleiro-Basteiro, J. Luis Rodriguez, and R. Burkholder, "An iterative physical optics approach for analyzing the electromagnetic scattering by large open-ended cavities," *Antennas and Propagation, IEEE Transactions on*, vol. 43, no. 4, pp. 356–361, 1995.

[36] F. Obelleiro, J. Rodriguez, and A. Pino, "A progressive physical optics (ppo) method for computing the electromagnetic scattering of large open-ended cavities," *Microwave and Optical Technology Letters*, vol. 14, no. 3, pp. 166–169, 1997.

[37] G. Thiele and T. Newhouse, "A hybrid technique for combining moment methods with the geometrical theory of diffraction," *IEEE Transactions on Antennas and Propagation,*, vol. 23, no. 1, pp. 62–69, 1975.

[38] E. Ekelman and G. Thiele, "A hybrid technique for combining the moment method treatment of wire antennas with the GTD for curved surfaces," *IEEE Transactions on Antennas and Propagation,*, vol. 28, no. 6, pp. 831–839, 1980.

[39] C. Lu and W. Chew, "Fast far field approximation for calculating the RCS of large object," *Micowave.Opt.Tech.Lett.,*, vol. 8, pp. 238–241, 1995.

[40] K. Chan and S. Wong, "Modal approach to RCS computation of electrically large inlets," in *IEEE Antennas and Propagation Society International Symposium*, vol. 3, 2002, pp. 114–117.

[41] D. Ross, J. Volakis, and H. Anastassiu, "Hybrid finite element-modal analysis of jet engine inlet scattering," *IEEE Transactions on Antennas and Propagation*, vol. 43, no. 3, pp. 277–285, 1995.

[42] S. H. Choi, D. Seo, and N. Myung, "Scattering analysis of open-ended cavity with inner object," *Journal of Electromagnetic Waves and Applications*, vol. 21, 2007.

[43] H. LIM and N. MYUNG, "A hybrid ipo-mom technique for wave scattering analysis of jet engine," *Conference on AP/EMC/EMT, Incheon, Korea*, 2009.

[44] K. Chan, S. Wong, and E. Riseborough, "Radar cross section modeling and measurements of inlets and cylinders with skew blades," *IEEE Transactions on Antennas and Propagation,*, vol. 54, no. 10, pp. 2930–2939, 2006.

[45] H. Lim, J. Yoo, C. Kim, K. Kwon, and N. Myung, "Radar cross section measurements of a realistic jet engine structure with rotating parts," *Journal of Electromagnetic Waves and Applications*, vol. 25, no. 7, pp. 999–1008, 2011.

[46] M. Gruden, M. Jobs, and A. Rydberg, "Measurements and simulations of wave propagation for wireless sensor networks in jet engine turbines," *IEEE Antennas and Wireless Propagation Letters*, vol. 10, 2011.

[47] ——, "Measurements and simulations of wave propagation for wireless sensor networks in jet engine turbines," *Antennas and Wireless Propagation Letters, IEEE*, vol. 10, pp. 1139–1142, 2011.

[48] D. Hill, *Electromagnetic fields in cavities: deterministic and statistical theory.* John Wiley & Sons, Inc., 2009.

[49] P. Corona, G. Ferrara, and M. Migliaccio, "Reverberation chambers as sources of stochastic electromagnetic fields," *IEEE Trans. on Electromagnetic Compatibility*, vol. 38, no. 3, pp. 348–356, Aug., 1996.

[50] D. A. Hill, "Electromagnetic theory of reverberation chambers," *U.S. Nat. Inst. Stand. Technol. Tech. Note 1506*, 1998.

[51] C. Bunting, "Statistical characterization and the simulation of a reverberation chamber using finite-element techniques," *IEEE Transactions on Electromagnetic Compatibility*, vol. 44, no. 1, pp. 214–221, 2002.

[52] G. J. Freyer and M. O. Hatfield, "Aircraft test applications of reverberation chambers," *IEEE Electromagnetic Compat. Int. Symp.*, pp. 491–496, Aug., 1994.

[53] D. R. Kempf, "EMV testing of aircraft: A comparison of the mode-stirred and standard methods," *IEEE Electromagn. Compat. Int. Symp.*, pp. 185–189, Aug. 1996.

[54] Y. Shriftin, "Statistical antenna theory." *Statistical antenna theory., by Shriftin, YS. Boulder, CO (USA): The Golem Press, 370 p.*, vol. 1, 1971.

[55] J. James and H. P.S, *Handbook of Microstrip Antennas.* Peter Peregrinus LTD, U.K, 1989.

[56] S. A. Mitilineos, S. K. Symeonidis, M. B. Ioannis, D. Iliopoulos, G. S. K. , S. P. Savaidis, and N. A. Stathopoulos, "Conformal patch antenna arrays design for onboard ship deployment using genetic algorithms," *Advances in Power Electronics*, vol. 2013, 2013.

[57] M. Gruden, M. Jobs, and A. Rydberg, "Design and evaluation of conformal patch antenna array for use with wireless sensor network inside jet engines," in *7th European Conference on Antennas and Propagation (EuCAP), 2013*, 2013.

[58] M. Hinnemo, M. Grudén, and A. Rydberg, "Design of a miniaturized patch antenna for easy deployment on metal surfaces," *Microwave and Optical Technology Letters*, vol. 55, pp. 723–727, 2013.

[59] M. Gruden, "Wireless sensor network systems in harsh environments and antenna measurement techniques," 2014.

[60] R. Holland and R. John, *Statistical electromagnetics*. CRC, 1999.

[61] A. krishna, T. Khattab, A. F. Abdelaziz, and M. Guizani, "A review of the analysis of electromagnetic fields inside jet engines," *Submitted to IEEE microwave magazine*, 2016.

[62] A. Abdelaziz, D. Trinchero, and T. Khattab, "New methodology for field analysis inside jet engine," IEEE AP-S and URSI National radio Science Meeting, Seattle, USA, 2011.

[63] A. Papoulis, *Probability, Random Variables, and Stochastic Processes*. New York: McGraw-Hill Book Co., 1965.

[64] D. Hill, "Plane wave integral representation for fields in reverberation chambers," *IEEE Trans.on Electromagn. Compat.*, vol. 40, pp. 209–217, 1998.

[65] L. Musso, "Assessment of reverberation chamber testing for automotive applications," *PbIl Thesis, Politecnico di Torino, Turin, Italy*, 2003.

[66] E. Lee and J. Wang, *Statistical methods for survival data analysis*. Wiley-Interscience, 2003, vol. 364.

[67] Y. S. Lee, J. Kwon, and S. Park, "Extension of a plane wave integral representation for fields in lossy reverberation chambers," *Electromagnetics,*, vol. 35, no. 4, 2015.

[68] A. Krishna, T. Khattab, A. F. Abdelaziz, and M. Guizani, "On the statistical distribution of electric field inside jet engines," *IEEE AP-S and URSI National radio Science Meeting, Florida, USA*, 2013.

[69] J.-I. Hong and C.-S. Huh, "Optimization of stirrer with various parameters in reverberation chamber," *Progress In Electromagnetics Research*, vol. 104, pp. 15–30, 2010.

[70] "Draft IEC 61000-4, section 21, reverberation chambers test methods," *Electromagnetic Compatibility(EMC) Part 4: Testing and Measurement Techniques*, 2001.

[71] E. Walton, J. Young, J. Moore, and K. Davis, "EM propagation in jet engine turbines," *Annual Meeting Symposium of the Antenna Meas. Tech. Assoc.,*, 2006.

[72] M. Gruden, M. Jobs, and A. Rydberg, "Empirical tests of wireless sensor network in jet engine including characterization of radio wave propagation and fading," *IEEE Antennas and Wireless Propagation Letters*, 2014.

[73] L. Koschel, K. Mahler, R. Felbecker, and M. Frey, "Rf-mimo for smart metering communication under harsh conditions," in *2014 IEEE Conference on Wireless Sensors (ICWiSE)*, Oct 2014, pp. 55–60.

[74] M. Lieberei and U. Zolzer, "Mimo channel measurements inside an aircraft cabin with planar transmit antennas," in *Communications (MICC), 2009 IEEE 9th Malaysia International Conference on*. IEEE, 2009, pp. 229–233.

[75] P. Kyritsi, D. C. Cox, R. A. Valenzuela, and P. W. Wolniansky, "Correlation analysis based on mimo channel measurements in an indoor environment," *Selected Areas in Communications, IEEE Journal on*, vol. 21, no. 5, pp. 713–720, 2003.

[76] P. Kyritsi and D. C. Cox, "Correlation properties of mimo radio channels for indoor scenarios," in *Signals, Systems and Computers, 2001. Conference Record of the Thirty-Fifth Asilomar Conference on*, vol. 2. IEEE, 2001, pp. 994–998.

[77] T. A. Lamahewa, R. A. Kennedy, T. D. Abhayapala, and T. Betlehem, "Mimo channel correlation in general scattering environments," in *Communications Theory Workshop, 2006. Proceedings. 7th Australian*. IEEE, 2006, pp. 93–98.

[78] L. Lanbo, Z. Shengli, and C. Jun-Hong, "Prospects and problems of wireless communication for underwater sensor networks," *Wireless Communications and Mobile Computing*, vol. 8, no. 8, pp. 977–994, 2008.

[79] C. Oestges, "Validity of the kronecker model for mimo correlated channels," in *Vehicular Technology Conference, 2006. VTC 2006-Spring. IEEE 63rd*, vol. 6. IEEE, 2006, pp. 2818–2822.

[80] D.-S. Shiu, G. J. Foschini, M. J. Gans, and J. M. Kahn, "Fading correlation and its effect on the capacity of multielement antenna systems," *IEEE Transactions on communications*, vol. 48, no. 3, pp. 502–513, 2000.

[81] D. Gesbert, H. Bolcskei, D. A. Gore, and A. J. Paulraj, "Outdoor mimo wireless channels: models and performance prediction," *IEEE Transactions on Communications*, vol. 50, no. 12, pp. 1926–1934, Dec 2002.

[82] I. S. Shifrin, *Statistical antenna theory*. Golem Press, 1971, vol. 7.

[83] A. Sibille, "Statistical antenna modeling," *29 th URSI General Assembly*, pp. 10–16, 2008.

[84] C. Roblin, "A preliminary approach of the statistical modelling of antennas for the UWB communications," *ICEAA-EESC'05*, 2005.

[85] R. D'Errico, C. Roblin, and A. Sibille, "A statistical analysis of antenna scattering in uwb arrays," in *Antennas and Propagation, 2009. EuCAP 2009. 3rd European Conference on.* IEEE, 2009, pp. 2562–2566.

[86] J. M. de Sa, *Applied Statistics Using SPSS, STATISTICA, MATLAB and R.* Springer„ 2007.

[87] M. Jobs, M. Gruden, and A. Rydberg, "Modelling of em propagation in simplified jet turbine structure using helical rays," *Electronics Letters*, vol. 51, no. 11, pp. 809–811, 2015.

[88] V. C. Chen, F. Li, S.-S. Ho, and H. Wechsler, "Micro-doppler effect in radar: phenomenon, model, and simulation study," *Aerospace and Electronic Systems, IEEE Transactions on*, vol. 42, no. 1, pp. 2–21, 2006.

[89] P. Hallbjorner and A. Rydberg, "Maximum doppler frequency in reverberation chamber with continuously moving stirrer," in *Antennas and Propagation Conference, 2007. LAPC 2007. Loughborough.* IEEE, 2007, pp. 229–232.

[90] K. Karlsson, X. Chen, P.-S. Kildal, and J. Carlsson, "Doppler spread in reverberation chamber predicted from measurements during step-wise stationary stirring," *IEEE Antennas and wireless propagation letters*, vol. 9, pp. 497–500, 2010.

[91] J.-H. Choi, J.-H. Lee, and S.-O. Park, "Characterizing the impact of moving mode-stirrers on the doppler spread spectrum in a reverberation chamber," *IEEE Antennas and Wireless Propagation Letters*, vol. 9, pp. 375–378, 2010.

[92] M. Jeong, B.-Y. Park, J. Choi, and S.-O. Park, "Doppler spread spectrum of a circularly moving receiver in an anechoic and a reverberation chamber," *Progress In Electromagnetics Research C*, vol. 48, pp. 125–132, 2014.

[93] C. A. Balanis, *Antenna Theory: Analysis and Design.* Wiley-Interscience, 2005.

[94] G. Kumar and K. Ray, *Broadband microstrip antennas.* Artech House, 2003.

[95] T. Lo, C.-O. Ho, Y. Hwang, E. Lam, and B. Lee, "Miniature aperture-coupled microstrip antenna of very high permittivity," *IET Electronics Letters*, vol. 33, pp. 9–10, 1997.

[96] M. Abbaspour and H. R. Hassani, "Wideband star-shaped microstrip patch antenna," *Progress In Electromagnetics Research Letters*, vol. 1, pp. 61–68, 2008.

[97] J. Liu, Q. Xue, H. Wong, and H. Lai, "Design and analysis of a low-profile and broadband microstrip monopolar patch antenna," *IEEE Transactions on Antennas and Propagation*, vol. 61, 2013.

[98] G. Ramesh, *Microstrip antenna design handbook*. Artech house, 2001.

[99] J. A. Ansari, P. Singh, N. P. Yadav, and B. R. Vishvakarma, "Analysis of shorting pin loaded half disk patch antenna for wideband operation," *Progress In Electromagnetics Research C*, vol. 6, pp. 179–192, 2009.

[100] I. J. Bahl, *Lumped elements for RF and microwave circuits*. Artech house, 2003.

[101] Y. Wang and C. Lee, "Versatile semi-disc microstrip antennas: Study and application," *Journal of electromagnetic waves and applications*, vol. 15, no. 12, pp. 1595–1613, 2001.

[102] X.-X. Zhang and F. Yang, "Study of a slit cut on a microstrip antenna and its applications," *Microwave and Optical Technology Letters*, vol. 18, no. 4, 1998.

[103] M. K. Meshram and B. R. Vishvakarma, "Gap-coupled microstrip array antenna for wide-band operation," *International Journal of Electronics*, vol. 88, no. 11, pp. 1161–1175, 2001.

[104] A. Derneryd, "Analysis of the microstrip disk antenna element," *IEEE Transactions on Antennas and Propagation*, vol. 27, no. 5, pp. 660–664, 1979.

[105] S. Vishvakarma and B. R. Vishvakarma, "Analysis of inclined slot-loaded patch for dual-band operation," *Microwave and optical technology letters*, vol. 48, no. 12, pp. 2436–2441, 2006.

[106] J. A. Ansari, A. Mishra, and B. R. Vishvakarma, "Half u-slot loaded semi-circular disk patch antenna for gsm mobile phone and optical communications," *Progress In Electromagnetics Research C*, vol. 18, pp. 31–45, 2011.

[107] S. Maci, G. B. Gentili, P. Piazzesi, and C. Salvador, "Dual-band slot-loaded patch antenna," *IEE Proceedings-Microwaves, Antennas and Propagation*, vol. 142, no. 3, pp. 225–232, 1995.

[108] K. Chung, J. Kim, and J. Choi, "Wideband microstrip-fed monopole antenna having frequency band-notch function," *IEEE Microwave and Wireless Components Letters*, vol. 15, no. 11, pp. 766–768, 2005.

[109] K. Parasnis, L. Shafai, and G. Kumar, "Performance of star microstrip as a linearly and circularly polarised tm2, 1 mode radiator," *Electronics Letters*, vol. 22, p. 463, 1986.

[110] L. Economou and R. J. Langley, "Patch antenna equivalent to simple monopole," *Electronics letters*, vol. 33, no. 9, pp. 727–729, 1997.

Chapter A: Analytical Approach Of segment1

A.1 Plane wave Representation

The jet engine analysis proved that, the complex metallic jet engine cavity creates a statistically uniform electric field similar to RC, once excited by an internal EM source. Hence, the Hill's plane wave integral representation for RC field can be used to analyze the characteristics of the field components of an ideal jet engine environment [64]. Fig. 3.2(b) is considered as a well stirred ideal environment similar to a mechanically stirred RC and the environment generates a statistically uniform field. Then, we will analyze the statistical properties for one electric field rectangular component at one receiving point inside the jet engine cavity.

The electric field at a particular position $\vec{r}$ inside the jet engine environment can be represented as a finite sum of plane wave contributions at that point as in (A.1), where $\vec{k}$ is the wave propagation vector and $\vec{E}(\vec{i})$ is the ith plane wave representation [64, 65].

$$\vec{E}(\vec{r}) =_{i=1}^{n} \sum \vec{E}(\vec{i}) exp(j\vec{k}.\vec{r}) \tag{A.1}$$

However, from the plane wave analysis it is clear that the mean value of the electric field, which is the sum of a large number of multipath rays with

random phase inside a well stirred cavity will be zero. i.e;

$$\left\langle \vec{E}(\vec{r}) \right\rangle = \int\int \left(\left\langle F(\vec{\Omega}) \right\rangle exp(j\vec{k}.\vec{r}) d\Omega \right) = 0 \tag{A.2}$$

Also, it is proved that the mean-square value of the electric field is independent of position as shown in (4.5), where E_0 is the constant amplitude of the plane wave.

$$\left\langle |\vec{E}(\vec{r})|^2 \right\rangle \equiv |E_0|^2 \tag{A.3}$$

Later, we analyze the statistical properties of one of the electric field rectangular component as shown in (A.4) [65]. The same analysis can be applied to all the other rectangular components. Hence,

$$E_Z = |E_0| cos(\theta) sin(\theta) cos(\phi) + j|E_0| cos(\theta) sin(\theta) sin(\phi) \tag{A.4}$$

The mean value and the variance of the the real ($E_{Z,r}$) and imaginary ($E_{Z,i}$) field component can be expressed as shown in (A.5) and (A.6) [64, 65].

$$Mean\left\{E_{Z,r}\right\} = Mean\left\{E_{Z,i}\right\} = 0 \tag{A.5}$$

$$Variance\left\{E_{Z,r}\right\} = Variance\left\{E_{Z,i}\right\} = \frac{|E_0|^2}{6} = \sigma^2 \tag{A.6}$$

The statistical characteristics of the amplitude and squared amplitude of the rectangular field component and the total field component can be derived as a function of mean and variance of the real and imaginary field component by using (A.5) and (A.6) [63, 65]. Hence, the mean value of the electric field component inside the engine cavity can be derived according to [64] as shown in (A.7) and (A.8) , where E_0 is a free parameter to match the amplitude of the fields resulting from the jet engine model with the fields amplitude measured in a real chamber. $|E_0|^2$ can be represented in terms of the cavity parameters as shown in (4.7), where $\mathbf{Q}$ and $\mathbf{V}$ can be evaluated using (A.9) and (A.10) [65].

$$\langle |E_z| \rangle = E_0 \cdot \sqrt{\mathbf{n}} \cdot \sqrt{\frac{\pi}{12}} \tag{A.7}$$

$$\left\langle |E_z|^2 \right\rangle = \mathbf{n} \frac{|E_0|^2}{3}, \tag{A.8}$$

$$\mathbf{Q} = \frac{16\pi^2 \mathbf{V}}{\lambda^3}, \tag{A.9}$$

$$\mathbf{V} = \pi \mathbf{R_r}^2 \mathbf{L}. \tag{A.10}$$

Furthermore, a detailed statistical analysis of sum of different plane waves ($\mathbf{n}$) inside a complex cavity is available in [65]. The analysis was based on a random plane wave coupling approach and the analysis proved that each plane wave has random propagation direction, polarization and phase, but constant amplitude (E_0). It should be noted that, the parameter E_0 can be used to

match the amplitude of fields resulting from the coupling model with the fields amplitude measured in an ideal well stirred environment. The mean value of the amplitudes of the field rectangular components and the mean value of the squared amplitudes of the field rectangular components resulting from the sum of $\mathbf{n}$ random plane waves are also studied using this plane wave coupling approach. The mean value and the variance of the rectangular field component inside the jet engine cavity can be analyzed using the same approach as in [65].

$$\langle |E_z| \rangle = E_0 \cdot \sqrt{\mathbf{n}} \cdot \sqrt{\frac{\pi}{12}} \tag{A.11}$$

A detailed analysis to match the field characteristics generated using the plane wave coupling approach and the field mean amplitude measured in a real chamber is also available in [65]. However, due to the complexity of this analytical approach to solve the entire jet engine model a novel SE based approach is proposed for the analysis of complex jet engine cavity.

Chapter B: Code for jet engine simulation

B.1 VB code for jet engine dynamic simulation

```
' ----------------------------------------------
' Script Recorded by Ansoft HFSS Version 10.0
' 9:06 PM  Sep 30, 2012
' ----------------------------------------------

Dim oAnsoftApp
Dim oDesktop
Dim oProject
Dim oDesign
Dim oEditor
Dim oModule

Set oAnsoftApp = CreateObject("AnsoftHfss.
    HfssScriptInterface")
Set oDesktop = oAnsoftApp.GetAppDesktop()
Set oProject = oDesktop.SetActiveProject("
    jet_engine_surface_hertzian_dipole_0_X190_Z45_b24_a_00120
    ")
```

```
For i= 0 To 119
Set oDesign = oProject.SetActiveDesign("HFSSDesign1")
oDesktop.RestoreWindow
Set oEditor = oDesign.SetActiveEditor("3D Modeler")
oDesign.AnalyzeAll
oProject.Save
Set oModule = oDesign.GetModule("FieldsReporter")
oModule.EnterQty "E"
oModule.CalcOp "CmplxMag"
oModule.ExportToFile _

  "C:\Users\aparna\Dropbox\HFSS\HFSS_ROTTAION_CURRENT\
     MAG_E_I_00120\position"&i&"
     _mag_current_00120_X190_Z45.reg", _
"C:\APZ_QU_FILES\HFSS_COORDINATE_FILE\grid_radius150_z66
   .pts", _
  "Setup1 : LastAdaptive", Array("Freq:=", "5GHz", "
     Phase:=", "0deg", "a:=", _
  "190mm", "antenna_length:=", "7.5mm", "
     antenna_location:=", "75mm", "antenna_rad:=", _
  "1mm", "b:=", "30mm", "blade_thickness:=", "2.5deg", "
     l:=", "20mm", "lambda:=", _
  "60mm", "length_outer:=", "180mm", "phii:=", "13.2deg
     ", "sector_thickness:=", _
  "22.5deg")
```

```
oProject.SaveAs "C:\APZ_QU_FILES\HFSS_ROTATION_CURRENT\
    Rotation_a_00120\jet_engine_surface_hertzian_dipole_"&
    i+1&"_X190_Z45_b24_a_00120.hfs" & _
  "s", true
oEditor.Rotate Array("NAME:Selections", "Selections:=",
    _
  "thickness1,thickness1_1,thickness1_2,thickness1_3,
     thickness1_4,thickness1_5,th" & _
  "ickness1_6,thickness1_7,thickness1_8,thickness1_9,
     thickness1_10,thickness1_11," & _
  "thickness1_12,thickness1_13,thickness1_14,
     thickness1_15,thickness1_16,thicknes" & _
  "s1_17,thickness1_18,thickness1_19,thickness1_20,
     thickness1_21,thickness1_22,th" & _
  "ickness1_23"), Array("NAME:RotateParameters", "
     CoordinateSystemID:=", -1, "RotateAxis:=", _
  "Z", "RotateAngle:=", "0.125deg")
Next
```

B.2 Matlab code for jet engine simulation

```
%clear all
rot_size = 119;
pt_size = 17;
% load Efield_a_180_blade_24_180_75.mat E
% load Cordinate_current_00075.mat corr
```

```
corr = xlsread('position0_mag_new_a_180_24_190_45.xlsx
    ','a1:c17')
%empty = []; %positions failed to simulate
%kk = 1;
for j = 1:pt_size

    for i = 0:rot_size



        E(i+1 + (j-1)*(rot_size+1),:) = xlsread(['
            position' int2str(i) '
            _mag_new_a_180_24_190_45.xlsx'],['d' int2str(
            j) ':F' int2str(j)]);


    end
end

%
for l= 1:pt_size
for k = 1:pt_size
    temp = (E(1 + (k-1)*(rot_size+1) :rot_size+1 + (k-1)
        *(rot_size+1),3));
   % temp = ((E(1 + (k-1)*(rot_size+1) :rot_size+1 + (k
       -1)*(rot_size+1),1)).^2 + (E(1 + (k-1)*(rot_size+1)
        :rot_size+1 + (k-1)*(rot_size+1),2)).^2);
    %temp = (E(1 + (k-1)*(rot_size+1) :rot_size+1 + (k
        -1)*(rot_size+1),1)).^2;
```

```
  %  temp = sqrt(sum((E(1 + (k-1)*(rot_size+1) :rot_size
      +1 + (k-1)*(rot_size+1),:)).^2,2));
     Ez2(:,k) = temp;
     Ez(:,k)=Ez2(:,k)
   % Rho(l,k)=corr2(Ez2(:,l),Ez2(:,k));
     mean_Ez2(k) = sum(temp)/(rot_size);
     mean_Ez2(k) = 1;
end
end
pos = 6
for k = 1:pt_size
     temp = sqrt(sum((E(pos + (k-1)*(rot_size+1) :pos + (
        k-1)*(rot_size+1),:)).^2,2));
     mean_E_position1_mag(k) = mean(temp);
end
theta = atan(corr(:,2)./corr(:,1));
polar(theta,mean_Ez2','ro')
%x = (Ez2(:,1))/mean_Ez2(1);
%x_axis = (min(x): (max(x) - min(x))/20 : max(x));
point = 10;
figure(2)
hist((Ez2(:,point))/mean_Ez2(point),10);
[N,x_axis] = hist((Ez2(:,point))/mean_Ez2(point),10);
N_norm = N/(rot_size+1);

%==New======
%Ez2_norm = (Ez2(:,point))/mean_Ez2(point);
```

```
index = [1 3 6 11];
for k = 1:length(index)
Ez2_norm = ((Ez2(:,index(k)))/mean_Ez2(index(k)));
figure(3)

subplot(2,2,k); normplot(Ez2_norm);
%legend('pt1','pt2','pt3')
end
mu=zeros(1,pt_size);
sig =zeros(1,pt_size);
mu_c = zeros(2,pt_size);
sig_c = zeros(2,pt_size);
for ii = 1:pt_size
    [mu(ii),sig(ii),mu_c(:,ii),sig_c(:,ii)]=normfit((Ez2
        (:,ii)));
end



% Computation of average Ez over all possible points
% Ez2_avg = mean(Ez2,2);
% Ez2_avg= Ez2_avg.^2;
% figure(3)
% hist((Ez2_avg)/mean(Ez2_avg),10);
% [Na,xa_axis] = hist((Ez2_avg)/mean(Ez2_avg),10);
% Na_norm = N/(rot_size+1);
```

Chapter C: Antenna Fabrication and Measurement Details

Fabrication and testing of the proposed antenna is the most important part during the antenna design procedure. The selection of substrate material is the first step during the design of the antenna system. In order to reduce the propagation delay, the substrate material used for the RF applications should possess low relative permittivity and low dielectric constant. It should be mentioned that, the choice of ϵ_r of the substrate depends mainly on the application of the antenna. The thickness of the substrate plays an important role in the antenna design process. As the thickness of the substrate material increases, the band width of the antenna will also increase. In this thesis, we use Rogers RT duroid 5880 substrate with ϵ_r =2.2, tanδ=0.0009, and h=0.381,mm.

Once the deign of the proposed antenna is complete, the antenna can be simulated using RF software. Later, a fine optimization of different antenna parameters can be executed to bring the antenna resonance at the designed frequency of operation with adequate S_{11} characteristics. Once, the required simulation characteristics are achieved a layout is generated for the fabrication process. The layout of the proposed antenna can be generated using either the simulation software or the CAD software. A detailed explanation of fabrication steps are available in the following section.

C.1 Fabrication process

The screen printing method is adopted for the fabrication of the antenna. Screen Printing method is the simple and easy method used for the fabrication of PCB. The three main steps involved in screen printing methods are: photo resist application, exposing (or printing) and developing.

Photo resist application

In this stage the substrate is coated with a photoresist by using the spin coating method. The photoresist viscous solution is dispensed onto the substrate, and the substrate will rotate promptly to yield a evenly thick photoresist layer of 0.5 to 2.5 μm thick. It should be noted that the spin coating frequently rotate at the speed of 1200 to 4800 RPM for almost 30 to 60 s. The film is sensitive to UV light. The coated substrate is then put into prebaking stage to remove the leftover photoresist solvent. The board will place in the oven for 20 min and then take from the oven to cool down to room temperature.

Image Expose (or printing)

Later, the CAD file of the proposed model is used to model the particular design on the board. The data will carry all the copper features and through hole details. This film helps to place an image on the photo resist. The substrate is then exposed to a high intensity ultraviolet light source for 30secs. This procedure allows the UV light to create the image of the proposed model on the substrate material. THis operation is similar to the development of the negative of the photograph. The unprotected substrate is then retained for almost 20 min and then a development machine is used to develop the board.

Image Develop

Image developing is performed in a developer solution using the developing machine . The developer deposes the photo resist from the concealed parts. These parts are the portions which were under the hazy areas of the photo tool). The exposed areas of the substrate remain untouched. Later, the proposed board will cleanse with water and then it will soak in a sulfuric acid solution for some time. Finally, the board will again cleanse with water.

Etching Process

The most important step is the Etching, which is the chemical process used for removing the unwanted copper from the PCB. It is important to put a mask on the particular pattern that should be remained after the etching process. The copper area which is not guarded by the etch resist will remove by this process. Hence, the final antenna pattern is retained by the careful elimination of all the unwanted copper. The available etching solutions are: Ferric Chloride, Ammonium Persulphate, etc.

Finally, the photoresist applied on the board will remove from the board after the etching process. In order to strip the photo resist the etched board will dip in to the sodium hydroxide solution for 10 min. Later, the PCB will remove from the solution and it will clean with water. Then, the PCB will dry completely and will check thoroughly for any kind of fabrication errors. The final produced PCB is shown in Fig.C.1. The various steps involved in the fabrication process are illustrated in Fig.C.2.

C.2 Antenna Measurements

The most important part of antenna design process is the measurement of the fabricated antenna. In this section, the different techniques used for the

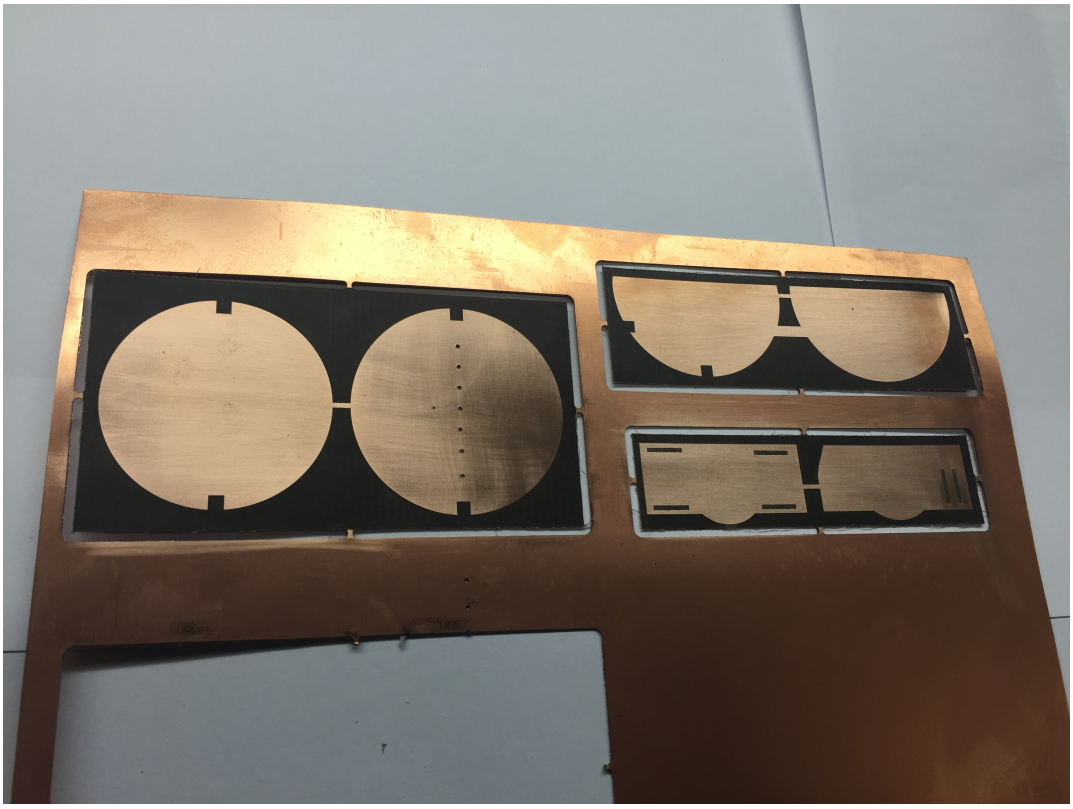

Figure C.1: Fabricated Antenna.

antenna measurement is provided. Two different equipment are used for the measurement procedure.

C.2.1 E5072A Network Analyzer

Agilent E5072A ENA Series Network Analyzer was used for analyzing the antenna parameters. The vector network analyzer (VNA) is mainly used for radio frequency design applications. Agilent E5072A ENA is an advanced network analyzer which provide wide range of applications. The microwave ENA Series vector network analyzers architecture consist of a signal generator, two test ports, display etc,. The two port set up helps to measure four standard S-parameters. It has a frequency range of 30 kHz to 8.5 GHz. The calibration of the port is done for the frequency range of interest using the calibration

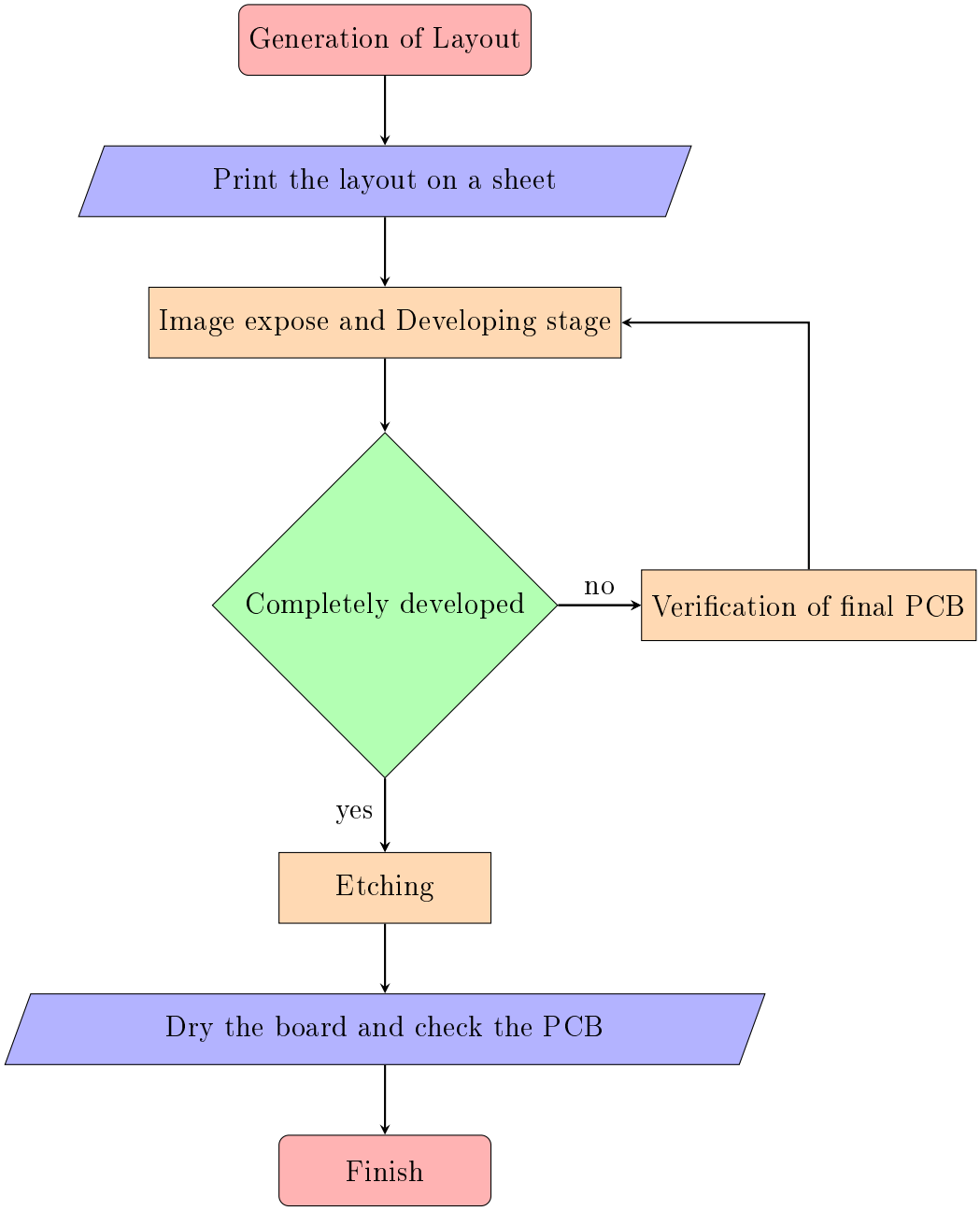

Figure C.2: Antenna fabrication process

kit 85032F (Type-N, 50Ω). The calibration kit is used to correct the system performance by using standard short, open and matched load set up (SOLT). Moreover, electronic calibration (ecal) set up is also available. This VNA pos-

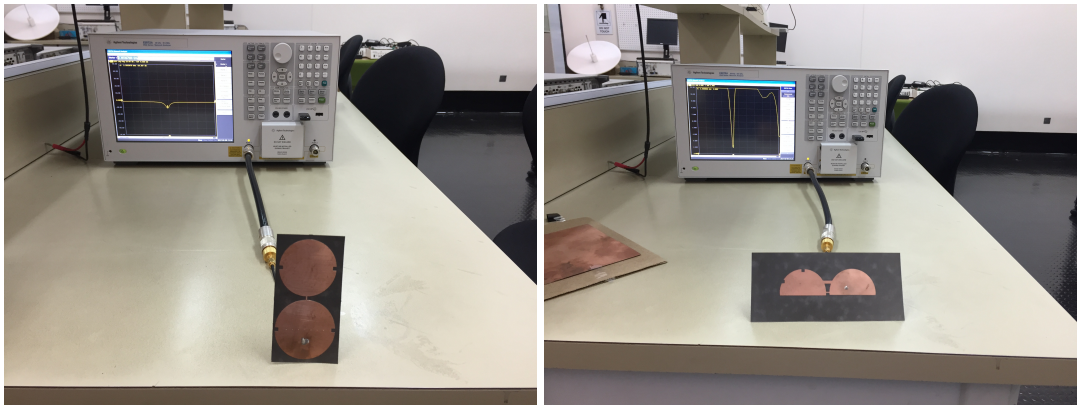

(a) (b)

Figure C.3: Measurement of the antenna using network analyzer.

sess high speed and accuracy, and it is relevant for the testing of passive and active components, such as antennas, filters, and high-power amplifiers.

In this thesis, we use E5072A VNA for the measurement of return loss characteristic of the antenna. In this procedure, the antenna is connected to any one of the port (port 1 or port 2) and operating the VNA in S_{11} or S_{21} mode as shown in Fig. C.3. The resonant frequency of the antenna is the frequency at which the antenna shows minimum return loss value. The VSWR of the antenna can also be measured using the VNA as shown in Fig.C.3. Later, the bandwidth of the antenna can be evaluated from the S_{11} plot. Moreover, the smith chart, phase of the transmission characteristics, etc, can also measured using the VNA.

C.2.2 Antenna Pattern Measurements Using Anechoic Chamber

Radiation pattern measurements for the proposed antennas is performed at CUSAT, Kerala, India in an Anechoic Chamber. . The Anechoic chamber has a quiet Zone, free from all types of EM distortions and has been designed for

a particular frequency range. It is important to mention that there are two types of chambers are available. The rectangular anechoic chambers, that are used mainly for frequencies above 1 GHz and tapered anechoic chambers for frequencies below 1 GHz.

Radiation Pattern measurement

The radiation pattern of the antenna under test (AUT) is the representation of the radiation characteristics of the antenna as a function of θ and ϕ coordinates. The radiation pattern of the AUT is measured in the Far-Field region for constant radial distance and frequency. The radiation pattern of the proposed antennas can be measured in transmit or receive mode. However, sometimes it is required to measure the characteristics under both conditions. The radiation pattern of the antenna can be measured as either 3D or 2D pattern according to available technology. The 2D pattern is called pattern cuts and it can be measured as elevation pattern, or azimuth pattern. In order to achieve the particular pattern cuts, the equipment must have the ability to rotate in various planes.

A photograph of the anechoic chamber is shown in Fig.C.4. The AUT and the test horn antenna set up are also shown. The distance between AUT and test horn can vary according to the frequency of operation. For our particular application the AUT and the test system was separated by a distance of 85 cm, as shown in Fig.C.5 (a). A microwave test receiver receives the signal from the AUT as shown in Fig. C.5 (b). The acquired data may be plotted and/or post processed using matlab code.

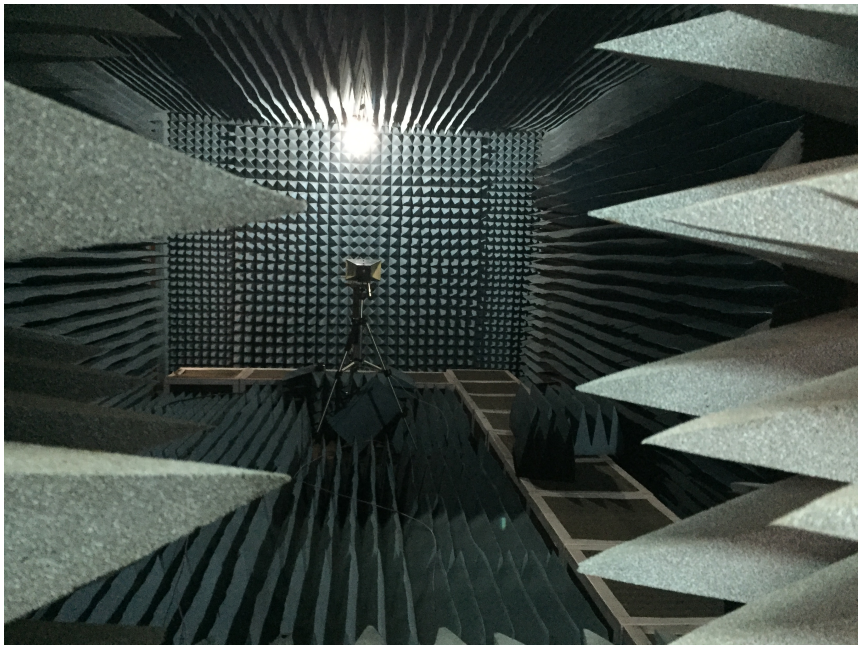

Figure C.4: Anechoic chamber.

(a) (b)

Figure C.5: Measurement of the antenna using anechoic chamber.